

Synthesis of fluorinated polymers in supercritical carbon dioxide (scCO₂)

This work is licensed under a Creative Commons License:
Attribution - Noncommercial - No Derivative Works 3.0 Unported
To view a copy of this license visit
<http://creativecommons.org/licenses/by-nc-nd/3.0/>

Online published at the
Institutional Repository of the Potsdam University:
<http://opus.kobv.de/ubp/volltexte/2008/1986/>
[urn:nbn:de:kobv:517-opus-19868](http://nbn-resolving.org/urn:nbn:de:kobv:517-opus-19868)
[<http://nbn-resolving.de/urn:nbn:de:kobv:517-opus-19868>]

Universität Potsdam
Arbeitsgruppe Prof. Sabine Beuermann

Synthesis of fluorinated polymers in supercritical carbon dioxide (scCO₂)

Dissertation
zur Erlangung des akademischen Grades
"doctor rerum naturalium"
(Dr. rer. nat.)
in der Wissenschaftsdisziplin "Polymerchemie"

eingereicht an der
Mathematisch-Naturwissenschaftlichen Fakultät
der Universität Potsdam

von
Muhammad Imran ul-haq
aus Gujrat, Pakistan

Potsdam, im Juni 2008

The following research work has been done from June 2005 to June 2008 at the Georg-August University of Göttingen, Göttingen and University of Potsdam in Potsdam/Golm, Germany.

Referent: Prof. Dr. Sabine Beuermann

Korreferent. 1: Prof. Dr. Jan Meuldijk

Korreferent. 2: Prof. Dr. Markus Busch

Tag der mündlichen Prüfung: 07.08.2008

Table of contents

1. Abstract	1
2. Introduction	3
2.1 Supercritical carbon dioxide scCO ₂	3
2.2 Polymer synthesis and scCO ₂	5
2.3 Fluoropolymers and scCO ₂	6
2.4 Supercritical CO ₂ in the production of nano-size particles	8
2.5 Rapid expansion of supercritical solution (RESS)	9
2.6 Objectives of this work	10
3. Theoretical background	12
3.1 Ideal polymerization kinetics	12
3.2 Transfer reactions	14
4. Experimental techniques	16
4.1 High pressure apparatus	16
4.1.1 Optical high-pressure cell	16
4.1.2 Heating and temperature control	17
4.1.3 Experimental set-up for polymerizations in scCO ₂	17
4.1.4 High pressure mixing autoclave	18
4.1.5 FT-IR/NIR spectrometer	20
4.1.6 Phase behaviour setup and measurements	20
4.1.7 RESS set-up	20
4.2 Characterization techniques	21
4.2.1 Size-Exclusion Chromatography	21
4.2.2 Nuclear Magnetic Resonance	22
4.2.3 ESI-MS Spectrometer	21
4.2.4 Scanning Electron Microscopy	22
4.2.5 Atomic Force Microscopy	22
4.2.6 Wide Angle X-ray Diffraction	22
4.2.7 Differential Scanning Calorimetry	22

4.2.8	Spectroscopic observations (FT-NIR)	22
5.	Experimental part	24
5.1	Materials	24
5.2	Experimental Procedure	25
5.2.1	Phase behaviour experiments	25
5.2.2	VDF polymerization in scCO ₂	25
5.2.3	VDF polymerization using CTAs	26
5.2.4	End-functionalization of PVDF-I	26
5.2.5	RESS process	27
6.	Results and Discussion	28
6.1	Homogeneous phase polymerization	28
6.1.1	Phase behaviour analysis	28
6.1.2	FT-NIR Spectroscopic Observations	29
6.1.3	MW control via initiation	31
6.1.4	Variation of monomer concentration	34
6.1.5	Microstructure of PVDF	35
6.1.6	Morphology of PVDF	36
6.1.7	Summary of results	37
6.2	Molecular weight control via degenerative transfer using Perfluorinated hexyl iodide (PFHI)	39
6.2.1	NIR spectroscopy and conversion	39
6.2.2	Effect of perfluorinated hexyl iodide concentrations	40
6.2.3	Living nature of polymerization	42
6.2.4	Rate of polymerization	43
6.2.5	Application of iodide end groups towards click chemistry	47
6.2.6	Summary of results	53
6.3	Bromotrichloromethane as chain transfer agent	54
6.3.1	Variation of chain transfer agent concentration	54
6.3.2	Rate of polymerization and CTA concentration	55
6.3.3	Summary of results	57
6.4	Polymerization in the presence of perfluorinated hexyl bromide and 1H-perfluorohexane	58
6.4.1	Molecular weight Control via employing CF ₃ -(CF ₂) ₅ -X	58

6.4.2	End groups analyses via $^1\text{H-NMR}$ spectroscopy	60
6.4.3	Chain transfer constants of $\text{CF}_3\text{-(CF}_2)_5\text{-X}$	62
6.4.4	Effect of $\text{CF}_3\text{-(CF}_2)_5\text{-X}$ concentrations on rate of polymerization	63
6.4.5	Summary of results	67
6.5	Polymer end group effect on morphology and crystallization of PVDF	68
6.5.1	Polymer samples for analyses	68
6.5.2	Positive ESI-MS analyses of PVDF	69
6.5.3	End groups analyses via $^1\text{H-NMR}$ spectroscopy	72
6.5.4	Morphology of different PVDF samples	74
6.5.5	DSC and crystallinity	78
6.5.6	Polymorphs of PVDF and FT-IR analyses	82
6.5.7	Wide angle X-ray diffraction: (WAXD)	84
6.5.8	AFM images of PVDF	86
6.5.9	Summary of results	88
6.6	Rapid expansion of supercritical solution (RESS) for PVDF	89
6.6.1	Effect of RESS process on MW of PVDF	89
6.6.2	Particle formation	90
6.6.3	Influence of polymer MW on particle size and distributions	91
6.6.4	Influence of polymer end groups on particle size distributions	94
6.6.5	Summary of results	96
7.	Summary and conclusions	98
8.	List of abbreviations	102
9.	Acknowledgements	105
10.	Publications	107
11.	Literature	109
	Curriculum Vitae	

Dedicated to my family and friends

1. Abstract

For the first time stabilizer-free vinylidene fluoride (VDF) polymerizations were carried out in homogeneous phase with supercritical CO₂. Polymerizations were carried out at 140°C, 1500 bar and were initiated with di-*tert*-butyl peroxide (DTBP). In-line FT-NIR (Fourier Transform- Near Infrared) spectroscopy showed that complete monomer conversion may be obtained. Molecular weights were determined via size-exclusion chromatography (SEC) and polymer end group analysis by ¹H-NMR spectroscopy. The number average molecular weights were below 10⁴ g·mol⁻¹ and polydispersities ranged from 3.1 to 5.7 depending on DTBP and VDF concentration. To allow for isothermal reactions high CO₂ contents ranging from 61 to 83 wt.% were used. The high-temperature, high-pressure conditions were required for homogeneous phase polymerization. These conditions did not alter the amount of defects in VDF chaining. Scanning electron microscopy (SEM) indicated that regular stack-type particles were obtained upon expansion of the homogeneous polymerization mixture.

To reduce the required amount of initiator, further VDF polymerizations using chain transfer agents (CTAs) to control molecular weights were carried out in homogeneous phase with supercritical carbon dioxide (scCO₂) at 120 °C and 1500 bar. Using perfluorinated hexyl iodide as CTA, polymers of low polydispersity ranging from 1.5 to 1.2 were obtained. Electrospray ionization- mass spectroscopy (ESI-MS) indicates the absence of initiator derived end groups, supporting livingness of the system. The “livingness” is based on the labile C-I bond. However, due to the weakness of the C-I bond perfluorinated hexyl iodide also contributes to initiation. To allow for kinetic analyses of VDF polymerizations the CTA should not contribute to initiation. Therefore, additional CTAs were applied: BrCCl₃, C₆F₁₃Br and C₆F₁₃H. It was found that C₆F₁₃H does not contribute to initiation. At 120°C and 1500 bar $k_p/k_t^{0.5} \sim 0.64$ (L·mol⁻¹·s⁻¹)^{0.5} was derived. The chain transfer constant (C_T) at 120°C has been determined to be $8 \cdot 10^{-1}$, $9 \cdot 10^{-2}$ and $2 \cdot 10^{-4}$ for C₆F₁₃I, C₆F₁₃Br and C₆F₁₃H, respectively. These C_T values are associated with the bond energy of the C-X bond.

Moreover, the labile C-I bond allows for functionalization of the polymer to triazole end groups applying click reactions. After substitution of the iodide end group by an azide group 1,3 dipolar cycloadditions with alkynes yield polymers with 1,2,3 triazole end groups. Using symmetrical alkynes the reactions may be carried out in the absence of any catalyst. This end-functionalized poly (vinylidene fluoride) (PVDF) has higher thermal stability as compared to the normal PVDF.

PVDF samples from homogeneous phase polymerizations in supercritical CO₂ and subsequent expansion to ambient conditions were analyzed with respect to polymer end groups, crystallinity, type of polymorphs and morphology. Upon expansion the polymer was obtained as white powder. Scanning electron microscopy (SEM) showed that DTBP derived polymer end groups led to stack-type particles whereas sponge- or rose-type particles were obtained in case of CTA fragments as end groups. Fourier-Transform Infrared spectroscopy and wide angle X-ray diffraction indicated that the type of polymorph, α or β crystal phase was significantly affected by the type of end group. The content of β -phase material, which is responsible for piezoelectricity of PVDF, is the highest for polymer with DTBP-derived end groups. In addition, the crystallinity of the material, as determined via differential scanning calorimetry is affected by the end groups and polymer molecular weights. For example, crystallinity ranges from around 26 % for DTBP-derived end groups to a maximum of 62 % for end groups originating from perfluorinated hexyl iodide for polymers with $M_n \sim 2200 \text{ g}\cdot\text{mol}^{-1}$.

Expansion of the homogeneous polymerization mixture results in particle formation by a non-optimized RESS (Rapid Expansion from Supercritical Solution) process. Thus, it was tested how polymer end groups affect the particles size distribution obtained from RESS process under controlled conditions ($T = 50^\circ\text{C}$ and $P = 200 \text{ bar}$). In all RESS experiments, small primary PVDF particles with diameters less than 100 nm were produced without the use of any liquid solvents, surfactants, or other additives. A strong correlation between particle size and particle size distribution with polymer end groups and molecular weight of the original material was observed. The smallest particles were found for RESS of PVDF with $M_n \sim 4000 \text{ g}\cdot\text{mol}^{-1}$ and C₆F₁₃I - derived end groups.

2. Introduction

Environmental concern over the emission of volatile organic solvents used in polymer synthesis has prompted researchers to look for less harmful alternatives. A very promising technology area should be the polymerization in supercritical fluids.¹ These fluids show gas like diffusivities while having liquid like densities that allow for solvation of many compounds. They exhibit a change in solvent density upon small variations in temperature or pressure without altering solvent composition.² In addition, the low viscosity of supercritical fluids and their ability to plasticize glassy polymers have implications on polymer processing and kinetics. The temperature and pressure at which the gas and liquid phases become identical is the critical point. In the supercritical environment only one phase exists. The fluid, as it is termed, is neither a gas nor a liquid and is best described as intermediate to the two extremes. This phase retains the solvent power common to liquids as well as the transport properties common to gases. A comparison of typical values for density, viscosity and diffusivity of the gases, liquids and SCFs are present in Table 2.1.

Property	Gas	SCF	Liquid
Density ($\text{kg}\cdot\text{m}^{-3}$)	1	100-800	1000
Viscosity (cP)	0.01	0.05-0.1	0.5-1.0
Diffusivity ($\text{mm}^2\cdot\text{s}^{-1}$)	1-10	0.01-0.1	0.001

Table 2.1: Comparison of physical and transport properties of gases, liquids and SCFs (supercritical fluids).

2.1 Supercritical carbon dioxide (scCO₂)

One of the supercritical fluids, which can be used in polymerization process as solvent is carbon dioxide (CO₂). Supercritical CO₂ is a clean and versatile solvent and a promising alternative to noxious organic solvents and chlorofluorocarbons. It has attracted particular attention as a supercritical fluid in the synthesis as well as processing areas for polymers due to the following properties:

- CO₂ is non-toxic, non-flammable, chemically inert, and inexpensive. A large amount is available as a by-product from NH₃ and ethanol industries and refineries.

- Supercritical conditions are easily achieved: $T_c^\circ = 31^\circ\text{C}$ and $P_c^\circ = 74$ bar.
- The solvent may be removed by simple depressurization.
- The density of the solvent can be tuned by varying the pressure.
- Many polymers become highly swollen and plasticized in the presence of CO_2 .

CO_2 can be acquired from natural reservoirs or recovered as a by-product of industrial chemical processes, so no new production of CO_2 is necessary and there will be no additional contribution to the greenhouse gases. Liquid CO_2 is a compressible fluid, while supercritical CO_2 has relatively high liquid-like densities and low gas-like viscosities. Both liquid and supercritical CO_2 have a tuneable density (and dielectric constant) that increases with increasing pressure or decreasing temperature.³ The solvency of supercritical CO_2 is often compared to that of fluorocarbon solvents.

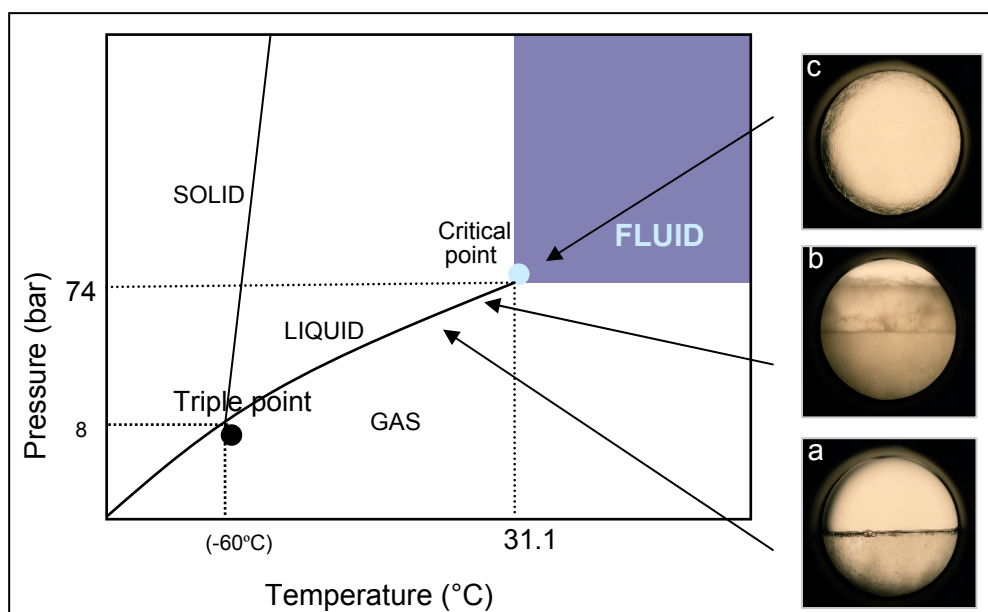


Figure 2.1: Phase diagram of CO_2 .⁴

The pressure-temperature diagram for carbon dioxide is presented in Figure 2.1 to illustrate the differences between the gas, liquid and supercritical states. The CO_2 in Figure 2.1a clearly shows two phases before the critical point and near to the critical point in Figure 2.1b two less distinct phases. The critical point is marked at the end of the gas-liquid equilibrium curve, and the supercritical fluid region is indicated by the shaded area. Supercritical CO_2 is represented by Figure 2.1c, which clearly exhibits one phase. It can be shown that by using a combination of isobaric changes in temperature with isothermal changes in pressure, it is possible to

convert a pure component from liquid to gas (and vice versa) via the supercritical region without incurring a phase transition.

2.2 Polymer synthesis and scCO₂

DeSimone and co-workers have shown that scCO₂ is an attractive medium for both homogeneous and heterogeneous radical polymerizations.⁵ Most of the investigations into polymerizations in scCO₂ are focused on reactions in heterogeneous phase as polymer solubility in scCO₂ is generally rather low. Recently, several studies showed a significant influence of scCO₂ on homogeneous phase polymerizations. For example, in butyl acrylate homopolymerization scCO₂ was shown to have a significant influence on the propagation and termination rate coefficients.⁶⁻⁸

Homogeneous phase polymerizations are attractive because of avoiding the use of a surfactant, which saves cost and also eliminates surfactant derived impurities in the polymer. The work-up after the reaction is easier as compared to heterogeneous phase processes. Homogeneous phase polymerizations are advantageous for carrying out continuous polymerizations in a tubular reactor, which would allow for a reduction in reactor size and increase the inherent safety of the process. Low molar mass polymers were targeted to improve the polymer solubility in solvents and to decrease the processing temperature during the fabrication of shaped articles (by molding or extrusion) or films (by solvent casting and extrusion) or for textile and paper coatings.⁹

Homogeneous phase reactions also provide favourable conditions for in-line spectroscopic monitoring of the polymerization. As demonstrated in the work of Buback et al., vibrational spectroscopy is particularly useful for measuring concentrations under supercritical conditions.¹⁰ The spectroscopic data allow for kinetic investigations under extreme conditions, which are not easily carried out otherwise, and gives insights into the homogeneity of the reaction mixture throughout the polymerization.¹¹

However, while many small molecules are soluble in CO₂, high molecular weight (MW) polymers are mostly insoluble in scCO₂. Besides low MW styrene-(meth)acrylate copolymers¹² some fluoropolymers,⁵ poly(siloxanes)¹³ and ether-carbonate copolymers¹⁴ show considerable solubility in dense CO₂. The solubility of fluoropolymers having a hydrocarbon backbone and a fluorocarbon pendant group in scCO₂ was reported to depend on both the number of fluorinated side groups and the molar mass of the side groups relative to that of the hydrocarbon main chain.¹⁵⁻¹⁷ In addition, solubility increases towards lower

polymer MW.¹⁸ With respect to technical applications of homogeneous phase polymerization in CO₂, primary interest thus focuses on the production of a relatively low MW polymer.¹⁹

2.3 Fluoropolymers and scCO₂

Fluorinated polymers gained large interest for technical applications due to their unique properties, e.g., excellent chemical, thermal, and mechanical stability as well as piezoelectric and pyroelectric properties.²⁰⁻²² These properties lead to technical applications, e.g., such as valves, coatings, films, cables, pipes and membranes for fuel cells.²³ Generally, these polymers are synthesized in heterogeneous phase, either in precipitation polymerizations or more frequently in emulsion polymerizations. The latter generally affords the use of fluorinated stabilizers,²⁴ which have a high potential for bioaccumulation.²⁵ Supercritical carbon dioxide (scCO₂) has emerged as an attractive alternative solvent.

Despite the benefits of homogenous phase polymerizations, literature reports focus on heterogeneous phase polymerizations of VDF.²⁶⁻³³ This holds not only for VDF but also for other fluoromonomers.^{24,34} In case of VDF one of the reasons for studying heterogeneous phase polymerizations may be seen in the fact that PVDF is a semicrystalline polymer (more than 50 % crystallinity). Sorption and swelling of the polymer upon addition of supercritical CO₂ shows significant differences to amorphous polymers, e.g., such as poly(methyl methacrylate).³⁵ Previously, it was shown that high molecular weight PVDF ($M_w > 181000 \text{ g}\cdot\text{mol}^{-1}$) has a rather limited solubility in pure CO₂.³⁶

The controlled synthesis of low molecular weight (MW) polymers is gaining greater importance because applications in coatings, detergents and water treatment industries continue to develop. The interest in the free-radical polymerization with respect to the preparation of these materials is originating from the fact that in contrast to ionic polymerization a greater number of monomers can be utilized. Although most common styrenic and meth(acrylic) polymers show only limited solubility, the synthesis of low molecular weight material in the presence of scCO₂ is a promising alternative process. Due to the significantly increased polymer solubility at low MW, high degrees of monomer conversion are accessible in homogeneous phase of scCO₂. Because polymer properties are strongly dependent on MW, it is of great interest to effectively control MW. One approach to molecular weight reduction involves the use of chain-transfer agents (CTAs). The knowledge of the transfer activity of a CTA, which is measured via the chain transfer rate coefficient, k_{tr} , is necessary to predict the molecular weight of the polymer obtained. Thus, one of the aims of

this work is to investigate the influence of CTAs on the rate of polymerization and also on the transfer process in free-radical polymerization in supercritical carbon dioxide.

It is generally accepted that end groups have no significant influence on macroscopic properties of polymers, because their weight is negligible as compared to the whole mass of the polymer, and because energy values for bonds in end groups and in the constitutive units are practically equal. It has been demonstrated that hydrogen and fluorine containing polymers, for example poly(vinylidene fluoride) (PVDF), are influenced, as far as thermal stability and fire resistance are concerned, by the end groups generated in the presence of different initiators.³⁷ In PVDF other properties, such as fluidity and electrical conductivity were demonstrated to be significantly influenced by end groups. End groups can also determine the crystallisation kinetics from the melt of thermoplastic fluoropolymers and hence the processing and end-use properties.²²

Poly(vinylidene fluoride) (PVF) is a fascinating polymer to study because of its unusual piezoelectric properties. Poly(vinylidene fluoride) (PVDF) is known to be a semicrystalline polymer with five different polymorphs, the so-called α , β , γ , δ , and ϵ forms.³⁸ The piezoelectricity is principally associated with the β phase. The connection between the crystalline structure and the resultant electrical properties has led to a number of studies in which attempts have been made to prepare different phases by altering thermal history,³⁹ mechanical deformation⁴⁰, γ irradiation⁴¹, or pressure.⁴² In addition, PVDF shows low acoustic impedance.⁴³ Polymeric piezoelectrics were used, e.g., as energy converters and different types of sensors in medicine. While pure PVDF has a modest dielectric permittivity, recently it was shown that hybrid materials consisting of PVDF and carbon nanotubes show very high permittivity that may find potential applications as actuators for artificial muscles.⁴⁴ Further attractive applications of VDF homo- and copolymers are seen as membranes for filtration⁴⁵ or for fuel cells.⁴⁶

The occurrence of these PVDF polymorphs depends on polymerization conditions and processing of the polymer, e.g., thermal treatment or application of an electrical field. Further, it was shown that polymer morphology may be affected by the use of scCO_2 .⁴⁷ The PVDF structural unit has a spiral shape because 1, 3 repulsion forces the F atoms out of linearity as shown in Figure 2.2.⁴⁸

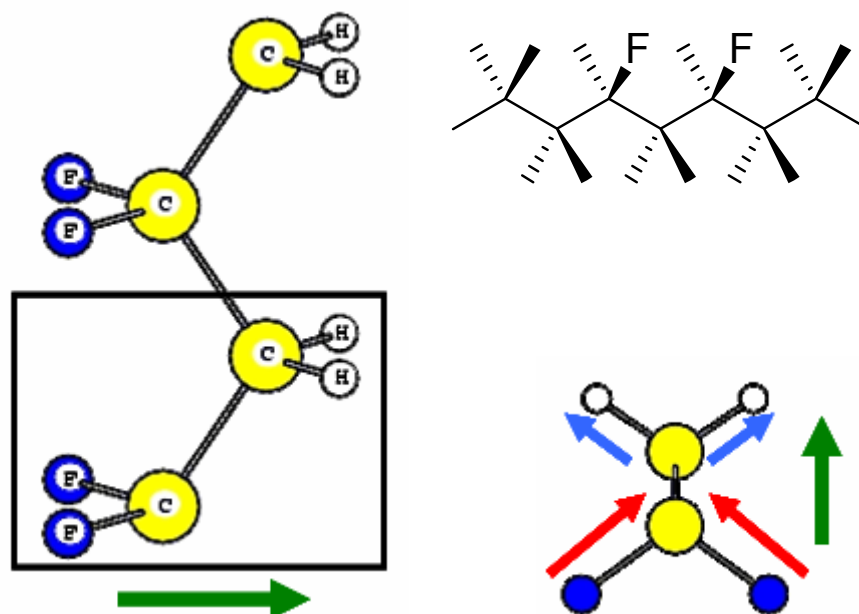


Figure 2.2: PVDF structural unit taken from ref. 48.

The nature of the CTA derived substituents determines the functionality introduced at the polymer chain ends. Literature shows only some on the chain-transfer activity, thus, the chain-transfer constant ($C_T = k_{tr}/k_p$) of these chain transfer agents are available for VDF. A few kinetic aspects related to these chain transfer agents for vinylidene fluoride have been studied in organic solvents.⁴⁹

2.4 Supercritical CO₂ in the production of nano-size particles

Milling, grinding, crystallization and spray drying are the particle formation methods commonly used in the coating, toner and drug delivery industries. Narrow particle size distribution, solvent recovery and avoiding the emissions of low volatile organic compounds (VOCs) are the major challenges associated with these methods. In addition, milling and grinding are not suitable for thermally unstable and low glass transition temperature or melting point compounds due to the frictional heat dissipated during processes. Therefore, the industries have been looking for new technologies, which would provide micron/nano size particles with a narrow particle size distribution using as small as possible quantities of VOC. This has motivated chemical engineers as well as chemists to apply a supercritical technology rather than classical methods. The supercritical technology utilizes the solubility of supercritical CO₂ in a polymer or vice versa.

In the last decade, the research on particle production using supercritical CO₂ has rapidly been growing. Various methods already exist that use supercritical CO₂ as a solvent or anti-solvent.

Recently, these methods have been broadly reviewed⁵⁰: rapid expansion of supercritical solutions (RESS), gas anti-solvent crystallization (GAS), supercritical anti-solvent precipitation (SAS), precipitation by compressed anti-solvent (PCA), solution enhanced dispersion by supercritical fluid (SEDS) and particles from gas saturated solutions (PGSS).

To have a brief idea over the listed methods, a comparison of all of them is summarized in Table 2.2. Moreover, a brief introduction has been provided for most commonly used supercritical methods.

	RESS	GAS/SAS/PCA	SEDS	PGSS
Process	discontinuous	Semi-continuous	Continuous	Continuous
Gas quantity	High	Medium	Medium	Medium
Organic solvent	Absent	Present	Present	Absent
Pressure	High	Medium	Medium	Low
Separation of gas	Easy	Easy	Easy	Easy

Table 2.2: The comparison of various supercritical methods.

2.5 Rapid expansion of supercritical solution (RESS)

The RESS method utilizes a dramatic change in the dissolving power of a solvent, when it is rapidly expanded from a supercritical pressure to a low pressure. After expansion, the solvent exists as a gas that makes the collection of the resulting particles (solute) much easier. RESS is based on crystallization or precipitation of a solute in order to facilitate the powder production. The method can generally be used, if the solubility of a solute (polymer) in supercritical CO₂ or another appropriate fluid is high. A fluid is pressurized and heated to ascertain the supercritical conditions needed for the process and passed through an extractor containing a solute in order to form single phase solution. Following this, the solution is depressurized over a nozzle to atmospheric pressure. The rapid depressurization leads to nucleation of the solute caused by the lowering of the solvation power and therefore particles are formed. After the depressurization, CO₂ turns into the gas phase and is purged out of the collecting device.

Numerous thermally labile substances have been processed with supercritical fluids. In particular, biocompatible and / or biodegradable polymers of pharmaceutical interest and significance were considered, since submicron polymer particles may be used as a carrier for

drugs or proteins and for controlled release applications.⁵¹⁻⁵³ Experimental investigations show, that the RESS-process enables the formation of submicron drug particles with improved dissolution behaviour.⁵⁴⁻⁵⁶ The feasibility of producing submicron L-poly(lactic acid) and DL-poly(lactic acid) particles by RESS has been demonstrated by Türk et al.⁵⁷ Recently, Sane and Thies have shown that RESS products from poly(l-lactide) (PLLA) consisted predominantly of nanoparticles 30 - 100 nm in diameter.⁵⁸ However, investigations on the application of RESS on fluorinated polymers are scarce. Particularly interesting are polymers with piezoelectric properties, as for example poly(vinylidene fluoride) (PVDF). Chernyak et al.⁵⁹ have reported experimental results on the formation of perfluoropolyether diamide droplets during the RESS process. For the system CO₂ + poly (heptadecafluoro-decylacrylate) the relationship between RESS processing conditions and product morphology was investigated by Blasig et al.⁶⁰ Sane and Thies have demonstrated that RESS can be used to produce nanoparticles (45 - 88 nm) of a fluorinated tetraphenylporphyrin.^{61,62}

2.6 Objectives of this work

In the context described above, the synthesis and characterization of fluoropolymers under scCO₂ in the pursuit of interesting and unusual properties are worthwhile. Homogeneous phase polymerizations are particularly interesting, because no stabilizer is required and these are comparably easy to scale-up to continuous processes. Homogeneous phase reactions also provide favourable conditions for in-line spectroscopic monitoring of the polymerization, which provides kinetic data (r_p and $k_p/k_t^{0.5}$). Identification of homogeneous phase reaction conditions is the first step towards the development of continuous polymerization processes. This work of fluoropolymer synthesis under supercritical carbon dioxide involves five parts:

- 1) - Synthesis of fluoropolymers with well defined properties under supercritical carbon dioxide in homogeneous phase.
- 2) - Use of different chain transfer agents to control the molecular weight and kinetics.
- 3) - Characterization of polymer material obtained with respect to morphology and polymer end groups.
- 4) - RESS process for production of poly(vinylidene fluoride) particles using carbon dioxide and characterization of these particles.
- 5) - End-functionalization of poly(vinylidene fluoride) using click reaction.

The first step is to determine the reaction conditions for polymerizations in homogeneous phase. For this purpose different CTAs will be used to improve the homogeneous phase reaction conditions along with controlling the molecular weight of the polymer e.g., such as morphology and crystallization.

Another aim of this work is to determine kinetic coefficients which can be used to model the polymerization process, because prerequisites for reliable modelling are a very detailed understanding of the mechanisms and kinetics. Furthermore the polymers obtained from homogenous phase reactions will be used for the RESS process to study whether small particles are accessible.

3. Theoretical background

Free radical polymerization is still the most widely used type of polymerization for polymer production. The main steps of reaction are the initiation of chains, propagation of the chains, termination of the chains and different types of transfer reactions.

3.1 Ideal polymerization kinetics

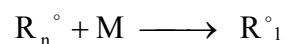
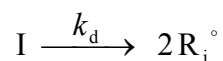
Ideal polymerization kinetics is based on four assumptions:

- All reactions are irreversible
- Monomeric species are only consumed in propagation steps
- All macroradicals show the same reactivity, irrespective of their chain length
- Termination takes place only by disproportionation or bimolecular radical combination

With these assumptions a kinetic scheme of a free radical polymerization can be characterized by three fundamental steps: the formation of radicals, chain growth of these radicals by propagation and termination of the radical chains.

Initiation

In the initiation reaction an initiator is decomposing into two primary radicals which can start the reaction. The formation of radicals can take place by thermal, chemical or photochemical activation of an initiator. This process involves two reactions.



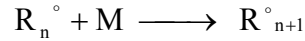
The initiator decomposition is a unimolecular reaction resulting in two initiator radicals with a rate coefficient k_d .

$$\frac{d c_{R,I}}{d t} = 2 \cdot k_d \cdot f \cdot c_I \quad (3.1)$$

Where $c_{R,I}$ is the radical concentration of initiator-derived radicals, k_d the initiator decomposition coefficient, f , the initiator efficiency and c_I the initiator concentration

Propagation

During the propagation step the monomer adds to a macroradical.



This leads to the following expression for the rate of propagation:

$$-\frac{d c_M}{d t} = k_p \cdot c_M \cdot c_R \quad (3.2)$$

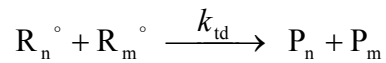
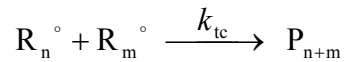
k_p : propagation rate coefficient

c_R : radical concentration

c_M : monomer concentration

Termination

Chain termination proceeds either via combination of two macroradicals R_n° and R_m° to a polymer molecule with chain length $n+m$, P_{n+m} , or by disproportionation of two macroradicals.



Generally, the individual rate of coefficients k_{tc} and k_{td} yield the overall termination rate coefficient, k_t :

$$k_t = k_{tc} + k_{td}$$

The termination rate is given by:

$$-\frac{d c_R}{d t} = 2k_t \cdot c_R^2 \quad (3.3)$$

Assuming steady state condition the number of formed radicals is equal to the number of consumed radicals:

$$2k_t \cdot c_R^2 = 2 \cdot k_d \cdot f \cdot c_I \quad (3.4)$$

$$c_R = \left(\frac{k_d \cdot f \cdot c_I}{k_t} \right)^{1/2} \quad (3.5)$$

Introducing this equation (3.5) into the equation 3.2, the overall rate of polymerization, r_p is derived according to:

$$r_p = -\frac{dc_M}{dt} = \frac{k_p \cdot c_M}{\sqrt{k_t}} \cdot \sqrt{k_d \cdot f \cdot c_I} \quad (3.6)$$

$$k = k_p \cdot \sqrt{k_d \cdot f \cdot c_I} \quad (3.7)$$

The overall rate of polymerization (r_p) is the first order with respect to the monomer concentration (c_M) and half order with respect to the initiator concentration (c_I). The overall rate coefficient k does not only depend on the rate coefficients of the chain propagation, initiator decomposition and chain termination, but also on the radical efficiency " f " which is a probability factor for a primary radical to react with monomer rather than to react with other radicals and become inefficient. To express the conversion of monomer as a function of time the differential rate equation has to be integrated. Calling $c_{M,0}$ and c_I the initial monomer and initiator concentration and regarding c_I to be constant with time, the result is:

$$\ln \frac{c_M}{c_{M,0}} = -k \cdot c_I^{0.5} \cdot t \quad (3.8)$$

If conversion of monomer (x) is of interest the corresponding equations are:

$$\frac{dx}{dt} = k \cdot c_I^{0.5} \cdot (1-x) \quad (3.9)$$

$$x = 1 - \exp(-k \cdot c_I^{0.5} \cdot t) \quad (3.10)$$

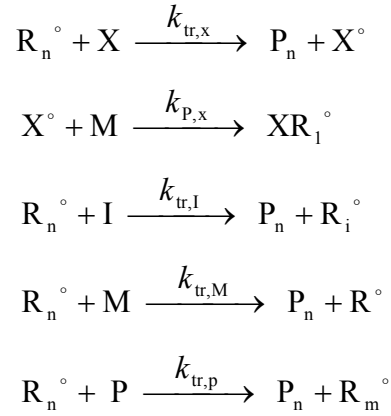
If the concentration of initiator is not constant with time and the initiator decomposition is a first order reaction, the following equations may be used to calculate the maximum conversion of monomer.

$$x_{\max} = 1 - \exp\left(-\frac{2k \cdot c_I^{0.5}}{k_d}\right) \quad (3.11)$$

3.2 Transfer reactions

According to the classical mechanism for free-radical polymerization, as shown in the following reaction scheme, a propagating radical R° , once generated, has three options to react. It may propagate, terminate in a radical-radical reaction, or undergo a chain-transfer reaction.

Chain transfer involves the reaction of a propagating chain R_n° with a transfer agent to terminate one polymer chain and produce a new radical X° , which initiates another chain XR_1° . The substrate for the chain transfer may be a chain-transfer agent (X), initiator (I), monomer (M), polymer (P) or some other component of the polymerization mixture.



$k_{tr,x}$, $k_{tr,M}$, $k_{tr,I}$ and $k_{tr,P}$ are the transfer rate coefficients to CTA, initiator, monomer and polymer, respectively.

$$C_T = \frac{k_{tr,x}}{k_p} \quad (3.12)$$

The chain-transfer constant, C_T , is defined as the ratio of $k_{tr,x}$ and k_p . The higher C_T , the lower is the concentration of chain-transfer agent that is required for a particular molecular weight reduction.⁶³

$$\frac{1}{DP_n} = \frac{1}{DP_{n_0}} + C_T \frac{[CTA]}{[M]} \quad (3.13)$$

This effect on polymer molecular weight is quantitatively given by the Mayo-equation⁶⁴ in (3.3) which expresses the reciprocal of the number average degree of polymerization, DP_n , as a function of the rates of chain growth and chain stopping.

4. Experimental Techniques

4.1 High-pressure apparatus

4.1.1 Optical high-pressure cell

The optical high-pressure cell used for spectroscopic investigations of chemically initiated VDF polymerizations under high pressure is illustrated in Figure 4.1. The cell is designed for pressures up to 3000 bar and temperatures up to 350°C. The cylindrical cell body and sealing flanges are made of a nickel-based alloy of high ultimate tensile strength (RGT 601, Material No. 2.4668, Arbed Saarstahl). The body length is 100 mm and the outer and inner diameters are 80 and 22 mm, respectively. Four holes bored perpendicular to the cylindrical axis allow for fitting of high-pressure capillaries and insertion of a sheathed thermocouple (6) directly into the sample volume. Unused borings are sealed with plugs. The cell is sealed at each end by a conical ram (5) (Material No. 2.4668, Arbed Saarstahl) which sits into the cell cone. The ram is pressed against the cell cone by the flange (2) (Material No. 2.4668, Saarstahl) which is secured by six high-pressure bolts (1) (Material No. 2.4969).

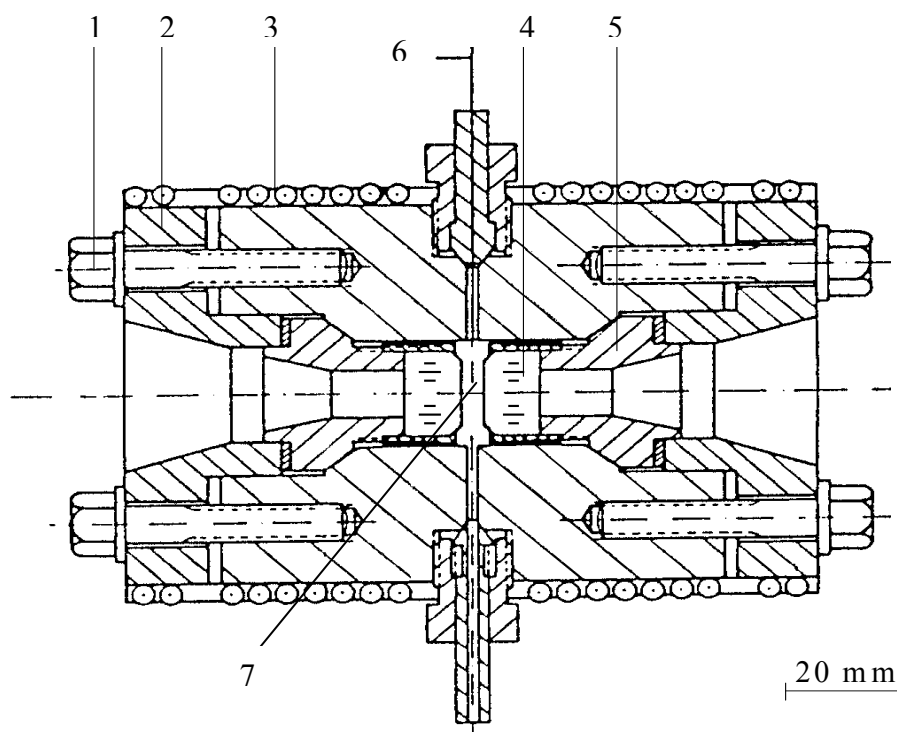


Figure 4.1: Optical high-pressure cell.

- (1) bolt, (2) flange, (3) heating jacket, (4) high-pressure window,
(5) ram, (6) sheathed thermocouple, (7) adjustable optical path length

Each high-pressure window (4) is fitted against the polished surface of the ram and held in place by a stainless steel cealing cap. To compensate surface area irregularities, a $\sim 12 \mu\text{m}$ thick Teflon foil is placed between the polished surfaces of the window. This set-up is self sealing under pressure in accordance with the Poulter principle. The high-pressure optical windows used in this work were synthetic sapphire crystals (diameter 18 mm, height 10 mm, UV grade, Roditi, Union Carbide) made by the Czochralski procedure. This material is transparent in the wavenumber range from 2000 to 50000 cm^{-1} . The optical high-pressure cell is mounted on a metal holder with a wooden grip for easy handling and fitting into the sample chamber of the FT-IR spectrometer.

4.1.2 Heating and temperature control

The optical high-pressure cell is heated by two heating jackets. They consist of a brass matrix, into which is embedded a sheathed resistance heating wire (CGE-Asthom). The closely fitting jackets slide over each end of the cell body (see Figure. 4.1 (3)). The temperature is measured via the sheathed thermocouple (Nickel-chromium against nickel, CIA S250, CGE-Alsthom) and regulated by a PID-controller (Eurotherm 815).

4.1.3 Experimental set-up for polymerizations in scCO_2

Figure 4.2 gives a schematic diagram of the experimental apparatus used to prepare the reaction mixture. The set-up is a modification of the previously used apparatus, which was detailed in ref. 6, used to prepare mixtures of CO_2 with liquid monomers. The initiator was filled into the inlet for liquid components. Then, the initiator was transferred into the mixing autoclave (A). The monomer VDF was compressed and pumped by the pneumatically driven pump (PM). The volume of VDF added to autoclave (A) was controlled by the syringe pump. Accordingly, CO_2 was compressed and pumped by the second PM. Again, the amount of CO_2 added to the autoclave (A) was controlled by the syringe pump. The mixture consisting of initiator, CO_2 and VDF inside autoclave A was stirred with a magnetic stir bar for one hour at the pressure of 350 bar to ensure homogeneous mixing of the components. To prevent polymerization, autoclave (A) was cooled to 0°C . Then, the mixture was transferred to the syringe pump and the pre-heated optical high-pressure cell (HZ) equipped with two sapphire windows. To avoid demixing during the filling procedure the pressure was kept constant by the HPLC pump, which moves the piston of the mixing autoclave (A) (dashed in Figure 4.2) and thus keeping the pressure constant. The final pressure inside the optical cell was adjusted with the syringe pump. Then the cell is disconnected from the pressure branch and inserted into the sample compartment of the FT-NIR spectrometer. In the majority of the experiments

the high pressure cell was filled directly inside the sample compartment of the spectrometer. A detailed description of the set-up and the high-pressure cell used was given elsewhere.^{6,65}

The pressure is measured using the pressure gauge from HBM (P3MB).

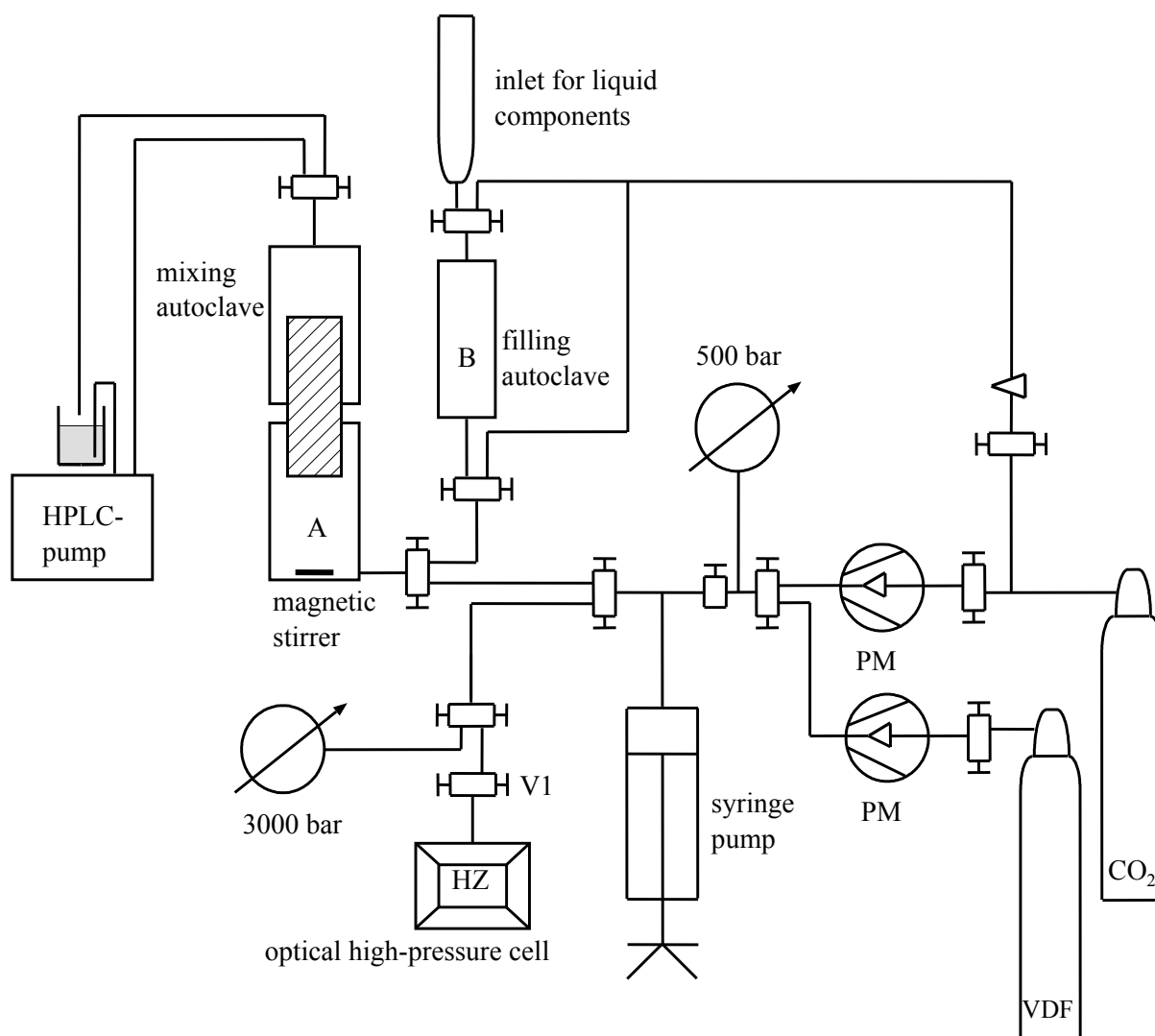


Figure. 4.2: Experimental apparatus: inlet for liquid components, filling autoclave (B), mixing autoclave (A), cylinder with CO₂, cylinder with monomer (VDF), manual syringe pump, magnetic stirrer, high-pressure cell (HZ), two ways valve (V1), pump for compression of gas (PM), HPLC pump.

4.1.4 High pressure mixing autoclave

Figure 4.3 gives the schematic diagram of the mixing autoclave, which allows for the production of the reaction mixture containing CO₂, vinylidene fluoride, initiator and chain transfer agent. The amount of the reaction mixture is sufficient for up to two experiments. At

the base of the autoclave a magnetic stirrer bar is placed, which allows the stirring of the reaction mixture. The mixture pressure is 500 bar and volume 100 cm³. The high pressure autoclave was fabricated in the workshop of the Institute of Physical Chemistry, Georg-August University Göttingen. The variation of the volume is achieved by a HPLC pump. A packing fits the moving piston against the base of autoclave. The base of the autoclave is fitted with the other part of the autoclave by a Teflon ring to avoid any leakage. A boring going from the side to the base into the centre serves as inlet and outlet. On the outside the autoclave is a cooling mantle, which allows for cooling of the reaction mixture to 0°C using a Kryostat. Thereby, polymerization inside the autoclave is avoided and the reaction mixture may be kept in the autoclave for up to 40 hours.

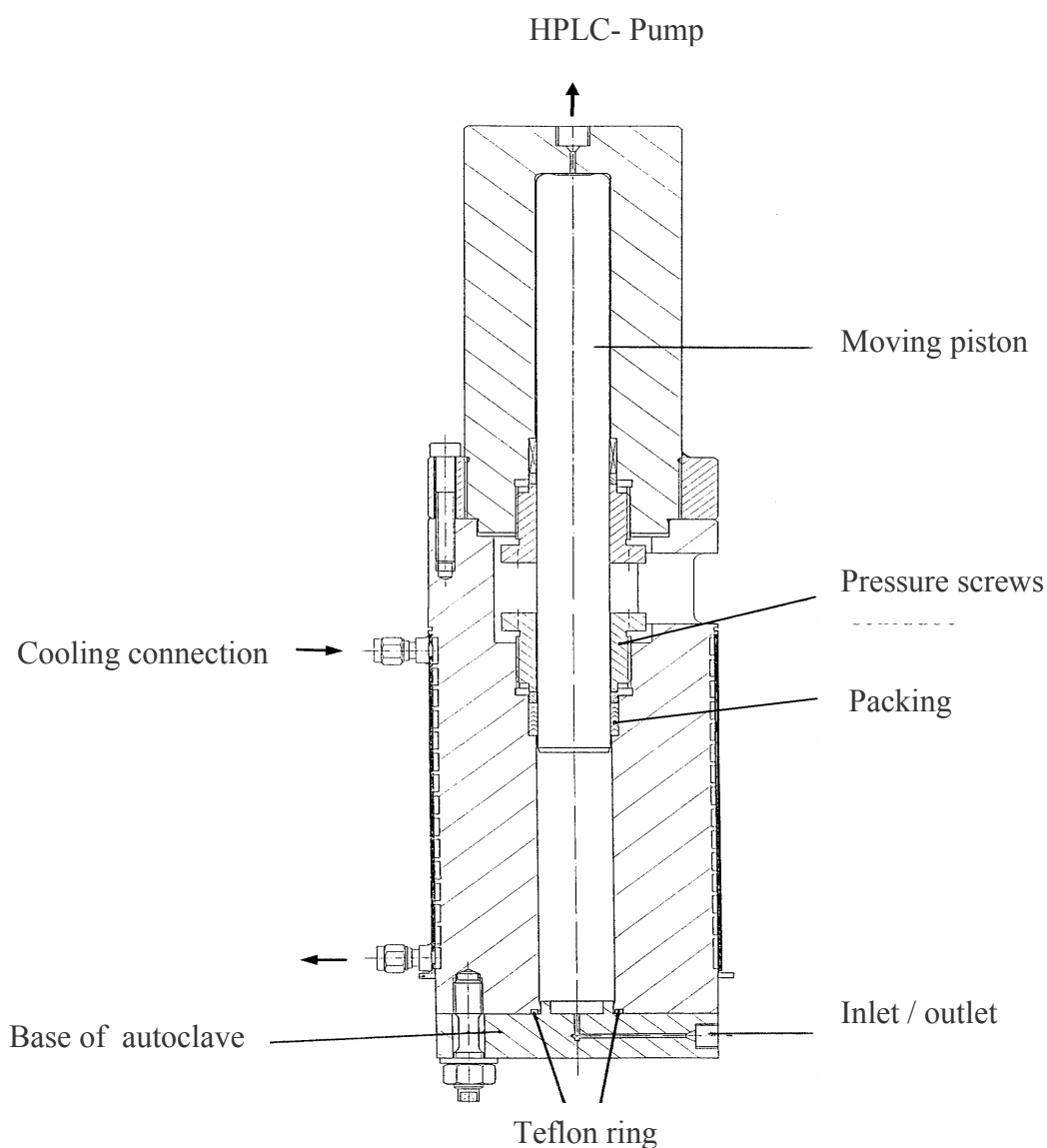


Figure 4.3: High pressure mixing autoclave

4.1.5 FT-IR/NIR spectrometer

Infrared and near infrared spectra were recorded either on a Bruker IFS-88 Fourier-Transform spectrometer or on a Bruker Vertex 70 FT-NIR spectrometer. To accommodate the heated optical high-pressure cell, the sample chamber of the spectrometer is enlarged (heightened) and fitted with a water-cooled cell holder (to prevent heat transfer). The chamber is purged with compressed air that has been freed from water and carbon dioxide.

The optical configuration of the present work consisted of a halogen source, a silicon-coated calcium fluoride beam splitter, and an InSb detector. This configuration allows for optimal recording in the spectral range of 4000 to 10000 cm^{-1} . The spectra were measured with a resolution of 2 cm^{-1} and a zerofilling factor of 2. Data acquisition and data processing were performed using the Opus software.

4.1.6 Phase behaviour set-up and measurements

Cloud point pressures were measured on a set-up consisting of a variable volume cell with a moving piston, which allows for changing the system pressure without modification of the composition of the system under investigation. The cell is equipped with a sapphire window to monitor the phase behaviour inside the cell with a video camera. The camera and a lamp are mounted on a boroscope, which may be placed directly in front of the sapphire window. A detailed description of the set-up used was given by Buback et al.⁶⁶

4.1.7 RESS set-up

Figure 4.4 gives a schematic diagram of the experimental apparatus used for RESS experiments. The apparatus consists of an extraction unit connected with a capillary nozzle, enabling experiments in the temperature range of 0 to 100 °C, and pressures up to 250 bars. For expansion of the polymer + CO₂ mixture the expansion chamber is connected through a nozzle. The bypass section was closed, supercritical CO₂ flew through the extractor and become enriched with the polymer. The scCO₂ + polymer mixture in the tubing leading to the nozzle was heated to the desired pre-expansion temperature using cable heaters. The mixture was expanded through the nozzle. The RESS experiments were carried out in collaboration with the research group of Prof. M. Türk at the University of Karlsruhe (TH). A detailed description of the set-up is given in ref. 67.

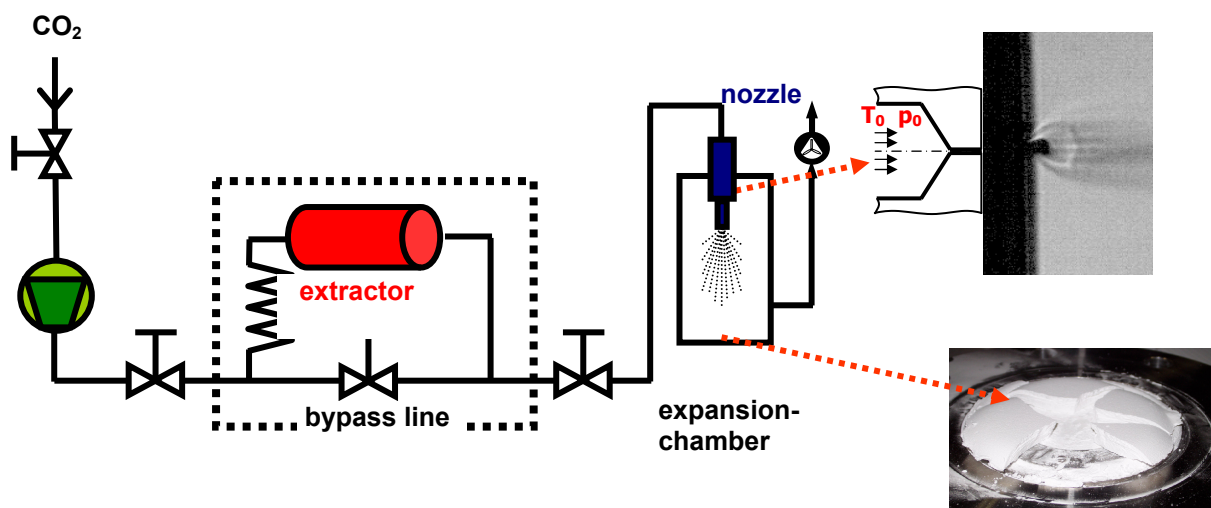


Figure 4.4: Schematic of the RESS apparatus.

4.2 Characterization techniques

4.2.1 Size-Exclusion Chromatography (SEC)

Size-exclusion chromatography (SEC) of the polymers was carried out with *N,N*-dimethylacetamide (DMAc) containing 0.1 % LiBr as eluent and a column temperature of 45°C. The flow rate of the eluent was 1.0 ml/min. The samples were analyzed on a SEC set-up consisting of an Agilent 1200 isocratic pump, an Agilent 1200 refractive index detector, and two GRAM columns (10 μ m, 8x300mm, pore sizes 100 and 1000) from Polymer Standards Services. The SEC set-up was calibrated using low polydispersity polystyrene standards (PSS), since PVDF standards were not available.

4.2.2 Nuclear Magnetic Resonance

Nuclear magnetic resonance spectra were acquired with a NMR spectrometer (Bruker 300 MHz). The spectra were measured using DMSO-*d*₆ and acetone-*d*₆ as solvent at room temperature.

4.2.3 ESI-MS Spectrometer

ESI-MS (electrospray ionization mass spectrometry) was performed to analyze the polymer end groups. The ESI spectra were recorded using a Q-TOF micro mass spectrometer (Micromass Manchester, UK) in the positive ion mode. All samples were injected (20 mL·min⁻¹) using a Harvard syringe pump. The capillary voltage was set to 2.7 kV and the

cone voltage within the range of 25 V. The source temperature was 80°C and the desolation temperature 150°C. The ESI mass spectra were measured for PVDF in CHCl₃ with traces of CH₃OH.

4.2.4 Scanning Electron Microscopy (SEM)

SEM images were recorded using Field Emission Scanning Electron Microscope (Hitachi S-4800) at accelerating voltage of 2.0 kV. The polymer sample was placed on to a sample holder (from Hitachi SEM) sputtered with gold/palladium in a sputter coater SCO 050 from Balzers.

4.2.5 Atomic Force Microscopy (AFM)

AFM measurements were performed in air at room temperature using a Nanoscope III Multimode AFM (digital Veeco Instruments Inc., Woodbury, USA) operating in tapping mode. Silicon tips with a resonance frequency of 285 kHz and a force constant of 42 N/m were obtained from NanoWorld AG (Neuchatel, Switzerland). The measurements as well as the following image editing were conducted with the Nanoscope 5.12r3 software. The PVDF films were prepared on silica using DMSO as solvent at room temperature.

4.2.6 Wide Angle X-ray Diffraction (WAXD)

The WAXD patterns of PVDF specimens were analyzed using a X-ray diffractometer (D8 X-ray diffractometer, Bruker AXS, Meadowside, UK) with a wavelength of 1.542 Å as X-ray source. The XRD spectra were measured at room temperature from 10 to 50 (2θ) with a step size of 0.028.

4.2.7 Differential Scanning Calorimetry (DSC)

Differential Scanning Calorimetry (DSC 2010, TA Instruments) was used to measure melting temperatures and melting enthalpies of the PVDF samples. For each sample 3 heating – cooling cycles were measured. For the determination of the degree of crystallinity the DSC data recorded during the third cycle was analyzed. The temperature was varied from 0 to 200 °C with a heating rate of 10°C per minute.

4.2.8 Spectroscopic observations (FT-NIR)

Figure 4.5 shows typical NIR spectra of vinylidene fluoride (dotted line) and of CO₂ (solid line) at 120°C, 200 and 1200 bar. The VDF spectrum was measured at 200 bar to reduce intensity and to allow for the presentation of both spectra in one Figure. The two small peaks

at 6214 and 6332 cm^{-1} refer to the absorbances of CO_2 and are unchanged. The spectrum of CO_2 also exhibits two prominent peaks at around 5087 cm^{-1} and 4959 cm^{-1} . The VDF spectrum shows distinct peaks between 6000 and 6350 cm^{-1} referring to the CH-stretching vibration at the double bond. The peak at 6303 cm^{-1} is used for quantitative analysis and the monomer conversion “ x ” is obtained from the ratio of peak integrals using Equation 4.1.

$$x = 1 - \frac{Int(t)}{Int(t=0)} \quad (4.1)$$

$Int(t=0)$ and $Int(t)$ are the integrals at time zero and at time t , respectively

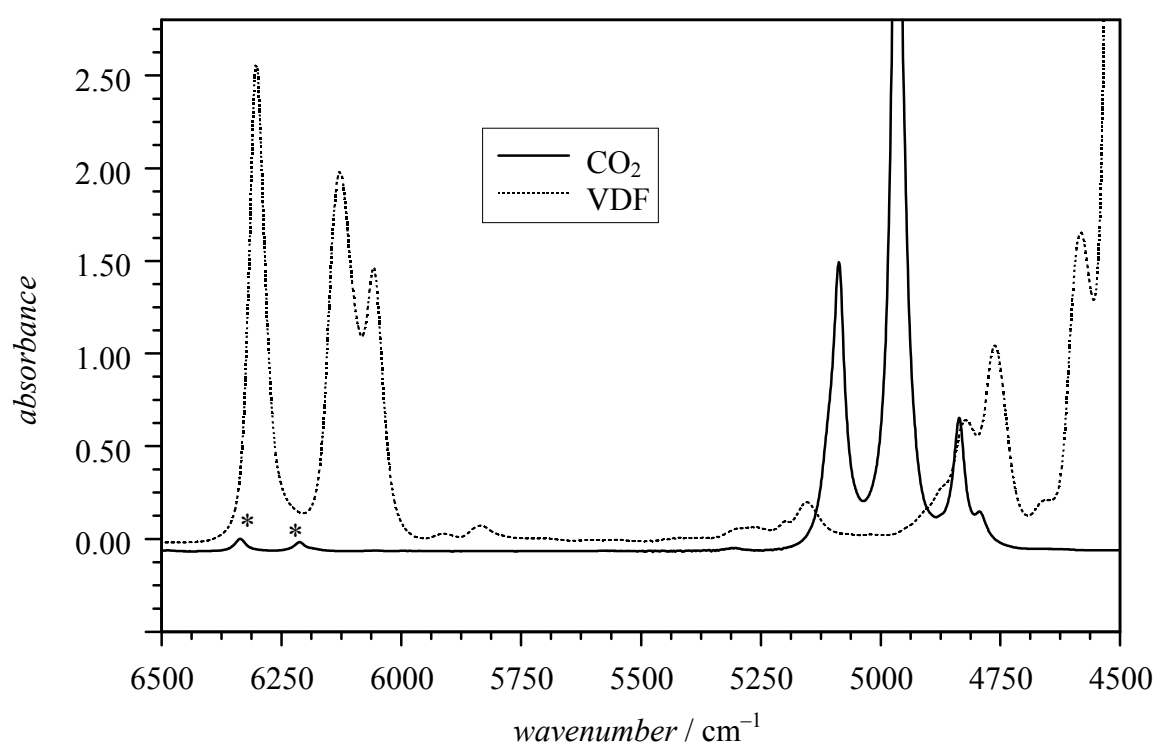


Figure 4.5: NIR spectra of vinylidene fluoride (dotted line) at 200 bar and CO_2 (solid line) at 1200 bar and 120°C (optical path length of 15 mm).

5. Experimental Part

5.1 Materials used

Monomer $\text{H}_2\text{C} = \text{CF}_2$

The monomer vinylidene fluoride (VDF, 99 % provided by Solvay S.A., Tavaux, France) was used in polymerization as received.

Carbon dioxide $\text{O}=\text{C}=\text{O}$

CO_2 (grade 4.5, Messer Griesheim, Krefeld, F.R.G) was used without further purification as solvent.

Initiator $(\text{H}_3\text{C})_3\text{C}-\text{O}-\text{O}-\text{C}(\text{CH}_3)_3$

Di-*tert*- butyl peroxide (DTBP, 99 % kindly provided by AKZO Nobel) was used as received as initiator.

Chain transfer agents

The following chain transfer agents (CTAs) of type $\text{CF}_3-(\text{CF}_2)_5-\text{Z}$ were used:

Z	Name	Abbreviation	Purity (%)	Company
I	Pefluorinated hexyl iodide	PFHI	-----	Dyneon
Br	Pefluorinated hexyl bromide	PFBH	98%	FluoroChem
H	1H- Perfluorohexane	HPFH	-----	Dyneon

In addition, the chain transfer agent bromotrichloromethane (BrCCl_3 , 99 % Acros, Germany) was used in this work. All chain transfer agents were used as received.

Other materials

Dimethyl formide DMF (99%, Carl Roth), Diethyl ether (99% Carl Roth), Sodium azide (99%, Sigma-aldrich), Dimethyl acetamide DMAc (99%, Carl Roth), Lithium bromide LiBr (99%, Carl Roth) and 2-butyne (98%, Alfa Aesar) were used as received.

5.2 Experimental procedures

5.2.1 Procedure for phase behaviour experiments

For measurement of the phase behaviour, polymer was weighed and placed into a high pressure cell. An amount of CO₂ required for the experiment was condensed in a cold (−10°C) small autoclave. After filling with CO₂ this small autoclave is connected with the high-pressure cell through a capillary connection. The temperature of the autoclave was slowly increased to transfer CO₂ into the cell. The difference in the weight of the autoclave shows the amount of CO₂ filled into the cell. The mixture in the high-pressure cell was stirred and heated to the experimental temperature. The system was pressurized until a single homogeneous phase was obtained. The temperature was kept constant for 15 minutes to establish stationary conditions. Then pressure was slowly lowered to the cloud point. To repeat the measurements the pressure was increased until a single phase was observed. Then, another temperature was chosen and phase behaviour measurements were repeated at the new temperature. After finishing the measurements, the pressure was lowered and the cell was cooled down to room temperature. CO₂ was removed by opening the valve of the cell and the cell was cleaned⁶⁸. For further details see ref. 66.

5.2.2 VDF polymerization in scCO₂

Figure 4.2 gives a schematic diagram of the experimental apparatus used to prepare the reaction mixture. The initiator was filled into the inlet for liquid components. Then, the initiator was transferred into the mixing autoclave (A). The monomer VDF was compressed and pumped by the pneumatically driven pump (PM). The volume of VDF added to autoclave (A) was controlled by the syringe pump. Accordingly, CO₂ was compressed and pumped by the second PM. Again, the amount of CO₂ added to the autoclave (A) was controlled by the syringe pump. The mixture consisting of initiator, CO₂ and VDF inside autoclave (A) was stirred with a magnetic stir bar for one hour at a pressure of 350 bar to ensure homogeneous mixing of the components. To prevent polymerization, autoclave (A) was cooled to 0°C. Then, the mixture was transferred to the syringe pump and the pre-heated optical high-pressure cell (HZ) equipped with two sapphire windows. To avoid demixing during the filling procedure the pressure was kept constant by the HPLC pump, which moves the piston of the mixing autoclave A (dashed in Figure 4.2) and thus keeping the pressure constant. The final pressure inside the optical cell was adjusted with the syringe pump. Then, the cell was disconnected from the pressure branch and inserted into the sample compartment of the FT-

NIR spectrometer. A detailed description of the set-up and the high-pressure cell used was given elsewhere.^{6,65,69} Pressure was measured using a pressure gauge from HBM (P3MB).

5.2.3 VDF polymerization using chain transfer agents

The same setup was used with little modification. The initiator along with CTA was filled into the inlet for liquid components and by passing CO₂ through the initiator, CTA mixture dissolved O₂ in the initiator was removed. Then, the initiator-CTA mixture was transferred into the mixing autoclave (A). The monomer VDF was compressed and pumped by the pneumatically driven pump (PM). The volume of VDF added to A was controlled by the syringe pump. Accordingly, CO₂ was compressed and pumped by a second PM. Again, the amount of CO₂ added to the autoclave A was controlled by the syringe pump. The mixture consisting of initiator, CTA, CO₂ and VDF inside autoclave A was stirred with a magnetic stirrer bar for one hour at the pressure of 350 bar to ensure homogeneous mixing of the components. To prevent polymerization, autoclave A was cooled to 0°C. Then, the mixture was transferred to the syringe pump and the pre-heated optical high-pressure cell (HZ) equipped with two sapphire windows. To avoid demixing during the filling procedure the pressure was kept constant by the HPLC pump, which moves the piston of the mixing autoclave A (dashed in Figure 4.2) and thus keeping the pressure constant. The final pressure inside the optical cell was adjusted with the syringe pump. In contrast to the above described procedure the cell was directly placed in the sample compartment of the FT-NIR spectrometer and filled. This approach minimizes the time lap which occurred in the above given case of disconnecting the cell and subsequent placement in the sample compartment of the spectrometer.⁷⁰ Pressure was measured using a pressure gauge from HBM (P3MB).

5.2.4 End – functionalization of PVDF-I by click reaction

PVDF synthesized using pefluorinated hexyl iodide as chain transfer agent ($M_n=2040 \text{ g}\cdot\text{mol}^{-1}$, 200 mg, 0.10 mmol), sodium azide (200 mg, 3.07 mmol), symmetrically alkyl substituted alkyne (2-butyne, 0.5 ml, 6.4 mmol), 15 ml of DMF were added in a flask. The flask was connected with a reflux condenser and the reaction mixture was stirred for 72 hours at a temperature of 90°C. As the reaction proceeds the colour of the solution changes from transparent to brown, because of elimination of iodine. Functionalized poly(vinylidene fluoride) was precipitated in water, filtered and washed with diethyl ether to remove the unreacted organic reactants and side products. The final product was dried under vacuum.

5.2.5 Experimental procedure for RESS process

The RESS process involves two steps and two units: the first one for dissolution of the polymer, and the second one for expansion, particle formation and collection. A schematic flow sheet of the RESS set-up is shown in Figure 4.4. In the first step, the polymer and the glass beads were mixed to prevent solute caking and added to the extractor. To minimize the unsteadiness of the flow and to accelerate thermal equilibrium, pure CO₂ flows through the thermostated bypass section into the thermostated high-pressure vessel and is expanded through a heatable capillary nozzle (50 μm inner diameter, length/diameter = 10) into the expansion chamber. In order to prevent cavitation in the pump the fluid was first cooled in a chiller. After equilibrium conditions (as indicated by constant pressure and temperature) were obtained, the bypass section was closed and supercritical CO₂ was allowed to flow through the extractor and to become enriched with the polymer. The experiments were performed at the temperature range of 0 to 100 °C and pressures up to 200 bars. The scCO₂ + polymer mixture in the tubing leading to the nozzle was heated to the desired pre-expansion temperature using cable heaters. The mixture was expanded through the nozzle heated at the pre-expansion temperature (T_0) into the expansion chamber ($V = 2.6 \text{ dm}^3$) at ambient conditions. Samples were collected onto SEM stages located on the sampling device. The average particle size and particle size distribution (PSD) were statistically determined from SEM images using image analysis (Image J Version 1.38). As a rule, about 600 particle diameters were considered in each PSD calculation.

6. Results and Discussion

6.1 Polymerization in homogeneous phase

It is interesting to study whether VDF may be polymerized in homogeneous phase at least to some extent. It was expected that unreacted VDF monomer may serve as a cosolvent. Phase behaviour data for the ternary system consisting of PVDF, VDF and CO₂ are not yet available. Since homogeneity is promoted by low polymer molecular weights,¹⁸ focus was on PVDF with M_n being below 10000 g·mol⁻¹. Besides being favourable with respect to the phase behaviour, rather low molecular weight polymers are interesting from a technical point of view, because, e.g., polymers applied in coatings are frequently of rather low MW.

This part (6.1) of the chapter 6 describes VDF polymerizations in scCO₂, initiated by conventional organic peroxide: di-*tert*-butyl peroxide, DTBP. This initiator was chosen because of its high efficiency,⁷¹ the decomposition kinetics⁷² in fluid phase polymerizations are known and its SADT (self accelerating decomposition temperature) is high.⁷³ Polymer molecular weights were controlled by the initiation rate.

6.1.1 Phase behaviour analysis

Phase behaviour of PVDF - scCO₂ systems

It was anticipated that PVDF should be soluble in VDF/scCO₂ mixtures or scCO₂ to some extent, which should allow for homogeneous phase polymerization of VDF at least up to intermediate monomer conversions. Since VDF polymerizations are highly exothermic⁷⁴ it was expected that high CO₂ contents would be required to allow for an isothermal reaction, if molecular weights should be controlled by the initiation rate. To estimate at which conditions polymerizations may be carried out in homogeneous phase the phase behaviour for a binary system consisting of CO₂ and low molecular weight PVDF ($M_n = 3000$ g·mol⁻¹, PDI = 3.65) was studied. First, 7 wt % PVDF was placed in the view cell. Then, CO₂ was added to the polymer. Figure 6.1.1a shows the polymer inside the cell at ambient conditions. Using a syringe pump the system volume was gradually decreased and as a consequence pressure was increased up to a value of 1000 bar. Figure 6.1.1b shows that a heterogeneous system is obtained. The cell was heated to 140 °C and equilibrated for 5 minutes. Then, pressure was further enhanced up to a value at which the system becomes homogeneous. Figure 6.1.1c indicates that a single phase is obtained at 140 °C and 1500 bar. To determine the cloud point pressure at which the system turns heterogeneous, the pressure was slowly decreased. At 1413

bar a phase transition for the mixture of PVDF and CO₂ is observed (see Figure 6.1.1d). Thus, the pressure of 1500 bar should be suitable for homogeneous phase polymerization of VDF.

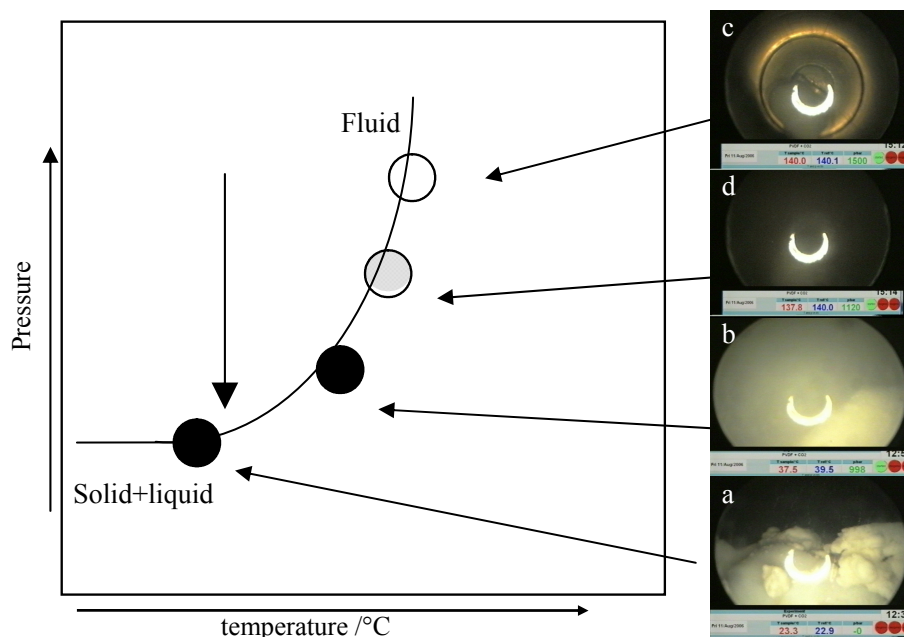


Figure 6.1.1: Typical experiment for measuring a cloud point. (a): polymer loaded to the cell at ambient conditions, (b): system is pressurized to 1000 bar; (c): system is pressurized up to 1500 bar until it becomes a single phase (d) system after lowering the pressure to 1413 bar.

6.1.2 FT-NIR Spectroscopic Observations

Based on the phase behaviour measurements polymerizations were carried out at 140°C and 1500 bar in an optical high-pressure cell equipped with two sapphire windows to monitor the variation of monomer concentration with time via quantitative near-infrared (NIR) spectroscopy in the region of the first overtones of the C-H stretching modes between 5600 and 6400 cm⁻¹. Additionally, in-line monitoring of the reaction mixture using NIR spectroscopy allows for checking the homogeneity during the course of the polymerization. Inhomogeneity is clearly indicated by a shift of the baseline toward higher absorbance resulting from increased scattering of the NIR light.¹¹ The optical cell also allows for visual inspection of the reaction volume and detection of inhomogeneities.

Figure 6.1.2 exhibits a spectral series recorded during a VDF polymerization using perfluorinated hexyl iodide as chain transfer agent. The absorbance band with the peak maximum at around 6303 cm⁻¹ is essentially due to the CH-stretching vibration at the C=C

double bond of VDF. The arrow in Figure 6.1.2 indicates the change in absorbance with time. The series of spectra in Figure 6.1.2 covers a time range of about 100 min. In the last spectrum no absorption is seen at 6303 cm^{-1} , showing that complete monomer conversion has reached. The two peaks at 6214 and 6332 cm^{-1} are due to the presence of CO_2 , as indicated by the asterisk in Figure 6.1.2. The pure CO_2 spectrum recorded at the pressure of 1200 bar and 120°C is given in Figure 4.5 (see chapter 4). At this high pressure and in the spectral range of interest the difference in temperature and pressure at which the CO_2 spectrum was recorded and the polymerization was carried out has only a minor influence on the CO_2 spectrum.

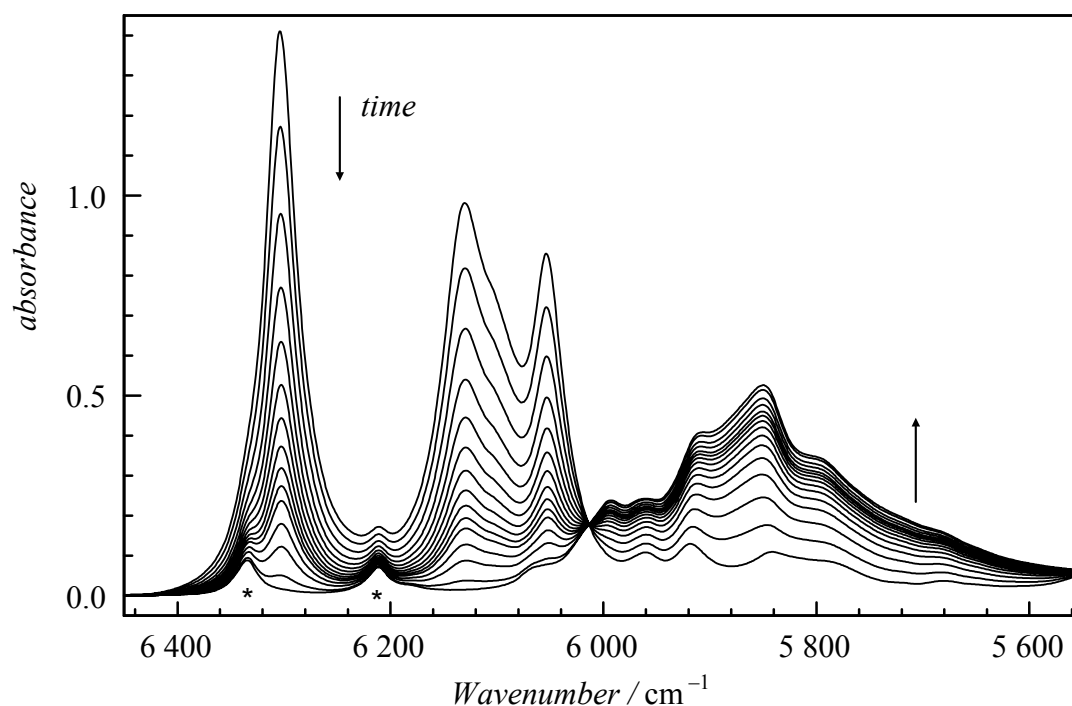


Figure 6.1.2: NIR spectral series recorded during a VDF polymerization in the presence of 73 wt.% CO_2 at 120°C and 1500 bar. The initial monomer concentration was $3.66\text{ mol}\cdot\text{L}^{-1}$, $c_{\text{DTBP}} = 0.061\text{ mol}\cdot\text{L}^{-1}$, $c_{\text{CTA}} = 0.25\text{ mol}\cdot\text{L}^{-1}$; optical path length 15 mm; final monomer conversion 98 %. * indicate absorbances due to CO_2 .

It has become standard practice⁷⁵⁻⁷⁷ to use the first overtone of the C-H stretching vibration for quantitative analysis of monomer conversion, which is calculated by integration of the peak at 6303 cm^{-1} over the high wavenumber half-band from the band maximum toward higher wavenumbers against a horizontal baseline determined by the absorbance at 6450 cm^{-1} .

6.1.3 MW control via initiation

To allow for homogeneous phase polymerizations experimental conditions were chosen to obtain low molecular weight material. To avoid the use of chain transfer agent molecular weights were controlled by the initiation rate. The influence of the DTBP concentration, c_{DTBP} , on polymer molecular weight was studied for polymerizations at 140 °C and 1500 bar with an initial VDF concentration of 3.47 mol·L⁻¹. The CO₂ content was 77 wt.%. DTBP concentrations were between 0.026 and 0.307 mol·L⁻¹. With the exception of the lowest c_{DTBP} in all cases the polymerization proceeded up to high degrees of monomer conversion in homogeneous phase.

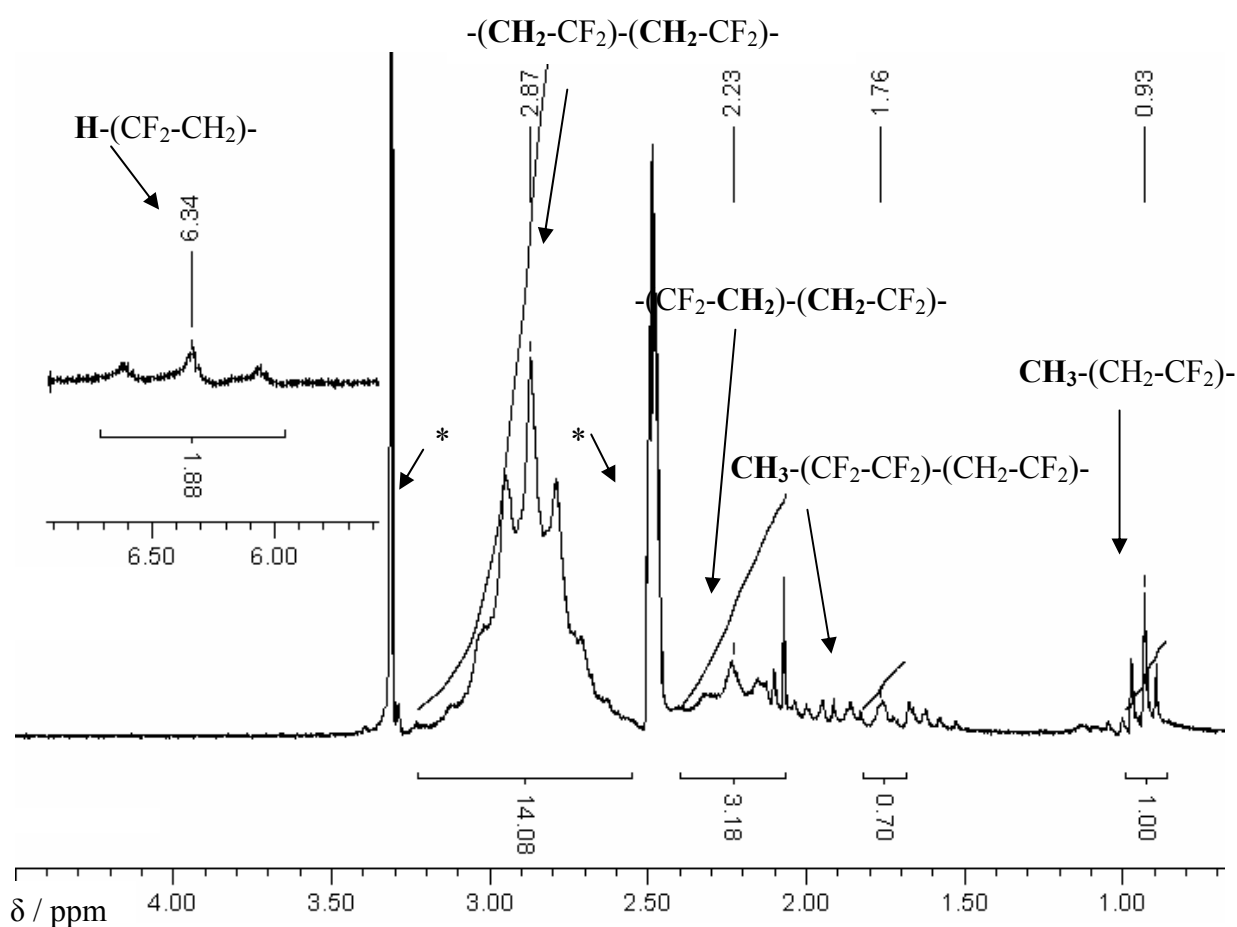


Figure 6.1.3: ¹H-NMR spectra of PVDF homopolymer initiated by DTBP at 140 °C and 1500 bar in scCO₂. * indicate peaks originating from DMSO-*d*₆.

The number average molecular weight, M_n , was calculated from ¹H-NMR spectra (Figure 6.1.3) using the following expression (1):

$$M_n = \frac{I(\text{CH}_2)/2}{(I(\text{CH}_3)/3)/2} \times M_{\text{VDF}} \quad (1)$$

Where $I(\text{CH}_2)$ is the integral of the CH_2 group of polymer and $I(\text{CH}_3)$ the integral of the CH_3 group of the initiator-derived end group and M_{VDF} molecular weight of VDF. The formula is based on termination via combination. A typical $^1\text{H-NMR}$ spectrum is shown in Figure 6.1.3. The peak assignment is given according to ref. 78. All the $^1\text{H-NMR}$ spectra show the presence of the characteristic multiplet centered at 2.87 ppm assigned to methylene groups of $-\text{CF}_2\text{CH}_2-\text{CF}_2\text{CH}_2-\text{CF}_2\text{CH}_2-$ sequence resulting from the normal tail-to-head VDF addition. The peaks at 1.76 ppm and 2.23 ppm are assigned to the $\text{CH}_3-(\text{CF}_2-\text{CF}_2)-(\text{CH}_2-\text{CF}_2)-$ and $(\text{CF}_2-\text{CH}_2)-(\text{CH}_2-\text{CF}_2)-$ groups. The $^1\text{H NMR}$ spectrum shows a triplet centered at 0.93 ppm assigned to the CH_3 end group. In addition, the $^1\text{H-NMR}$ spectrum shows a triplet ($^2J_{\text{HF}} = 55.2$ Hz) of triplets ($^3J_{\text{HH}} = 4.4$ Hz) centred at 6.30 ppm attributed to the terminal proton in the $-\text{CH}_2\text{CF}_2\text{H}$ end group arising from transfer to the polymer, as observed by various research groups.⁷⁹⁻⁸¹

M_n values calculated according to expression (1) are listed in Table 6.1.1. As expected, the molecular weights are decreasing with increasing c_{DTBP} . For 0.077 and 0.307 $\text{mol}\cdot\text{L}^{-1}$ DTBP M_n of 7700 and 2700 $\text{g}\cdot\text{mol}^{-1}$, respectively, were obtained. The value for the lowest DTBP concentration is significantly higher. Since the polymerization mixture turned heterogeneous, the numbers in Table 6.1.1 referring to this experiment is given in italics. SEC analyses were carried out to derive molecular weight distributions (MWDs) and associated polydispersities, PDI . The M_n values obtained are also contained in Table 6.1.1 and for comparison the values are plotted as a function of DTBP concentration in Figure 6.1.4. It is evident that the variation of M_n with c_{DTBP} is very similar for both types of analyses. M_n values from NMR are generally higher than the values from SEC. The reason for this deviation may be seen in the SEC calibration with polystyrene standards, due to the lack of PVDF standards.

Entry	p/bar	$[\text{DTBP}]/\text{mol}\cdot\text{L}^{-1}$	$M_n(\text{NMR})/\text{g}\cdot\text{mol}^{-1}$	$M_n(\text{SEC})/\text{g}\cdot\text{mol}^{-1}$	PDI	Phase behaviour
<i>1</i>	<i>1500</i>	<i>0.026</i>	<i>19200</i>	<i>17600</i>	<i>2.3</i>	<i>Heterogeneous</i>
2	1500	0.077	7700	6800	3.1	Homogeneous
3	1500	0.131	5100	4600	3.9	Homogeneous
4	1500	0.181	4200	3000	3.7	Homogeneous
5	1500	0.230	3100	2500	3.7	Homogeneous
6	1500	0.307	2700	2200	4.5	Homogeneous

Table 6.1.1: Experimental details for the variation of initiator concentration in VDF polymerizations in 77 wt.% CO_2 at 140 °C and 1500 bar, 3.47 $\text{mol}\cdot\text{L}^{-1}$ of VDF.

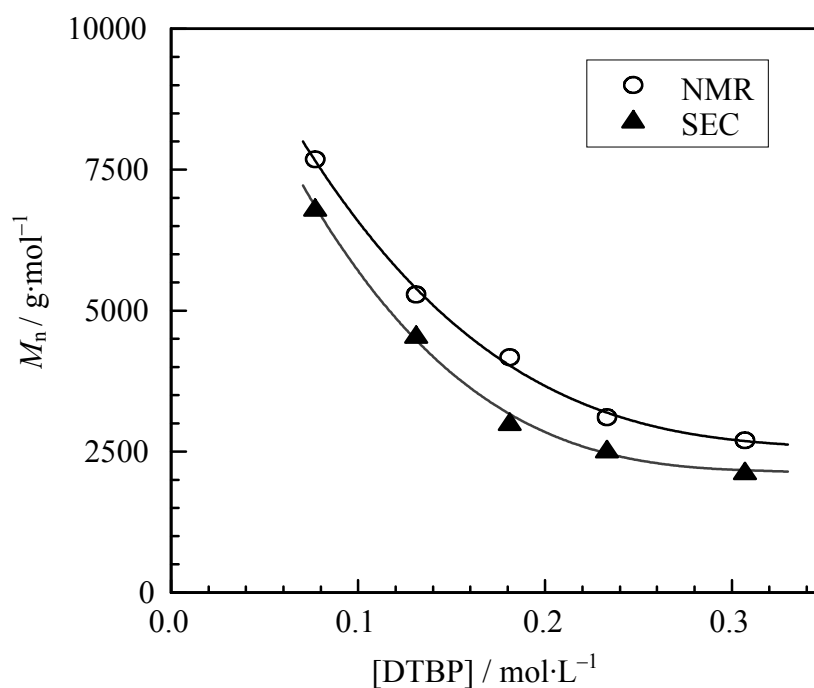


Figure 6.1.4: Variation of M_n with initiator concentration for VDF polymerizations at 140 °C and 1500 bar with 3.47 mol·L⁻¹ of VDF.

The polydispersities listed in Table 6.1.1 indicate that broad molecular weight distributions were obtained in all cases. For example, Figure 6.1.5 gives the MWD for PVDF from polymerization with 0.077 mol·L⁻¹ DTBP, the lowest initiator concentration allowing the reaction in homogeneous phase. PDI values increase from 3.1 at 0.077 mol·L⁻¹ DTBP to a maximum value of 4.5 at the highest DTBP concentration. In principle, high polydispersities could be due to depropagation at the high temperatures of the experiment. However, since almost complete monomer conversion is reached contributions from depropagation should be negligible. Thus, high polydispersity values may be caused by chain transfer to polymer resulting in branched material.⁷⁹⁻⁸¹

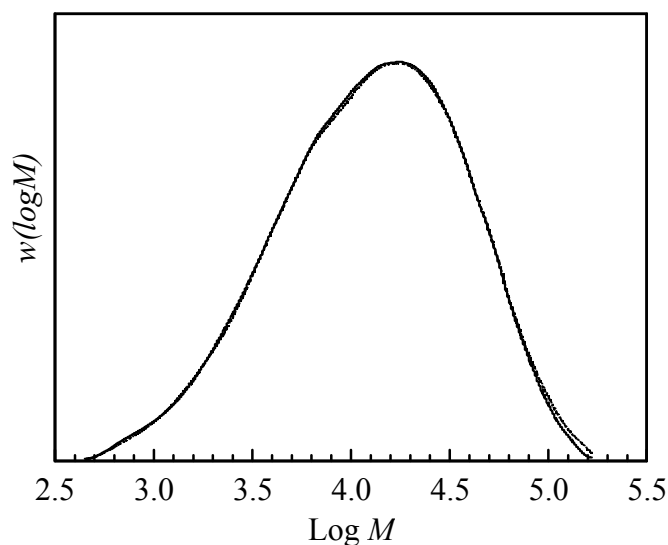


Figure 6.1.5: MWD of PVDF polymerized at 140 °C and 1500 bar with an initial VDF concentration of 3.47 mol·L⁻¹ and a DTBP concentration of 0.077 mol·L⁻¹.

6.1.4 Variation of monomer concentration

In a second set of experiments the VDF concentration, c_{VDF} , was varied from 6.18 to 2.88 mol·L⁻¹. These VDF concentrations are associated with 61 and 83 wt.% of CO₂, respectively. All other experimental conditions were held constant. The results are summarized in Table 6.1.2. Again, M_n values from SEC are in reasonable agreement with NMR-derived values. As expected M_n increases with enhanced monomer concentration. The polydispersities were becoming higher with increasing VDF concentration from 3.2 at 2.88 mol·L⁻¹ to 5.7 at 6.18 mol·L⁻¹. These rather high PDI values may be attractive for polymer processing, since they may contribute to improved flow characteristics and processing behaviour.⁸² It is remarkable to note that in all cases monomodal molecular weight distributions were obtained, in contrast to precipitation polymerizations carried out at high monomer concentrations, in which bimodal distributions were found.⁸³

Entry	[DTBP]/ mol·L ⁻¹	[VDF]/ mol·L ⁻¹	M_n (NMR)/ g·mol ⁻¹	M_n (SEC)/ g·mol ⁻¹	<i>PDI</i>
7	0.131	2.88	3000	4300	3.2
8	0.131	3.47	5100	4600	3.9
9	0.131	4.53	5300	5500	4.8
10	0.131	6.18	8300	9200	5.7

Table 6.1.2: Experimental details for VDF polymerizations at 140 °C and 1500 bar in solution with scCO₂ and varying VDF concentrations.

The results in Table 6.1.2 show that the PDI increases with the initial monomer concentration, at otherwise constant conditions. Previously, it was reported that the average number of branches per PVDF molecule increases with VDF concentration.⁸³ These findings compare reasonably well with the measurement of branch points on a VDF/ hexafluoropropylene/ tetrafluorethylene (72/18/10) copolymer synthesized at 85°C. Consideration of the terpolymer is relevant, since it primarily consists of VDF units. In addition, branching is unlikely to occur on hexafluoropropylene and tetrafluorethylene units, because there are no H atoms in either molecule.⁸³ Thus, the reason for high PDI values may be seen in branching, which becomes more likely as the concentration of monomer is increased. Depropagation is unlikely to be the origin of the high PDI values, because again high monomer conversions were obtained.

6.1.5 Microstructure of PVDF

PVDF is a semicrystalline polymer that is composed of mostly head-to-tail linkages (-CF₂- is denoted as “head” and -CH₂- as “tail”). Typical commercial polymers show 3-6 mol.% defects, which are formed by head-to-head or tail-to-tail linkages (head-head -CH₂-CF₂-CF₂-CH₂-; head-tail -CH₂-CF₂-CH₂-CF₂-; tail-tail -CF₂-CH₂-CH₂-CF₂-). It is believed that the extent of defects is mainly influenced by the polymerization temperature and initiator concentration.⁸⁴ Thus, it was tested whether the high-pressure and high-temperature conditions of this study influence the amount of defects in the polymer. Quantitative information on the occurrence of these defects is accessible from ¹⁹F-NMR and ¹H-NMR spectroscopy.⁷⁹⁻⁸¹ A ¹H-NMR spectrum of a polymer obtained at 140°C and 1500 bar was depicted in Figure 6.1.3. The normal to inversed addition ratio could be assessed from the integrals of the characteristic peaks occurring in ¹H-NMR spectra according to Equation (6.1).⁷⁸

$$F_{\text{PVDF}} = \frac{I_{2.9} + I_{2.2/2} + I_{0.93/3}}{2 \cdot I_{1.8/3} + I_{2.2} + I_{2.9}} = 0.937 \quad (6.1)$$

F_{PVDF} is the mole fraction of regular PVDF sequences and “ I ” represents the integral of the signal centered at different ppm, e.g., $I_{2.3/2}$ refers to the integral of the peak at 2.3 ppm, which corresponds to two protons. Equation (6.1) gives the sum of the integrals of the peaks assigned to normal VDF adducts over the sum of the integrals of the peaks belonging to VDF (normal and reversed monomer units). The signals attributed to the end group arising from the initiators are also considered in Equation (6.1).

According to Equation (6.1) the mole percentage of defects for the PVDF samples produced in scCO₂ is about 6.4 mol.%, which is within the reported range (6 mol.%) for PVDF produced by conventional aqueous methods. Thus, the high-temperature and high-pressure conditions of above experiments do not lead to additional defects in the microstructure of PVDF. This finding is important, since a large fraction of defect structures may lead to a lowering in thermal stability of the material.

6.1.6 Morphology of PVDF

Visual observation of PVDF samples after expansion to ambient pressure indicated that polymerizations carried out in the heterogeneous phase lead to large aggregates or coagulated material, whereas in the case of homogeneous phase reactions a fine powder was obtained. To obtain further information on the morphology, PVDF obtained from reactions in homogeneous phase and from reactions where the reaction mixture turned heterogeneous were subjected to SEM. The results are given in Figures 6.1.6 and 6.1.7. The images on the left refer to material from homogeneous phase polymerization, where the particles were formed during the expansion. The images on the right refer to polymer that precipitated during the polymerization. Thus, particle formation occurred already prior to expansion.

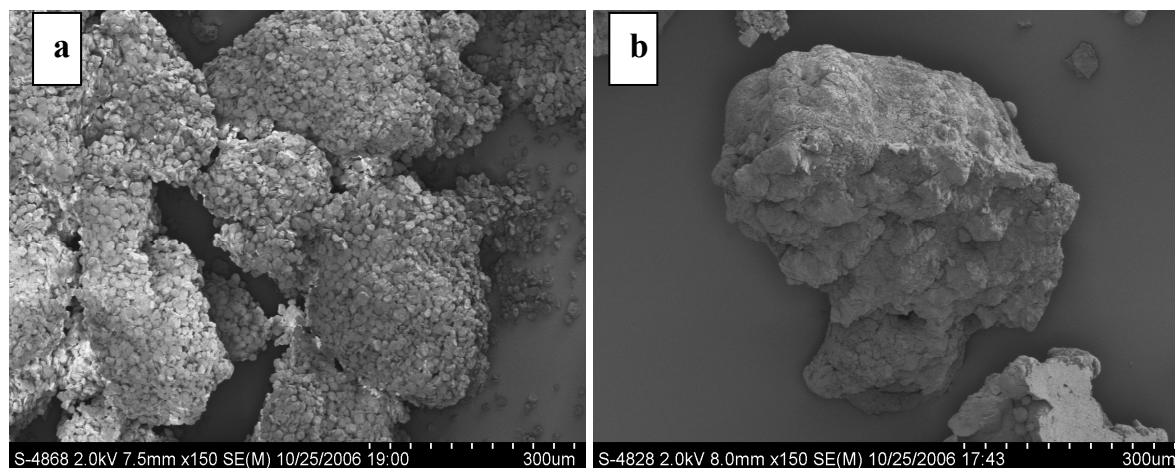


Figure 6.1.6: Low magnification SEM images of PVDF homopolymers. (a) PVDF polymerized in homogeneous phase at 140 °C, 1500 bar, 0.307 mol·L⁻¹ DTBP and 3.47 mol·L⁻¹ of VDF. (b) PVDF polymerized in heterogeneous phase at 140 °C, 1500 bar, 0.026 mol·L⁻¹ DTBP and 3.47 mol·L⁻¹ of VDF.

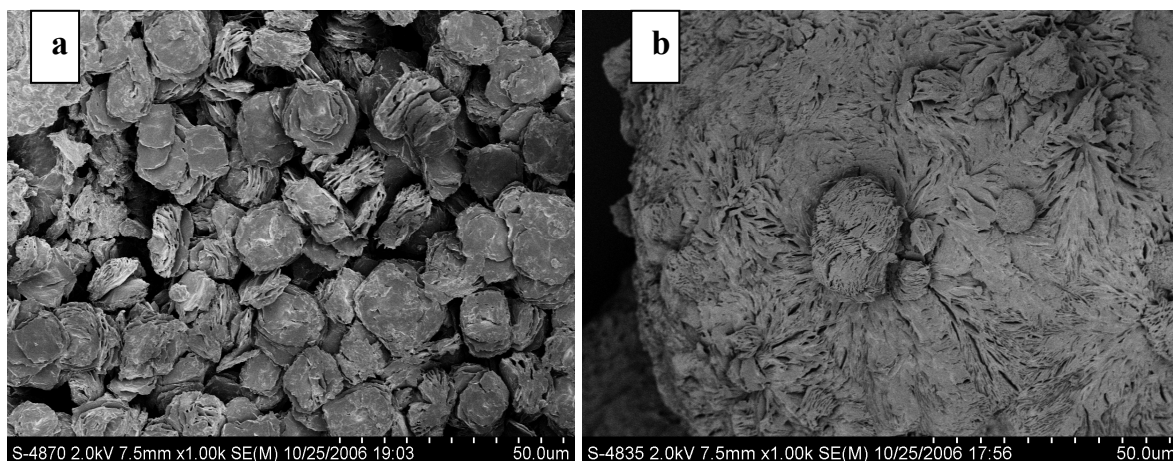


Figure 6.1.7: High magnification SEM images of PVDF homopolymer polymerized in scCO_2 . (a) PVDF polymerized in homogeneous phase at 140 °C, 1500 bar, $0.307 \text{ mol}\cdot\text{L}^{-1}$ DTBP and $3.47 \text{ mol}\cdot\text{L}^{-1}$ of VDF. (b) PVDF polymerized in heterogeneous phase at 140 °C, 1500 bar, $0.026 \text{ mol}\cdot\text{L}^{-1}$ DTBP and $3.47 \text{ mol}\cdot\text{L}^{-1}$ of VDF.

The SEM images of the PVDF material support the visual impression. In case of homogeneous phase reactions small lamellas were obtained, which formed small stacks of layered material. The size of these stacks is around $10 \mu\text{m}$ and the polydispersity is low. SEM images of PVDF with $M_n = 2000$ and with $M_n = 8000 \text{ g}\cdot\text{mol}^{-1}$ do not show significant differences. The stack-type particles formed larger aggregates. From precipitation polymerization only non-uniform coagulated material with very different particle sizes was collected.

The expansion of the homogeneous reaction mixture after the polymerization was finalized may be regarded as a non-optimized RESS (rapid expansion from supercritical solution) process.⁸⁵ In RESS processes particle formation occurs upon expansion of a homogeneous CO_2 -rich phase containing small amounts (up to a few wt.%) of a second component. Typically, selection of pre-expansion and expansion parameters allows for modification of the particle sizes and particle size distributions.⁸⁶ The details of the RESS process are given in chapter 6.6.

6.1.7 Summary of results

Although PVDF is a semicrystalline polymer its solubility in scCO_2 is sufficiently high to allow for homogeneous phase polymerization of VDF up to complete monomer conversion for CO_2 contents ranging from 61 to 83 wt.%. Polymer molecular weights were derived from $^1\text{H-NMR}$ and SEC. As expected, M_n is decreasing upon increasing DTBP concentration or

lowering VDF concentration. $^1\text{H-NMR}$ based M_n values for polymerizations in homogeneous phase range from 2700 to 7700 $\text{g}\cdot\text{mol}^{-1}$. For M_n of 19000 $\text{g}\cdot\text{mol}^{-1}$ the reaction mixture turned heterogeneous during the polymerization. Generally, large polydispersities ranging from 3.1 to 5.7 were obtained. The high-temperature, high-pressure and high DTBP concentration conditions applied did not alter the microstructure of PVDF: from $^1\text{H-NMR}$ spectrum was concluded that amount of structural defects is 6.4 mol %, which is close to the literature value of 6 mol %. SEM analyses showed that polymer obtained in a homogeneous phase reaction led to regular stack-type particles upon expansion, whereas expansion following a heterogeneous polymerization led to polymer particles with high polydispersity.

The present work indicated that VDF polymerizations may be carried out in an environmentally benign reaction medium up to complete monomer conversion in homogeneous phase in the absence of any fluorinated additives.

6.2 Molecular weight control via degenerative transfer using perfluorinated hexyl iodide (PFHI)

An attractive way of controlling MW is the application of living radical polymerizations. For fluorinated monomers degenerative transfer is particularly interesting.⁸⁷ Perfluorinated hexyl iodide (PFHI) is a very well suited CTA for VDF monomer and has been studied in using different fluorinated solvents in precipitation polymerization. It has been suggested that CO₂ either forms a weak complex with, or clusters near the fluorine atom of the C-F bond (because C-F is more polar than C-H), thereby enhancing the fluoropolymers solubility several fold in CO₂.⁸⁸ Thus, fluorinated chain transfer agents may not only control molecular weight, but may also improve the phase behaviour of the system. In chapter 6.2 it will be studied whether living conditions are accessible in scCO₂ using PFHI. In addition, it is important to determine up to which conversion livingness may be observed. Further, the polymerization kinetics will be investigated.

6.2.1 NIR spectroscopy and conversion

As pointed out in section 6.1.2, monomer concentrations may be obtained from FT-NIR spectra. After modification of the set-up the optical high pressure cell is filled directly in the spectrometer. Thus the entire reaction may be monitored. A typical 3D spectra series recorded. A typical 3D spectra series recorded during a VDF polymerization at 120 °C and 1500 bar with 73 wt.% CO₂, $c_{DTBP} = 0.061 \text{ mol}\cdot\text{L}^{-1}$ and $c_{CTA} = 0.25 \text{ mol}\cdot\text{L}^{-1}$ is shown in Figure 6.2.1. The peak at 6303 cm^{-1} is assigned to the C–H stretching vibration at the double bond. In the last spectrum no absorption is seen at 6303 cm^{-1} , showing that complete monomer conversion has reached. The reaction time was 100 min. The two small peaks at 6214 and 6332 cm^{-1} refer to the absorbances of CO₂ and are unchanged. The baselines of the spectrum were not corrected and, thus, indicate that the system was homogeneous throughout the entire polymerization.

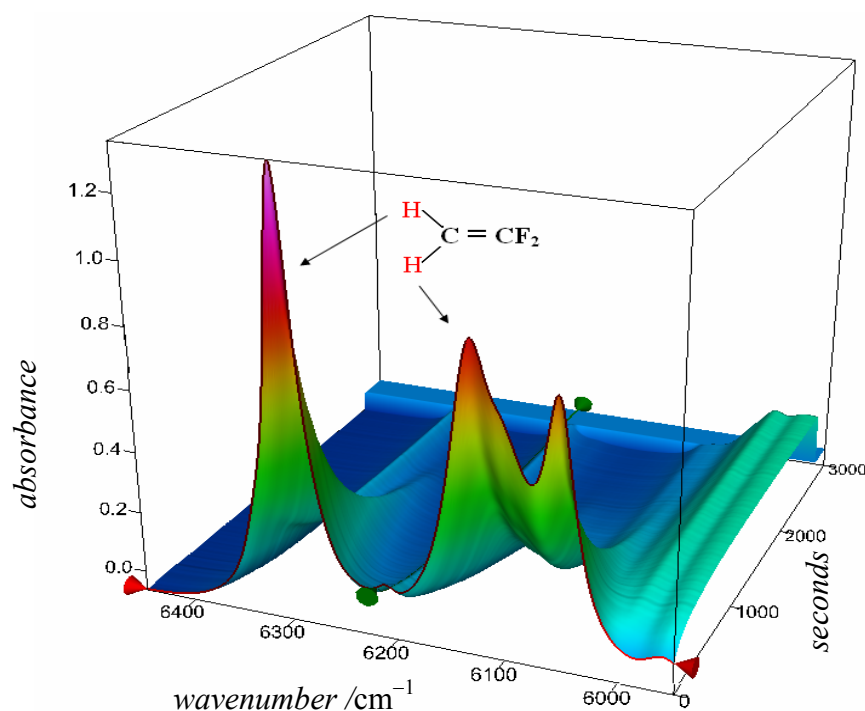


Figure 6.2.1: 3D NIR spectral series recorded during a VDF polymerization in the presence of 73 wt % CO₂ at 120 °C and 1500 bar. The initial concentrations were 3.66 mol·L⁻¹ VDF, 0.061 mol·L⁻¹ DTBP, 0.25 mol·L⁻¹ PFHI; optical path length 15 mm; final monomer conversion 98%.

6.2.2 Effect of perfluorinated hexyl iodide concentrations

Experiments were carried out to study the effect of perfluorinated hexyl iodide (PFHI) concentration on the rate of polymerization, average molecular weight and the MWDs. The results are summarized in Table 6.2.1.

No.	PFHI / (mol·L ⁻¹)	VDF / (mol·L ⁻¹)	M_n / (g·mol ⁻¹)	x (%)	PDI	r_p (40%) (mol·L ⁻¹ ·s ⁻¹)
1	0.07 ^(a)	3.66	3000	30	1.30
2	0.05	3.66	6700	90	1.51	2.72×10^{-3}
3	0.10	3.66	4000	96	1.49	4.02×10^{-3}
4	0.15	3.66	2500	>97	1.42	4.90×10^{-3}
5	0.20	3.66	1800	>97	1.23	6.33×10^{-3}
6	0.25	3.66	1600	>98	1.19	7.32×10^{-3}

Table 6.2.1: PFHI and VDF concentrations as well as product properties; number average molecular weight, M_n ; final conversion, x ; polydispersity index, PDI ; rate of

polymerization, r_p ; $0.061 \text{ mol}\cdot\text{L}^{-1}$ DTBP at 120°C , 1500 bar and CO_2 content of 73 wt %. (a) entry with out initiator. r_p refers to 40 % monomer conversion.

VDF polymerizations were carried out at 120°C and 1500 bar in the presence of $\text{C}_6\text{F}_{13}\text{I}$ concentrations ranging from 0.073 to $0.25 \text{ mol}\cdot\text{L}^{-1}$ in order to investigate the influence of chain transfer agent concentration (c_{CTA}) on molecular weight. The initial concentrations of monomer and DTBP were $3.66 \text{ mol}\cdot\text{L}^{-1}$ and $0.061 \text{ mol}\cdot\text{L}^{-1}$. The first entry in Table 6.2.1 indicates that polymerization performed without initiator and resulted polymer material. This observation shows that PFHI can take part in initiation step. The reaction in presence of PFHI remains homogeneous even at 120°C and it shows that PFHI not only control the molecular weight of the polymer but also improve the phase behaviour of the reaction. As the concentration of PFHI increased the monomer conversion up to 98 % in homogenous phase is possible. The low polydispersity value of 1.19 is the indication of living polymerization because conventional free radical polymerization of VDF lead to polydispersity values around 3 (see chapter 6.1).

Figure 6.2.2 shows the molecular weight distributions obtained from SEC analysis. A clear shift to lower molecular weights is observed upon increasing the CTA concentration. In all cases rather narrow monomodal MWDs were obtained. The associated number average molecular weights and polydispersities are listed in Table 6.2.1, together with CTA concentrations and the monomer conversions reached.

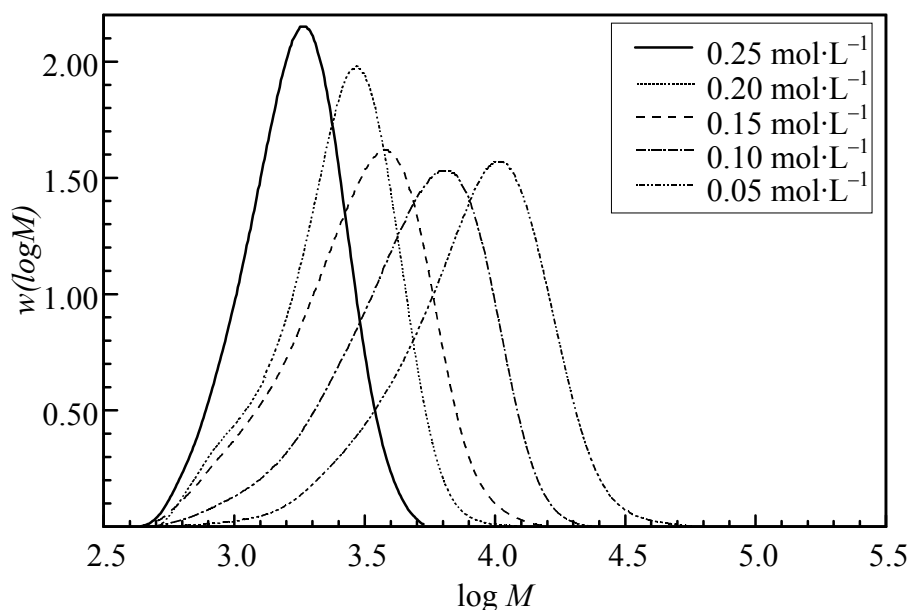


Figure 6.2.2: Molecular weight distributions for polymer obtained from VDF polymerization at 120°C and 1500 bar in the presence of 73 wt.% CO_2 , with $0.061 \text{ mol}\cdot\text{L}^{-1}$ DTBP, $3.66 \text{ mol}\cdot\text{L}^{-1}$ VDF and 0.05 to $0.25 \text{ mol}\cdot\text{L}^{-1}$ $\text{C}_6\text{F}_{13}\text{I}$.

The results presented in Figure 6.2.3 show that there is a quite prominent effect of perfluorinated hexyl iodide (CTA) concentration on the M_n . As the concentration of CTA is increased there is decrease in the M_n value. This indicates that CTA is responsible for M_n control. In fact the PDI decreases from 1.51 to 1.19 as the concentration of CTA is increased. The SEC results show that MWD is unimodal with a narrow PDI of 1.19 at the highest CTA concentration.

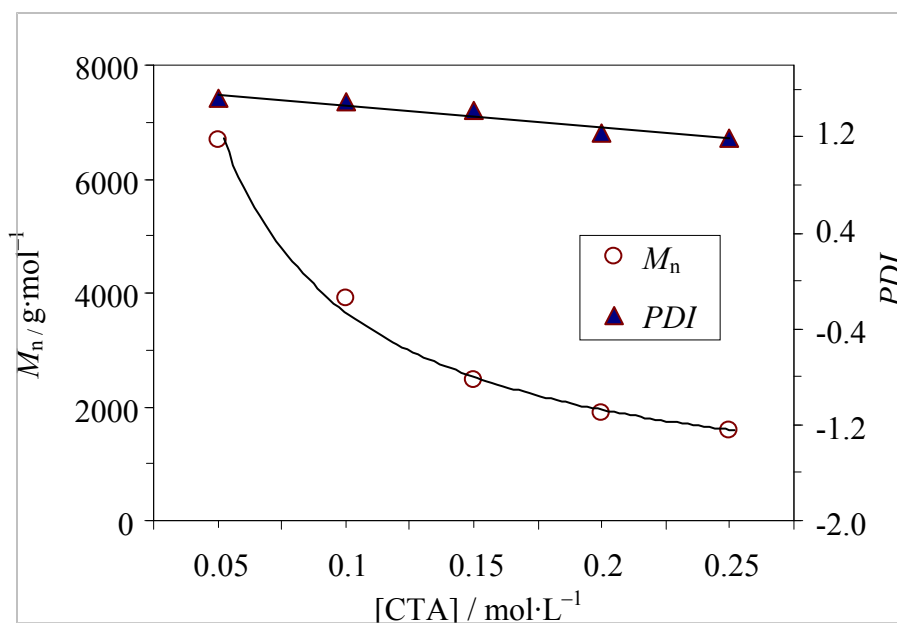


Figure 6.2.3: M_n vs CTA concentration data from VDF polymerization at 120°C, 1500 bar with 73 wt. % CO₂.

6.2.3 Living nature of polymerization

As expected the M_n values are lowered significantly upon increasing CTA concentration. The polydispersities are also quite low ranging from 1.5 to 1.2 at the highest CTA concentration. Polydispersity values around 1.2 may not be obtained from conventional radical polymerizations and are indicative of a living radical polymerization system. To test for livingness a set of polymerizations at the same reaction conditions was carried out using 0.081 mol·L⁻¹ CTA and 0.061 mol·L⁻¹ DTBP. The reactions were stopped after different conversions ranging from 23 to 86 % and MWDs of the polymers were measured. The associated M_n values are plotted as a function of monomer conversion, x , derived from the NIR spectra in Figure 6.2.4.

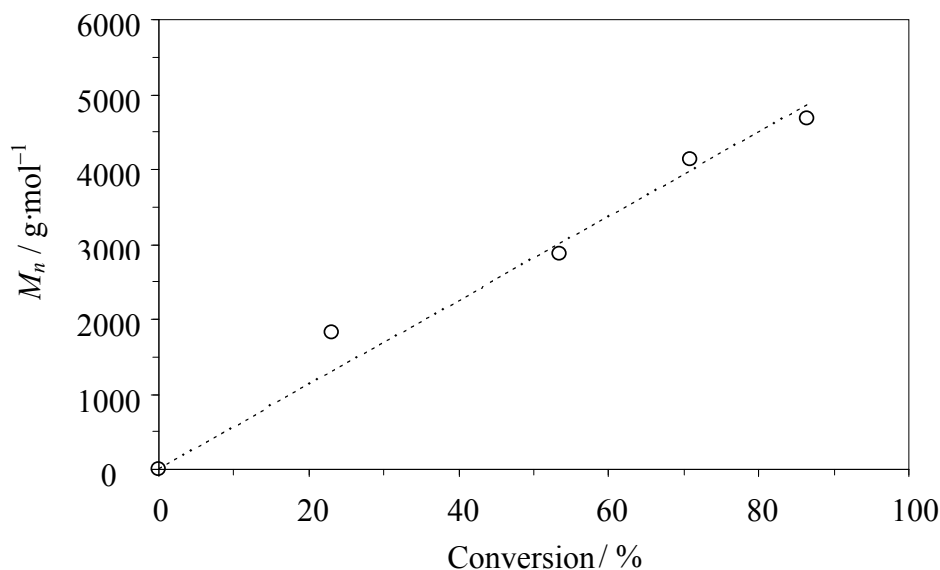


Figure 6.2.4: M_n vs. conversion data derived from VDF polymerizations at 120 °C, 1500 bar with $c_{\text{DTBP}} = 0.061 \text{ mol}\cdot\text{L}^{-1}$ and $c_{\text{CTA}} = 0.081 \text{ mol}\cdot\text{L}^{-1}$. dotted line: linear fit of the experimental data.

The data in Figure 6.2.4 indicates already for a rather low c_{CTA} of $0.081 \text{ mol}\cdot\text{L}^{-1}$ a linear increase of M_n with monomer conversion, which is typical for living radical polymerizations. The control over molecular weight in this case is possible up to high conversion of monomer. In this case high pressure leads to better control even at high conversion as reported in the case of styrene.⁸⁹ The finding of a living system is in good agreement with literature reports on iodine transfer polymerizations of VDF in acetonitrile at 75°C employing fluorinated alkyl iodides for low conversion.⁸⁷ The chain transfer constant, C_T , is presented in section 6.4.

6.2.4 Rate of polymerization

To study the kinetics of the VDF polymerizations the FT-NIR spectra recorded during the polymerizations were integrated as described above and monomer conversions were calculated. Figure 6.2.5 gives the variation of conversion with time for VDF polymerizations at 120°C and 1500 bar. The data were restricted to 40 % of conversion because of the pressure drop associated with the isochoric reaction cell. Up to 40 % of conversion the pressure decreases from the initial value of 1500 bar to around 1300 bar. At the end of the reaction at complete monomer conversion the residual pressure was 1100 bar. Thus, the following discussion will be restricted up to conversions of 40 %. We refrained from keeping the pressure constant by adding more CO_2 to the reaction cell to avoid the associated variation in mixture composition, because not only the phase behaviour would have been negatively

influenced, but also the kinetic analysis would have been more complicated.

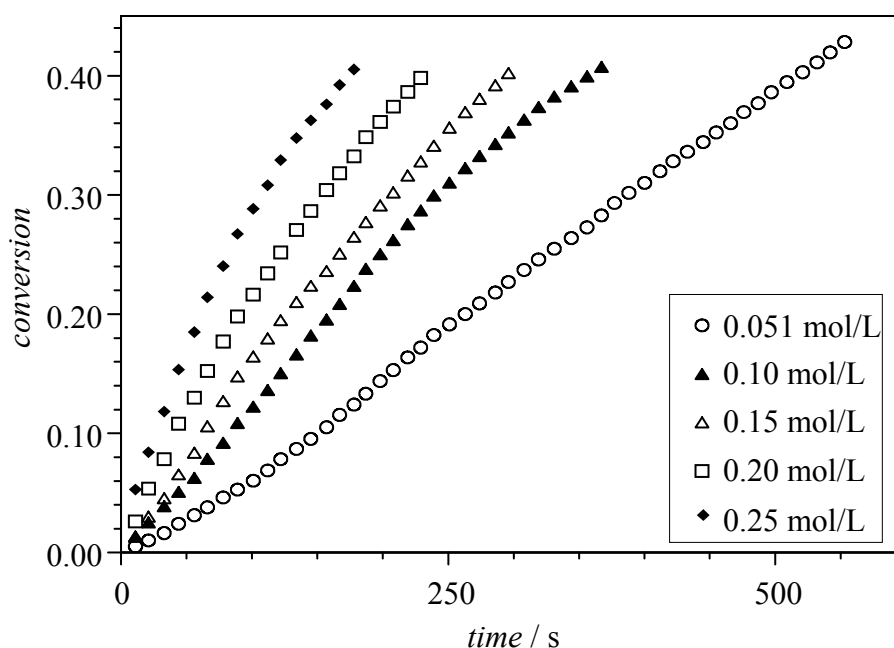


Figure 6.2.5: Conversion-time data from VDF polymerization at 120 °C, 1500 bar with 73 wt.% of CO₂, 0.061 mol·L⁻¹ DTBP, 3.66 mol·L⁻¹ VDF and C₆F₁₃I concentrations as indicated.

Surprisingly, the conversion vs. time data in Figure 6.2.5 shows that the polymerizations proceed faster with increasing c_{CTA} : While 40 % VDF conversion was reached within 125 s at the highest c_{CTA} , 516 s were required to reach 40 % conversion at the lowest c_{CTA} . Another difference can be observed from the time dependence of the conversion data. At the lowest c_{CTA} of 0.05 mol·L⁻¹ from 5 to 40 % conversion a rather linear increase in x with time is found. This behaviour is typical for living systems and is in good agreement with the molecular weight data presented in Figure 6.2.4. At the higher CTA concentrations an initial steep increase is followed by a levelling-off of the increase. The conversion – time data were used to calculate the rate of polymerization, r_p , according to $r_p = -dc_M / dt$. Figure 6.2.6 gives r_p as a function of time.

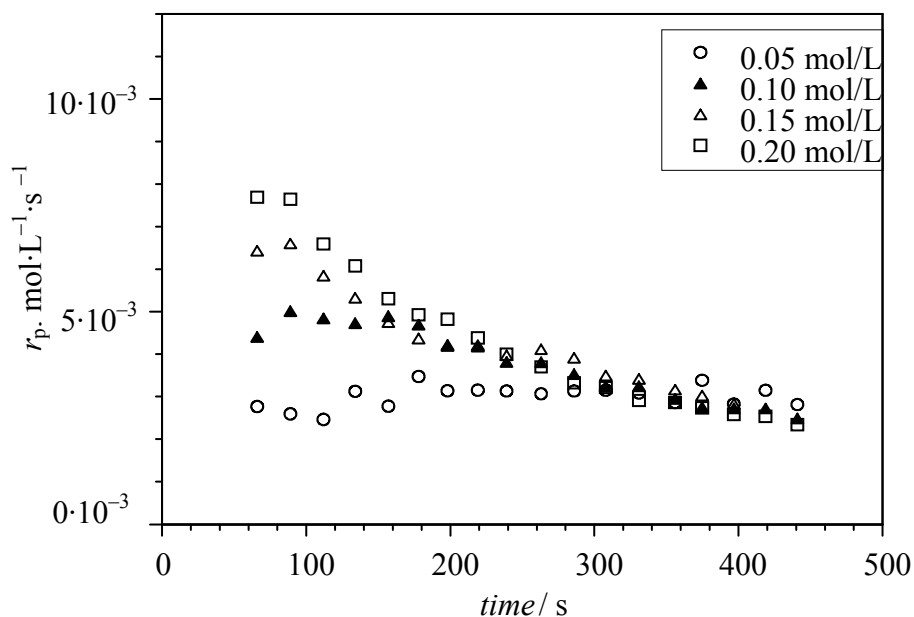
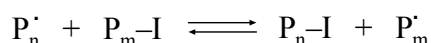


Figure 6.2.6: Time dependence of r_p for VDF polymerizations at 120 °C and 1500 bar with $c_{\text{VDF}} = 3.66 \text{ mol}\cdot\text{L}^{-1}$ and $c_{\text{DTBP}} = 0.061 \text{ mol}\cdot\text{L}^{-1}$. $\text{C}_6\text{F}_{13}\text{I}$ concentrations as indicated in the legend.

Within experimental uncertainty the rate of polymerization is almost constant at the lowest c_{CTA} of $0.051 \text{ mol}\cdot\text{L}^{-1}$. With increasing c_{CTA} higher initial values of r_p are observed. At the highest c_{CTA} of $0.25 \text{ mol}\cdot\text{L}^{-1}$ r_p is approximately 3 times higher than at the lowest c_{CTA} . At higher times the r_p values approach the data for $c_{\text{CTA}} = 0.051 \text{ mol}\cdot\text{L}^{-1}$. At around 320 s no significant difference is seen in r_p of the four polymerizations. This finding may be explained considering the characteristics of living radical polymerizations. The prerequisite of successful living radical polymerizations is suppressing chain stopping events by decreasing the concentration of free radicals. To achieve this goal active propagating radicals are in a dynamic equilibrium with a larger amount of dormant species,⁹⁰ e.g., as in iodine transfer polymerizations.⁹ The mechanism may be described as reversible addition fragmentation transfer and is illustrated in Scheme 6.1.⁸⁷

Scheme 6.1



The reversibility of the chain stopping event with an iodine atom is based on the weakness of the C-I bond. The original CTA agent also contains such a labile C-I bond, which may break at higher temperatures resulting in the formation of radical species. Thus, the CTA may contribute to the initiation process and increase the initiation rate. As a consequence the rate of polymerization is enhanced. The finding that the r_p -time curves in Figure 6.2.6 coincide at

around 320 s suggests that at this time already all of the original perfluorinated hexyl iodide is decomposed. To test the ability of $C_6F_{13}I$ to initiate polymerization the reaction mixture without any DTBP was prepared. The concentration of the CTA was $0.073 \text{ mol}\cdot\text{L}^{-1}$ and the VDF concentration $3.66 \text{ mol}\cdot\text{L}^{-1}$ as before. At $120 \text{ }^\circ\text{C}$ and 1500 bar 30 % of conversion were obtained in 900 min. To test whether the monomer itself may initiate the polymerization an additional reaction with $BrCCl_3$ as CTA was carried out in the absence of any DTBP at the same conditions. Since no conversion was obtained in this control experiment it may be concluded that the perfluorinated hexyl iodide significantly contributes to the initiation. Control experiments without DTBP and without $C_6F_{13}I$ at otherwise identical conditions did not yield any polymer.

The rate of polymerization is related to the individual rate coefficients according to Equation (6.2):

$$r_p = -\frac{dc_M}{dt} = \sqrt{f \cdot k_d \cdot c_I} \cdot \frac{k_p}{\sqrt{k_t}} \cdot c_M \quad (6.2)$$

with the initiator efficiency, f , the initiator decomposition rate coefficient, k_d , the initiator concentration, c_I , propagation and termination rate coefficients, k_p and k_t , respectively, and the monomer concentration, c_M . Equation (6.2) follows that the coupled parameter $k_p/k_t^{0.5}$ may be calculated according to Equation (6.3):

$$\frac{k_p}{\sqrt{k_t}} = -\frac{dc_M}{dt} \cdot \frac{1}{\sqrt{f \cdot k_d \cdot c_I}} \cdot \frac{1}{c_M} \quad (6.3)$$

Equation (6.3) only accounts for initiation by DTBP decomposition. Thus, it may only be applied at reaction times where no contribution from decomposition of the perfluorinated hexyl iodide is to be expected. Previously, it was shown that the polarity of the medium has a significant impact on k_d of the peroxide initiators.⁹¹ Thus, it was to be expected that k_d of DTBP for the VDF polymerization may be higher than k_d determined in a non-polar environment. However, decomposition data for DTBP in such polar media are not yet available. Thus, for a first analysis the k_d data published for DTBP decomposition in *n*-heptane as a function of pressure and temperature were adopted.⁷² During high-pressure high-temperature ethene polymerizations the efficiency for DTBP derived radicals was determined to be 1.^{71,72} This value should also hold for the system under investigation in this work.

With $k_d = 1.7 \cdot 10^{-5} \text{ s}^{-1}$, $f = 1$ and $r_p = 3.07 \cdot 10^{-3} \text{ mol} \cdot \text{L}^{-1} \text{ s}^{-1}$ at 40 % conversion a value of $1.5 \text{ L}^{0.5} \cdot \text{mol}^{-0.5} \cdot \text{s}^{-0.5}$ is derived for $k_p/k_t^{0.5}$ according to Equation (6.3). For comparison with literature⁹² $k_p/k_t^{0.5}$ has to be estimated for 75 °C and ambient pressure. The activation volume $\Delta V^\ddagger (k_p/k_t^{0.5}) = -25 \text{ cm}^3/\text{mol}$ was taken from Mueller et al.⁹³ The activation energy of $k_p/k_t^{0.5}$ was estimated to be similar to the corresponding value for ethene polymerizations due to structural similarity of the monomers. The electron withdrawing F-atoms at the double bond in VDF are expected to decrease the electron density at the double to some extent and the reactivity of the monomer towards the attack of radical should be slightly enhanced compared to ethene polymerizations. Further, the electron withdrawing F-atoms will contribute to some stabilization of the propagation radical, thus, increasing the stability of the radical compared to radicals in ethene polymerizations. Thus, the activation energy of k_p , which is largely determined by radical stability and monomer reactivity should be similar to $E_A(k_p) = 34 \text{ kJ} \cdot \text{mol}^{-1}$ for ethene.⁹⁴ Similarly, $E_A(k_t)$ for both monomers should differ significantly. Generally, $E_A(k_t)$ is between 0 and $10 \text{ kJ} \cdot \text{mol}^{-1}$.⁹⁵ Thus, the ethene value of $5 \text{ kJ} \cdot \text{mol}^{-1}$ should constitute a good estimate for VDF. To estimate $k_p/k_t^{0.5}$ at 75 °C $E_A(k_p/k_t^{0.5}) = 31.5 \text{ kJ} \cdot \text{mol}^{-1}$ was used. As a result $k_p/k_t^{0.5} = 0.15 \text{ L}^{0.5} \cdot \text{mol}^{-0.5} \cdot \text{s}^{-0.5}$ is obtained at ambient pressure and 75 °C. Considering the uncertainties of the parameters used this value is remarkably close to a literature value of $k_p/k_t^{0.5} = 0.14 \text{ L}^{0.5} \cdot \text{mol}^{-0.5} \cdot \text{s}^{-0.5}$ published for a kinetic analysis based on NMR conversion data.⁹² To obtain reliable data for $k_p/k_t^{0.5}$ additional experiments required using CTAs that do not contribute to initiation (section 6.3, 6.4).

6.2.5 Application of iodide end group towards click chemistry

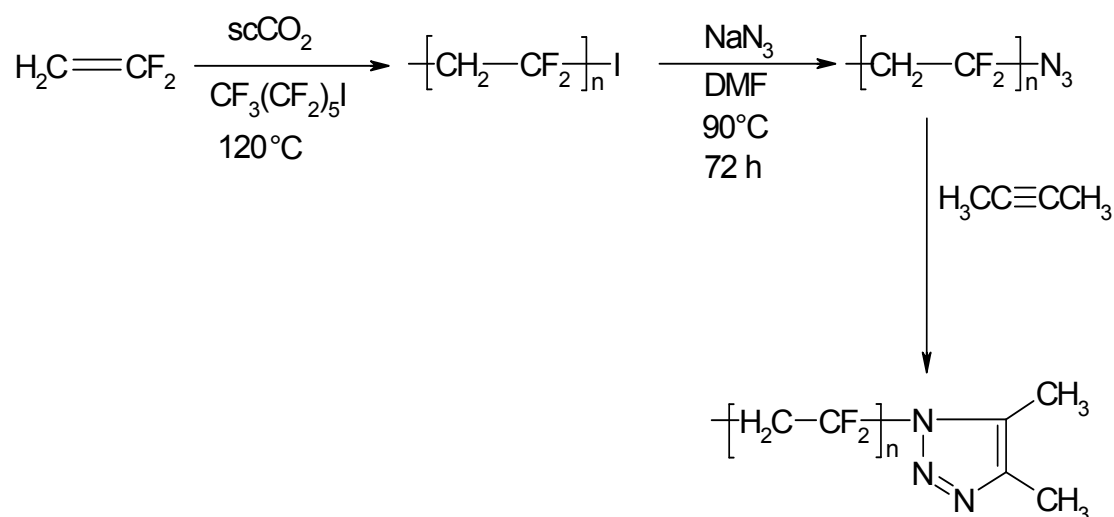
Controlling the molecular structure of polymers is a key issue for modern polymer synthesis, because more and more complex macromolecules are needed in the rapidly growing fields of nanotechnology or nanobiotechnology.⁹⁶ To fulfill this demand, synthetic polymer chemists may be able to develop versatile techniques of macromolecular engineering, enabling work at the interface between polymer science and other synthetic fields such as biochemistry or inorganic chemistry.^{97,98} Thus, the control over polymer functionalities (side groups or chain ends) is essential, since functional groups can be used for performing further modifications such as the reinitiation of polymerizations, creation of supramolecular linkages, conjugation of macromolecules or adsorption of polymers on surfaces.

Recently, Sharpless et al. popularized the 1,3-dipolar cycloaddition of azides and terminal alkynes, catalyzed by copper(I), in organic synthesis.⁹⁹ Such reactions were proven to be very practical, because they can be performed in high yield, in multiple solvents (including water),

and in the presence of numerous other functional groups.¹⁰⁰ Moreover, the formed 1,2,3-triazole is chemically very stable. Due to their efficiency and simplicity, these cycloadditions were classified as “click” reactions.¹⁰¹ Combination of chain-end functionality control via iodine transfer polymerization (ITP) and the efficiency of click chemistry is an interesting pathway for the synthesis of end-functional polymers, because iodine chain ends originating from ITP can be easily transformed into azides, and a plethora of functional alkynes is commercially available. In this chapter 6.2 the end-functionalization of poly(vinylidene fluoride) with iodide end groups (PVDF-I) by click reaction is reported. This end-functionalized PVDF is expected to have a higher thermal stability as compared to the normal PVDF.

Functionalization of PVDF-I

Well-defined PVDF with $C_6F_{13}I$ -derived end groups, $M_n = 2000 \text{ g}\cdot\text{mol}^{-1}$ and $PDI = 1.3$ was used for further synthesis. Due to the rather labile C–I bond it was expected that these polymers can be successfully transformed into various triazole functional end groups with alkyl substituents (methyl, ethyl and propyl) by a one-step reaction: substitution of the terminal iodine atom by an azide function as intermediate and subsequent 1,3-dipolar cycloaddition of the terminal azide and functional alkynes (methyl, ethyl and propyl). The scheme for the functionalization with 2-butyne is shown in scheme 6.2.



Scheme 6.2: Transformation of iodide end-functional poly (vinylidene fluoride) into 1-poly(vinylidene fluoride)-4, 5-dialkyl-1, 2, 3-triazole end functional groups.

No	Starting material	Reactant	Product	Substituent on triazole ring
1	PVDF-I	NaN_3	PVDF- N_3	-----
2	PVDF- N_3	2-butyne	PVDF- Triazole	4, 5-dimethyl
3	PVDF- N_3	3-hexyne	PVDF- Triazole	4, 5-diethyl
4	PVDF- N_3	4-octyne	PVDF- Triazole	4, 5-dipropyl

Table 6.2.2: Results of reactions of the original PVDF sample (PVDF-I) after performing click reactions with the different alkynes.

Figure 6.2.7 shows the original PVDF-I material and the polymer after functionalization to the azide group. The brown colour should be due to I_2 . The so-called “click” cycloaddition¹⁰² was performed without any catalyst because of the symmetric nature of the alkynes employed. The polymer end groups were determined by $^1\text{H-NMR}$ and FT-IR spectroscopy and by ESI-MS analyses.

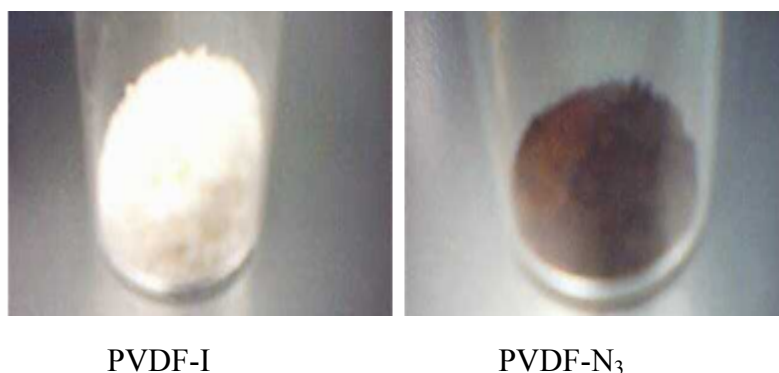


Figure 6.2.7: Visual appearance of PVDF with iodide (left) and azide end group (right).

End groups analyses

A poly(vinylidene fluoride) sample with iodide end groups from polymerization in scCO_2 was purified and analyzed by $^1\text{H-NMR}$. The spectrum is given in the lower part of Figure 6.2.8. The two signals due to each chain end of the PVDF chains were detected: signals from 3.62 to 3.87 ppm (b, a) are due to the methylene group in the VDF unit directly attached to an iodide moiety (a, b). The signals from 2.6 to 3.2 ppm are due to the methylene protons present in the polymer backbone (d). The peak present at 3.25 ppm corresponds to the methylene protons attached to $\text{CF}_3(\text{CF}_2)_5$ (c). Integration of both signals allowed for the calculation of the

fraction of initiated chains, which are effectively capped by an iodine atom after polymerization. There is no indication of end groups from initiator, which was confirmed by ESI-MS analysis (Chapter 6.5). To perform a 1,3-dipolar azide/alkyne cycloaddition at the iodide-chain end, the iodide functional PVDF was transformed into an azide functional polymer by nucleophilic substitution. This reaction was quantitative as verified by $^1\text{H-NMR}$ (Figure 6.2.8, middle). After seventy two hours of reaction the signal of methylene group (CH_2) neighbouring the iodide (3.62 and 3.87 ppm) completely shifted upfield (1.14 ppm) due to the substitution of iodide by azide (e). Integration of the new signal confirmed that the chain end transformation was quantitative. The obtained azide functional PVDF was subsequently involved in “click” reactions with various symmetric alkynes (methyl, ethyl and propyl substituted alkynes) to prepare PVDF with triazole end groups. Typically, in the absence of an appropriate catalyst, the reaction between azides and terminal alkynes is quite slow, because these alkynes are poor 1,3-dipole acceptors. The upper spectrum in Figure 6.2.8 was recorded for PVDF after reaction between the azide group and a methyl substituted alkyne. After the click reaction, in all cases the signal due to the methylene protons neighbouring the azide group are shifted to the high field to 3.90 and 4.08 ppm. In case of 2-butyne the methyl group directly attached to the triazole ring is present between 2.5 and 3 ppm (h). The 3-hexyne methyl peak is present at 1.14 ppm. In case of 4-octyne a methyl peak is observed at 0.96 ppm. Integration of both signals at 3.62 ppm (g) and 3.87 ppm (h) referring to the azide compound confirmed quantitative transformation of azide end groups into triazole end groups. Hence, the entire one-step transformation of ITP chain ends into triazole moieties was found to be quantitative.

The occurrence of triazole end groups was also confirmed by electrospray-ionization mass spectrometry. Characteristic peaks referring to a VDF chain with a C_6F_{13} end group originating from the chain transfer agent and the second end group being a triazole group with two methyl substituents were found at e.g. m/z of 608.1, 672.1 and 736.1.

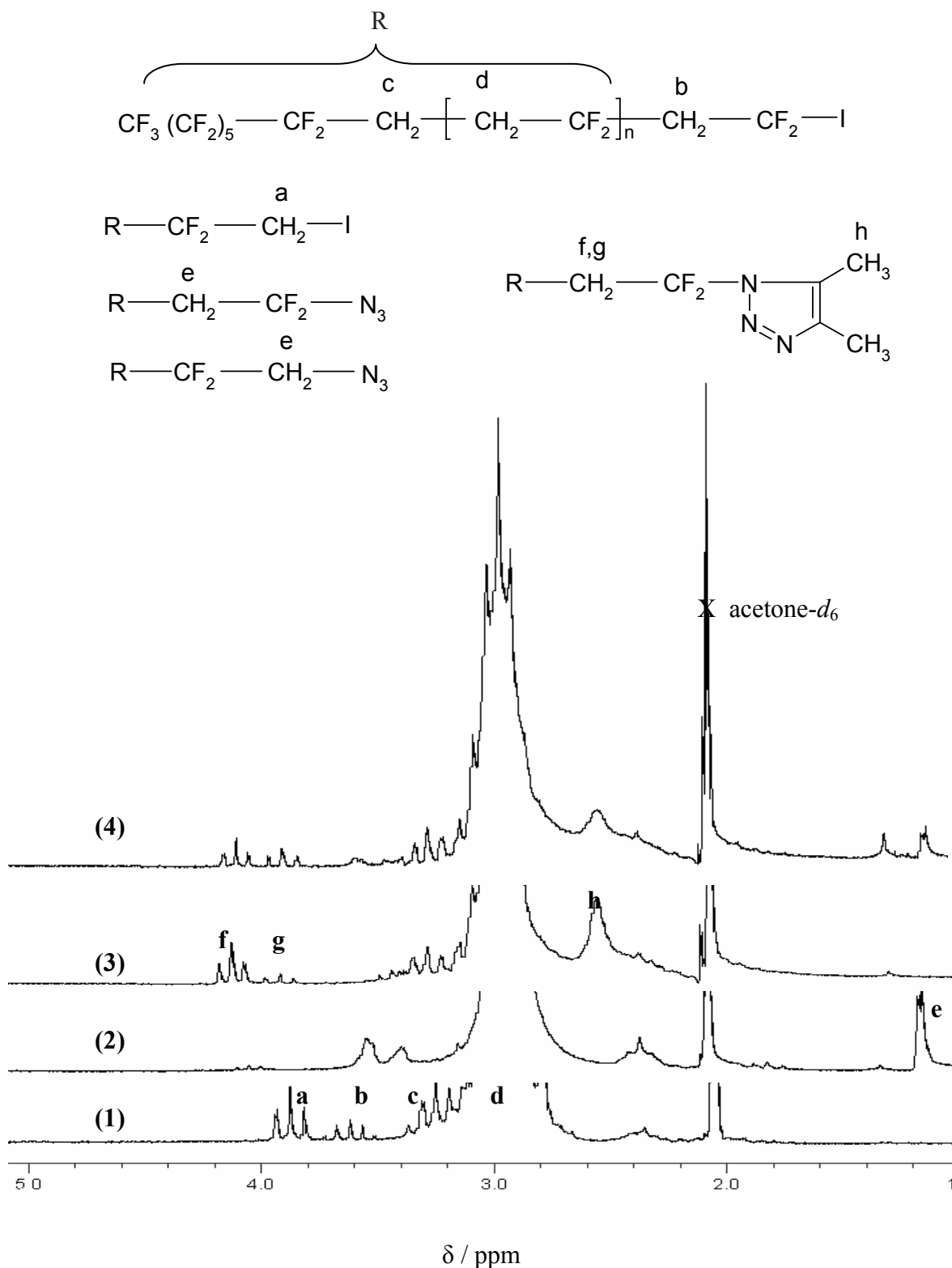


Figure 6.2.8: ^1H -NMR spectra (zoom of the region 1–5 ppm) of poly(vinylidene fluoride) with the following end groups: Iodide (1), $-\text{N}_3$ (2), 4,5-dimethyl 1,2,3-triazole (3), 4,5-diethyl 1,2,3-triazole (4). Spectra were recorded at room temperature in acetone- d_6 .

FT-IR analyses

In addition to $^1\text{H-NMR}$, FT-IR may be used to monitor the transformation of iodide to triazole end groups. An FT-IR spectrum of PVDF-I shows a prominent peak at 613 cm^{-1} assigned to C-I as indicated in Figure 6.2.9 (a). After the formation of a PVDF- N_3 this peak is no longer present and instead of this another peak around 2100 cm^{-1} is present Figure 6.2.9 (b). Instead, another peak around 2100 cm^{-1} is present. The peak at 2100 cm^{-1} is a characteristic peak of C- N_3 as reported in literature.¹⁰³ After the click reaction in Figure 6.2.9(c) a typical peak belonging to C=C and N=N is present at 1650 cm^{-1} , which indicates the formation of a triazole ring.

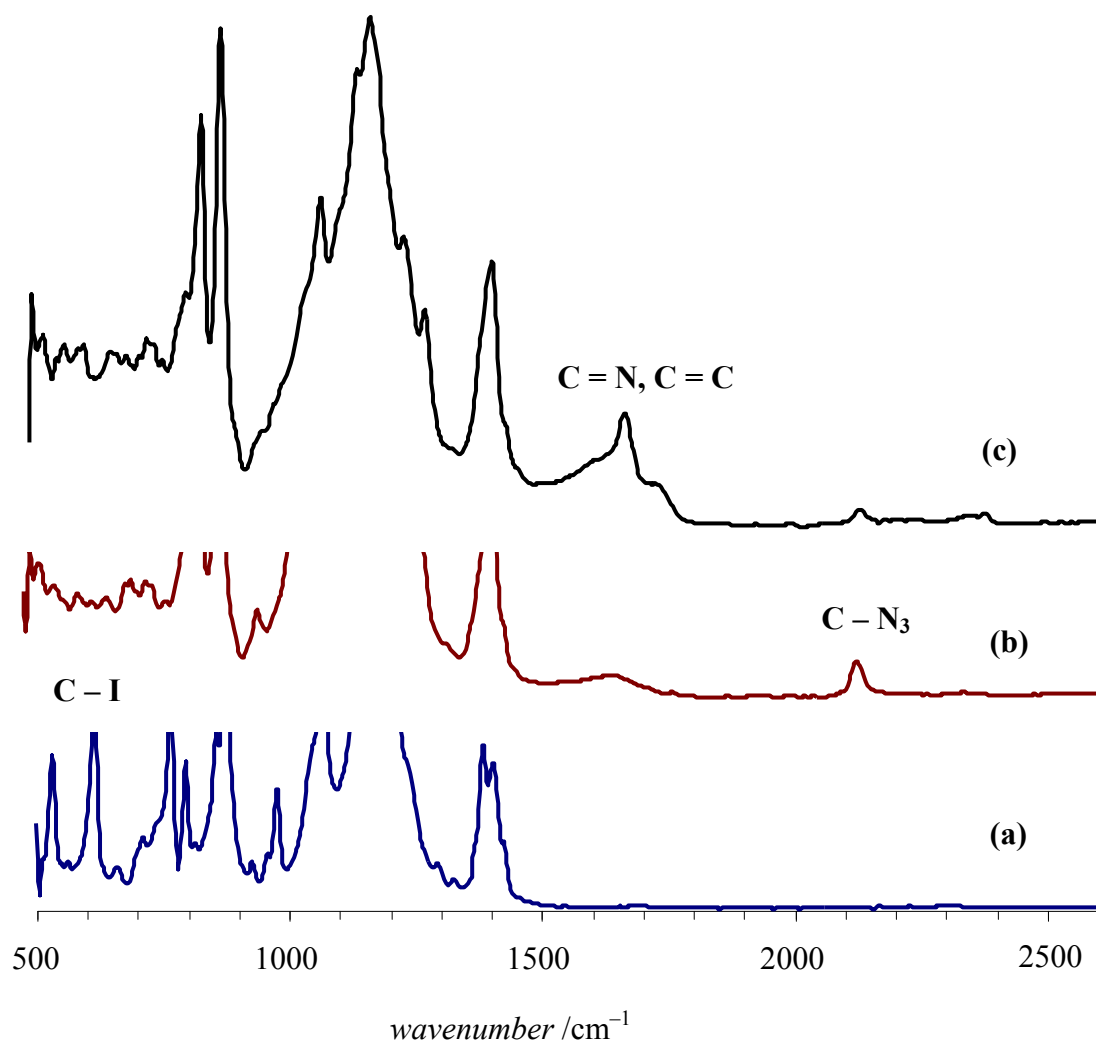


Figure 6.2.9: FT-IR spectra of PVDF-I (a), PVDF- N_3 (b) and 1-PVDF 4,5-dimethyl-1,2,3-triazole (c) end groups.

Molecular weight analyses

Molecular weight distributions of the original PVDF material with iodide end groups and of the final material after performing the click reactions with three different symmetrical alkynes were measured by SEC.

No.	alkynes	$M_n / (\text{g}\cdot\text{mol}^{-1})$	<i>PDI</i>
1	PVDF-I	2000	1.39
2	2-butyne	2200	1.16
3	3-hexyne	2600	1.23
4	4-octyne	2800	1.25

Table 6.2.3: SEC results of the original PVDF sample (PVDF-I) and after performing Click reactions with the alkynes indicated.

The results listed in Table 6.2.3 indicate that M_n is slightly enhanced with increasing size of the triazole substituents. Furthermore, Table 6.2.3 shows that polydispersities, *PDI*, of the material after performing the click reaction are slightly lower than the original material. The lowering in *PDI* should be due to additional purification steps.

6.2.6 Summary of results

VDF radical polymerizations in homogeneous phase with scCO_2 may be carried out up to complete monomer conversion at 120 °C and 1500 bar. The linear increase in M_n with time and conversion indicates that a living radical polymerization is occurring. It is remarkable to note that polymer from reactions up to complete monomer conversion shows a polydispersity of 1.2. The monomer conversion – time data may be used to estimate the rate of polymerization and $k_p/k_t^{0.5}$. However, the rate data indicates that $\text{C}_6\text{F}_{13}\text{I}$ does not only control molecular weight but also significantly contributes to the initiation rate.

PVDF obtained from homogeneous phase iodine transfer polymerization in supercritical CO_2 with iodide end groups allows for efficient end-functionalization of the polymer. After substitution of the iodide end group by an azide group 1,3-dipolar cycloadditions with alkynes yield polymers with 1-PVDF 4,5-dialkyl-1,2,3-triazole end groups. This end-functionalized PVDF is expected to have a higher thermal stability as compared to the normal PVDF. Using symmetrical alkynes the reactions may be carried out in the absence of any catalyst.

6.3 Bromotrichloromethane (BrCCl₃)

Since perfluorinated hexyl iodide contributes to initiation, it is not a suitable CTA for experiments directed towards determination of r_p and $k_p/k_t^{0.5}$. Thus, a different CTA had to be found, that does not initiate polymerization such as bromotrichloromethane. VDF polymerizations were carried out at 120°C and 1500 bar in the presence of BrCCl₃ concentrations ranging from 0.230 to 0.921 mol·L⁻¹ in order to investigate the influence of chain transfer agent concentration (c_{CTA}) on molecular weight.

6.3.1 Variation of BTCM concentration

A series of experiments was carried out to study the effect of bromotrichloromethane (BTCM) concentration on the rate of polymerization, average molecular weight and the MWDs. The results are summarized in Table 6.3.1. The first entry in Table 6.3.1 indicates that there is no initiation from the chain transfer agent. A clear shift to lower molecular weights is observed upon increasing the BTCM concentration which indicates that BTCM controls the molecular weight. Further results presented in Table 6.3.1 show that BTCM not only controls the molecular weight of the polymer but also improves the phase behaviour of the reaction. At low CTA concentration the reaction medium is homogeneous up to 30 % conversion, whereas at the highest concentration of CTA monomer conversion up to 95 % in homogenous phase. With the change in the BTCM concentration morphology also changes from fine white powder to a tacky material.

Entry	DTBP mol·L ⁻¹	CTA mol·L ⁻¹	x (%)	M_n g·mol ⁻¹	PDI	r_p (15%) mol·L ⁻¹ ·s ⁻¹	Reaction medium	Morphology
1	(a)	0.230	-----	-----	-----	-----	-----	<i>No polymer</i>
2	0.061	0.230	30	6000	2.8	5.5×10^{-4}	Homogeneous initially but became heterogeneous	<i>Fine white powder</i>
3	0.061	0.453	60	4400	1.8	4.6×10^{-4}	Homogeneous initially but became heterogeneous	<i>Fine white powder</i>
4	0.061	0.683	74	2900	1.6	4.1×10^{-4}	homogeneous initially but became heterogeneous	<i>White powder</i>
5	0.061	0.921	95	2100	1.6	3.8×10^{-4}	Homogeneous completely	<i>Gel like polymer</i>
6	0.061	1.15	96	1900	1.5	2.9×10^{-4}	Homogeneous completely	<i>Gel like polymer</i>

Table 6.3.1: Bromotrichloromethane and VDF concentrations as well as product properties (number average molecular weight, M_n ; final conversion, x ; polydispersity index, PDI ; rate of polymerization*, r_p ; reaction medium, morphology, for VDF polymerization with $0.061 \text{ mol}\cdot\text{L}^{-1}$ DTBP, $3.66 \text{ mol}\cdot\text{L}^{-1}$ VDF at 120°C , 1500 bar and 73 wt % content of CO_2 . ^(a) entry without initiator. ^(*) up to 15 % conversion, r_p (15%).

6.3.2 r_p and chain transfer concentration (BrCCl_3)

The conversion – time data was used to calculate the rate of polymerization, r_p , according to $r_p = -dc_M / dt$. Figure 6.3.1 gives r_p as a function of time. The r_p data indicates that the BrCCl_3 concentration has a minor effect on r_p and a lowering of r_p with increase in BrCCl_3 concentration is observed. The rate of polymerization for $0.23 \text{ mol}\cdot\text{L}^{-1}$ of BrCCl_3 is $5.5 \times 10^{-4} \text{ mol}\cdot\text{L}^{-1}\cdot\text{s}^{-1}$, whereas similar concentration of PFHI leads to r_p of $6.3 \times 10^{-3} \text{ mol}\cdot\text{L}^{-1}\cdot\text{s}^{-1}$. The lower values of r_p for BrCCl_3 as compared to perfluorinated hexyl iodide are due to no contribution in the initiation step from CTA. At the highest c_{CTA} of $1.15 \text{ mol}\cdot\text{L}^{-1}$ r_p is approximately 2 times lower than at the lowest c_{CTA} .

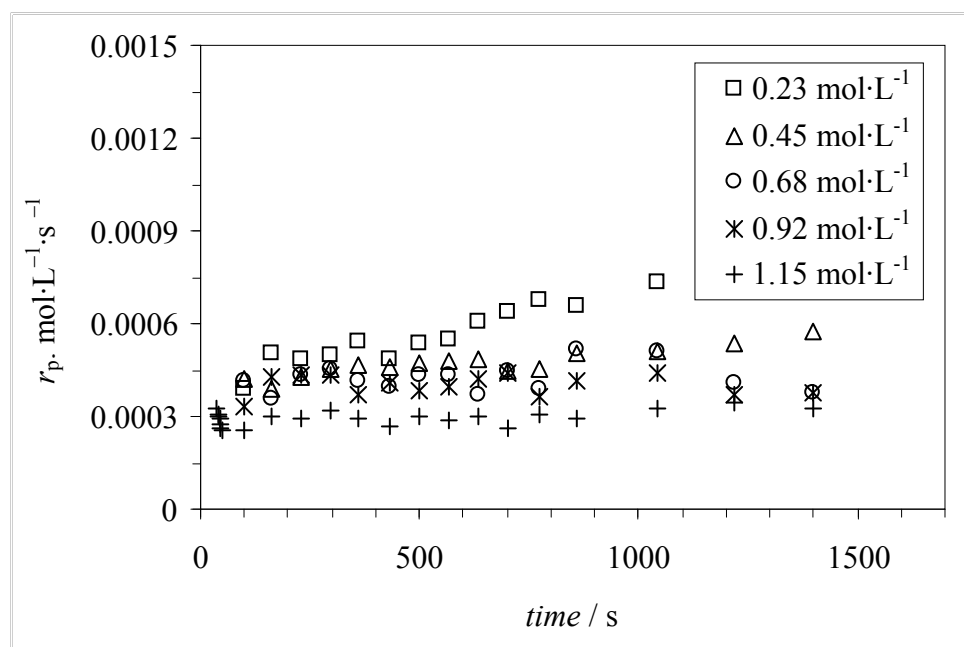


Figure 6.3.1: r_p - time plot from VDF polymerization at 120°C , 1500 bar with 73 wt. % CO_2 , $0.061 \text{ mol}\cdot\text{L}^{-1}$ DTBP, $3.66 \text{ mol}\cdot\text{L}^{-1}$ VDF under different BTCM concentrations.

The results show that the rate of polymerization is independent of time within experimental accuracy. From the data given in Figure 6.3.2 $k_p/k_t^{0.5}$ was determined using Equation 6.3.

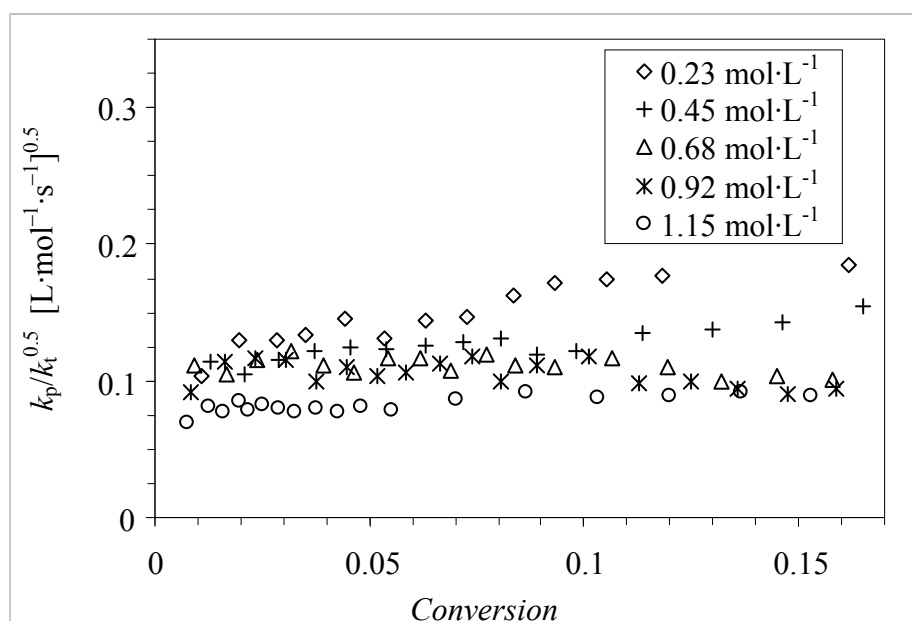


Figure 6.3.2: $k_p/k_t^{0.5}$ - conversion plot from VDF polymerization at 120°C, 1500 bar with 73 wt. % CO₂, 0.061 mol·L⁻¹ DTBP, 3.66 mol·L⁻¹ VDF under different bromotrichloromethane concentrations.

The results presented in Figure 6.3.2 show that $k_p/k_t^{0.5}$ is independent of conversion. CTA concentration has a slight effect on $k_p/k_t^{0.5}$. The value of $k_p/k_t^{0.5}$ for 0.23 mol·L⁻¹ of BrCCl₃ is 0.08 (L·mol⁻¹·s⁻¹)^{0.5}, whereas the lowest concentration of PFHI (0.05 mol·L⁻¹) leads to $k_p/k_t^{0.5}$ value of 1.5 (L·mol⁻¹·s⁻¹)^{0.5}. The higher value for PFHI as compared to BrCCl₃ is due to the contribution from PFHI towards the rate of polymerization as it takes part in the initiation step.

A reason for the observed variation of $k_p/k_t^{0.5}$ with BrCCl₃ may be seen in the chain length dependence of the termination rate coefficient. The lower concentration of BrCCl₃ leads to a chain length of 32, which is associated with a higher k_t value and it results into a lower value of $k_p/k_t^{0.5}$. At the lower value of CTA the chain length is 93, associated with a lower value of k_t leading to a higher value of $k_p/k_t^{0.5}$. The $k_p/k_t^{0.5}$ values derived from these experiments are in reasonable agreement with the value presented in literature for heterogeneous phase polymerization 0.19 (L·mol⁻¹·s⁻¹)^{0.5}.³³

Ameduri and coworkers reported a number of side reactions for systems with extremely high BrCCl₃ concentrations.⁴⁹ Thus, it seemed important to study whether these side reactions also

contribute to the kinetic analyses of this chapter and to confirm the kinetic data derived. Therefore additional CTAs were employed. The details of these CTAs are given in chapter 6.4.

6.3.3 Summary of results

The molecular weight was controlled by using bromotrichloromethane as chain transfer agent together with the modest amount of initiator. The kinetic data obtained from these experiments do not show an involvement of the chain transfer agent in the initiation step. A slight decrease of the rate of polymerization with increasing chain transfer agent concentration was observed, which may be explained by the chain length dependence of the termination rate coefficient. In all experiments the coupled parameter $k_p/k_t^{0.5}$ was independent of monomer conversion up to 15 % conversion. At 120°C $k_p/k_t^{0.5}$ was estimated to be around $0.1 \text{ (L}\cdot\text{mol}^{-1}\cdot\text{s}^{-1})^{0.5}$.

6.4 Polymerization in the presence of perfluorinated hexyl bromide and 1H-perfluorohexane; kinetics and transfer efficiency

Part 6.4 of chapter 6 focuses on the kinetic aspects of VDF polymerization using two additional chain transfer agents of the general structure $C_6F_{13}X$ to obtain reliable kinetic data for $k_p/k_t^{0.5}$. $C_6F_{13}X$, with X being Br or H, seemed interesting to use, because no contribution to initiation is expected to occur. Molecular weight distribution, chain transfer constants along with rate of polymerization will be discussed and compared with the corresponding results for $C_6F_{13}I$ as CTA. The following abbreviations will be used:

- Perfluorinated hexyl iodide ($CF_3-(CF_2)_5-I$) (PFHI)
- Perfluorinated hexyl bromide ($CF_3-(CF_2)_5-Br$) (PFBH)
- 1H- Perfluorohexane ($CF_3-(CF_2)_5-H$) (HPFH)

6.4.1 Molecular weight control via employing ($CF_3-(CF_2)_5-X$)

VDF polymerizations with ~ 73 wt. % CO_2 at 120 °C and 1500 bar were carried out using the above-mentioned CTAs. The initiator concentration was 0.061 mol·L⁻¹ and the chain transfer agent concentrations as detailed in Table 6.4.1. It also contains number average molecular weights, M_n , polydispersities, *PDI*, conversions reached and states whether the reaction mixture was homogeneous or heterogeneous. It should be noted that heterogeneous refers to the occurrence of two phases that are not completely miscible. Precipitation of polymer was not observed. In order to compare the chain transfer activity of the three CTAs comparable amounts of CTA were used, rather than adjusting CTA concentration to yield polymer with a targeted molecular weight. A series of polymer reactions was carried out using different CTA concentrations. For comparison, Table 6.4.1 contains some data for PFHI as CTA already discussed in section 6.2.

Sample	CTA	[CTA] (mol·L ⁻¹)	M_n / (g·mol ⁻¹)	x (%)	PDI	Phase
PFHI	C ₆ F ₁₃ I	0.07 ^(a)	3000	30	1.30	Homogeneous
PFHI-0	C ₆ F ₁₃ I	0.05	6700	90	1.51	Homogeneous
PFHI-3	C ₆ F ₁₃ I	0.20	1800	97	1.23	Homogeneous
PFBH-1	C ₆ F ₁₃ Br	0.051	16900	90	3.01	<i>Heterogeneous</i> ^{b)}
PFBH-3	C ₆ F ₁₃ Br	0.220	8800	96	2.85	<i>Heterogeneous</i> ^{b)}
PFBH-4	C ₆ F ₁₃ Br	0.464	5600	97	2.24	Homogeneous ^{b)} up to 20 %
HPFH -1	C ₆ F ₁₃ H	0.051	32100	92	3.67	<i>Heterogeneous</i> ^{b)}
HPFH -2	C ₆ F ₁₃ H	0.224	34200	95	2.08	<i>Heterogeneous</i> ^{b)}
HPFH -3	C ₆ F ₁₃ H	0.442	32500	96	2.40	<i>Heterogeneous</i> ^{b)}

Table 6.4.1: Molecular weight and conversion data obtained from VDF polymerizations in 73 wt.% CO₂ at 120 °C and 1500 bar with 0.061 mol·L⁻¹ DTBP. The data for C₆F₁₃I were already contained in Table 6.2.1. ^(a) no initiator, ^(b) the reaction mixture shows two phases, precipitation does not occur.

PFHI not only controlled the molecular weight of the polymer but also improved the phase behaviour of the reaction, whereas under similar conditions PFBH and HPFH led to a heterogeneous phase. Under the highest PFBH concentration the reaction medium was homogeneous up to 20 % conversion, whereas the highest concentration of PFHI led to the monomer conversion of 95 % in homogenous phase. In contrast to the iodo and bromo compounds, the data in Table 6.4.1 indicate that an increase in C₆F₁₃H concentration did not cause any lowering of M_n . Thus, C₆F₁₃H shows poor performance as a chain transfer agent. Some chain transfer activity is anticipated, since polydispersities are slightly lower at higher CTA concentration. However, no obvious trend is observed, which may also be due to the rather poor mixing of the system (no active stirring in the high-pressure cell).

Polydispersity values around 1.2 as obtained for the PFHI samples are indicative of a living radical polymerization system. The other two CTAs, PFBH and HPFH, led to polydispersity values 2.2 to 3.7, which are indicative of conventional radical polymerizations

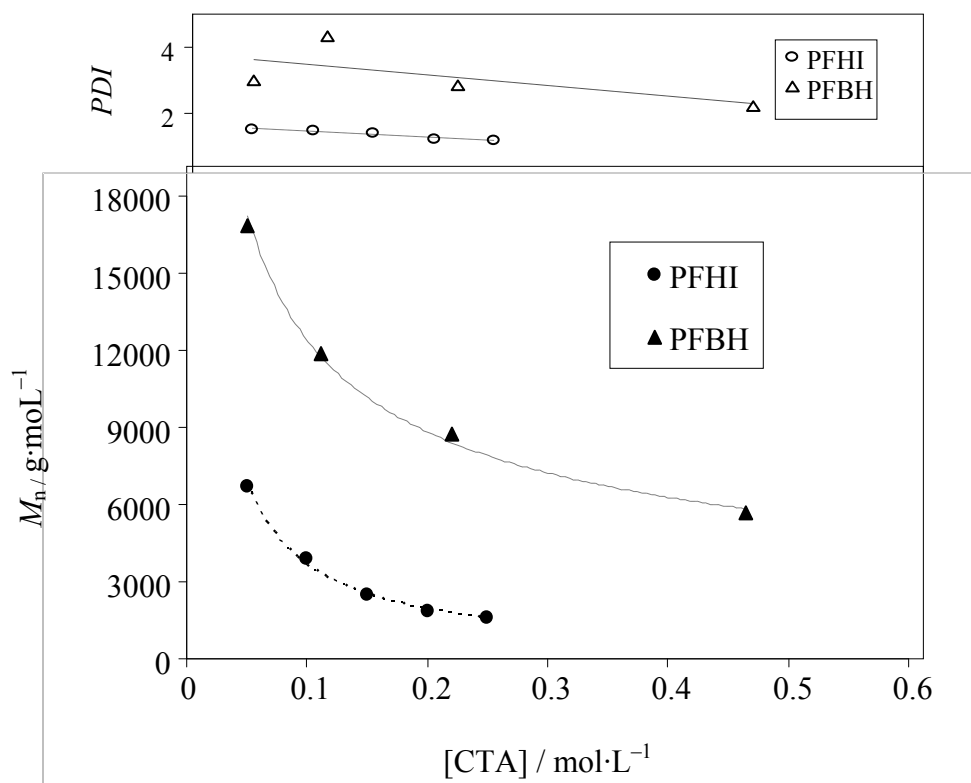


Figure 6.4.1: M_n vs. CTA concentration for PVDF from polymerizations at 120 °C and 1500 bar with 73 wt. % CO₂ using PFHI and PFBH as CTAs.

The molecular weight data obtained for polymerizations with either C₆F₁₃I or C₆F₁₃Br are depicted in Figure 6.4.1. As anticipated, the data in Figure 6.4.1 and Table 6.4.1 show that C₆F₁₃Br is less efficient as chain transfer agent. For a CTA concentration of 0.05 mol·L⁻¹ the use of C₆F₁₃Br yields PVDF with $M_n = 1.6 \cdot 10^4$ g·mol⁻¹ whereas C₆F₁₃I resulted in $M_n = 6.7 \cdot 10^3$ g·mol⁻¹. In all experiments with C₆F₁₃Br the polydispersities are significantly higher than for the samples from reactions with the corresponding iodo compound. As expected for a chain transfer agent, upon increasing concentration of C₆F₁₃Br a lowering of M_n and polydispersity is found.

6.4.2 End groups analyses via ¹H-NMR spectroscopy

To confirm the interpretation of the molecular weight data ¹H-NMR spectra of PVDF samples obtained in the presence of C₆F₁₃Br and C₆F₁₃I were measured to determine the polymer end groups. The spectra are given in Figures 6.4.2 and 6.4.3, respectively.

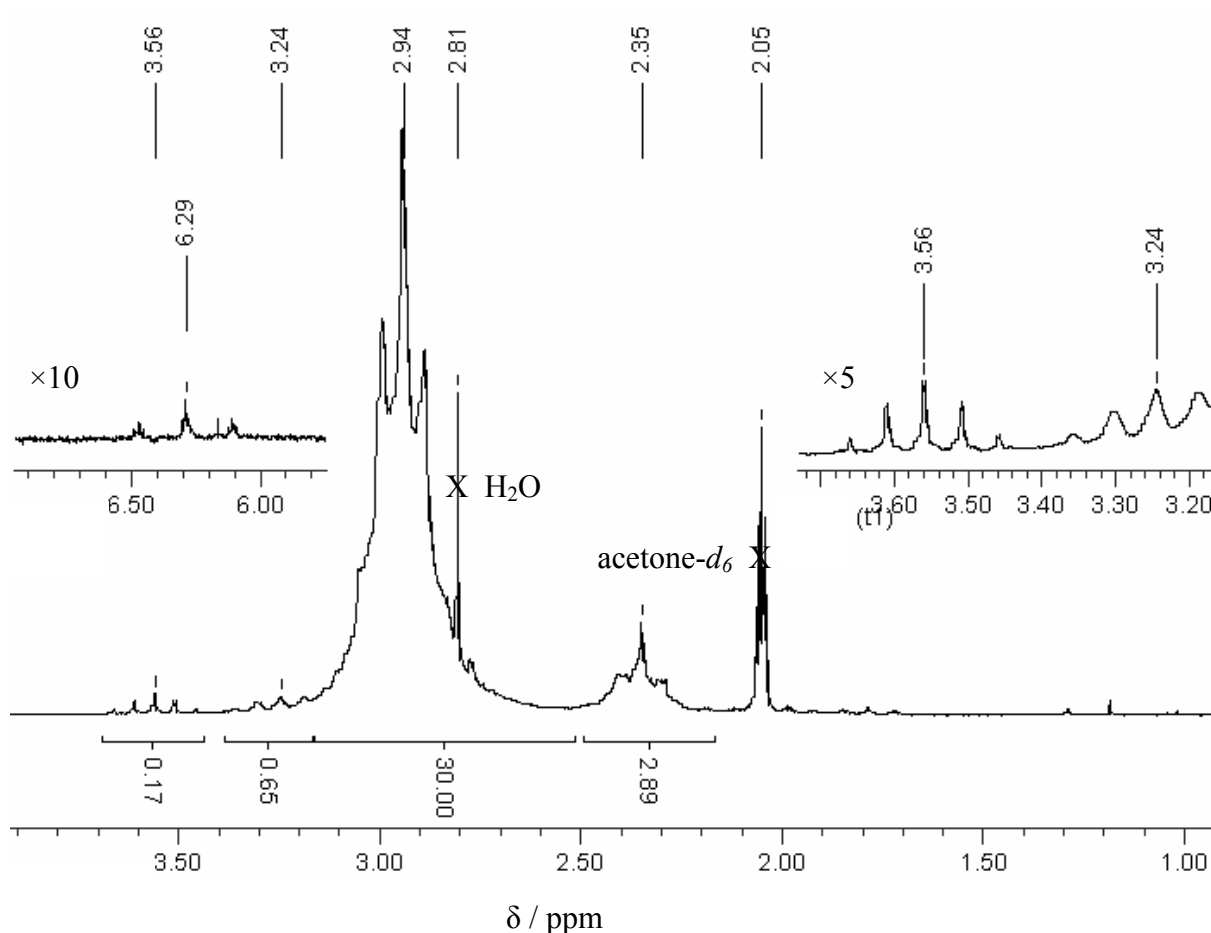


Figure 6.4.2: ^1H -NMR spectrum of polymer obtained from VDF polymerization using perfluorinated hexyl bromide ($0.464 \text{ mol}\cdot\text{L}^{-1}$) at $120 \text{ }^\circ\text{C}$, 1500 bar with 73 wt. % CO_2 . NMR solvent: acetone- d_6

The ^1H -NMR spectrum in Figure 6.4.2 shows peaks that may be assigned to end groups derived from $\text{C}_6\text{F}_{13}\text{Br}$:³⁷

$-\text{CH}_2\text{-CF}_2-$ (multiplet, 2.94 ppm, 2H), $-\text{CH}_2\text{-CF}_2\text{-Br}$ (quintet, 3.25 ppm, 2H), $-\text{CF}_3\text{-(CF}_2)_4\text{-CF}_2\text{-CH}_2-$ (triplet, 3.24 ppm, 2H), $-\text{CF}_2\text{-CH}_2\text{-Br}$ (triplet, 3.56 ppm, 2H), $\text{H-CF}_2\text{-CH}_2-$ (triplet of triplet, 6.3 ppm, H)

The signals at 2.05 and 2.81 ppm in the NMR spectrum of Figure 6.4.2 refer to the solvent acetone and water traces. Significant contributions from initiator-derived end groups (signals of methyl protons at $\sim 1 \text{ ppm}$) are not seen in the spectrum in Figure 6.4.2. Thus, it may be concluded that chain transfer is the dominating chain initiating and chain stopping event in the presence of $\text{C}_6\text{F}_{13}\text{Br}$. The ^1H -NMR spectrum in Figure 6.4.3, referring to polymerizations with $\text{C}_6\text{F}_{13}\text{H}$, indicates that $\text{CF}_3\text{-(CF}_2)_4\text{-CF}_2\text{-CH}_2-$ end groups that should result in a peak at 3.24 ppm are not contained in the polymer. Moreover, $\text{C}_6\text{F}_{13}\text{H}$ should also result in

$-\text{CH}_2\text{-CF}_2\text{-H}$ as end group associated with a distinct peak at 6.3 ppm.⁸⁷ However, even the ten fold magnification of the spectrum shows only a peak of negligible intensity at 6.3 ppm. The integral of the peak is mainly due to the scatter of the baseline. Thus, it is concluded that $\text{C}_6\text{F}_{13}\text{H}$ does not undergo significant chain transfer. The peak at 1.02 ppm belongs to the initiator derived end group $\text{CH}_3\text{-CH}_2\text{-CF}_2\text{-}$. Additionally, the triplet seen around 1.8 ppm refers to $\text{CH}_3\text{-CF}_2\text{-CH}_2\text{-}$.

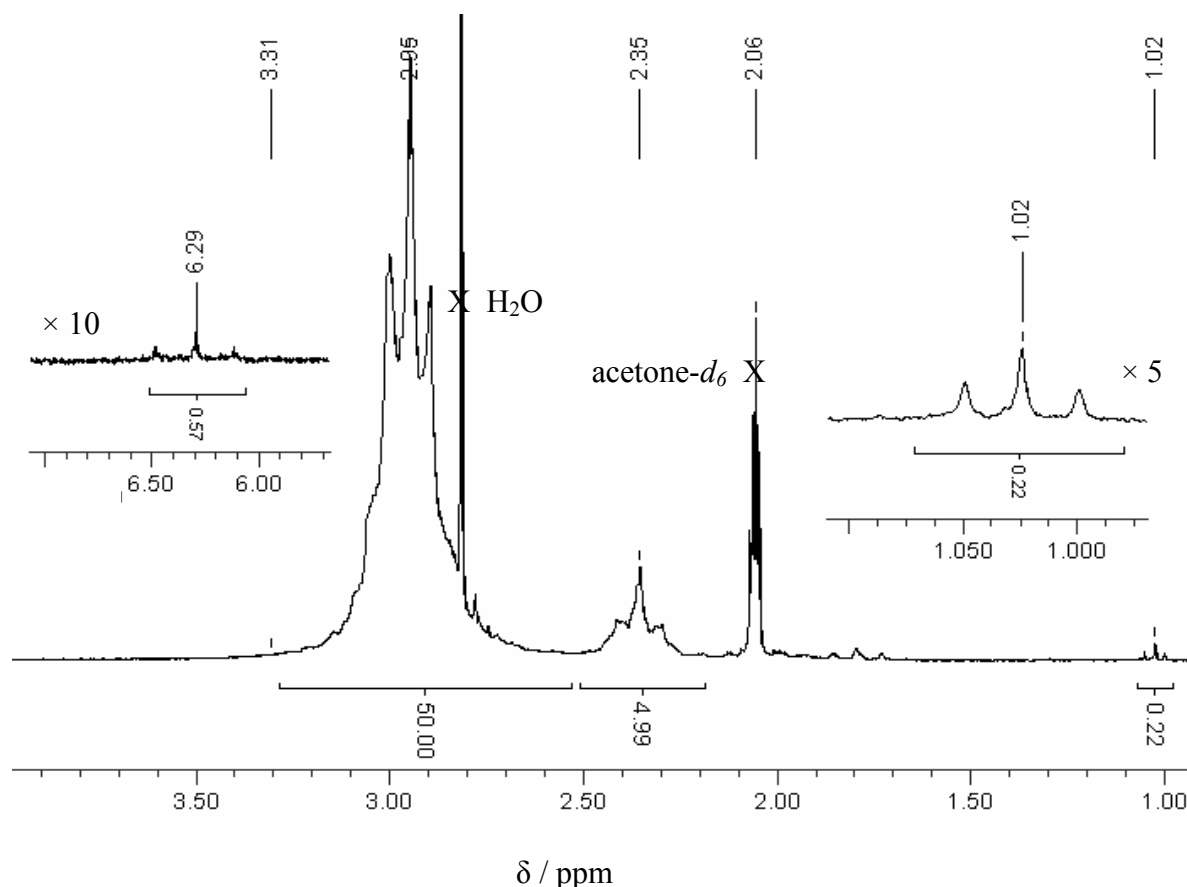


Figure 6.4.3: ^1H -NMR spectrum of polymer obtained from VDF polymerization using 1H-perfluorohexane ($0.224 \text{ mol}\cdot\text{L}^{-1}$) at $120 \text{ }^\circ\text{C}$, 1500 bar with 73 wt. % CO_2 . NMR solvent: acetone- d_6 .

6.4.3 Chain transfer constants of $\text{CF}_3\text{-(CF}_2)_5\text{-X}$

To quantify the chain transfer activity of these three CTAs the chain transfer constants, C_T , were determined from a Mayo plotⁱ of $1/DP_n$ vs. $[\text{CTA}]/[\text{VDF}]$, with $DP_n = M_n/M_{\text{VDF}}$ and the concentrations of CTA, $[\text{CTA}]$, and VDF, $[\text{VDF}]$. Data for all three systems is given in Figure

ⁱ To compare the chain transfer activity of all three transfer agents the Mayo method was used to derive C_T values. As pointed out in literature, for living systems other approaches may be better suited, which rest on the measurement of the consumption of monomer and of the initial chain transfer agent. However, since the conversion of $\text{C}_6\text{F}_{13}\text{I}$ as a function of time was not accessible the simple Mayo approach was chosen.

6.4.4. The C_T values derived from the slopes of the linear fits show that perfluorinated hexyl iodide is the most efficient chain transfer agent ($C_T = 8 \cdot 10^{-1}$) as compared to the two other CTAs. The C_T value for $C_6F_{13}Br$ is intermediate with $C_T = 9 \cdot 10^{-2}$. For $C_6F_{13}H$ a very low C_T of $2 \cdot 10^{-4}$ was determined, which is 1.5 orders of magnitude lower than the value for the bromine compound and 3.5 orders of magnitude lower than for the iodine compound. The decreasing order of the C_T values for the VDF polymerization in the presence of three chain transfer agents is as follow:

$$C_T(C_6F_{13}I) = 8 \cdot 10^{-1} > C_T(C_6F_{13}Br) = 9 \cdot 10^{-2} > C_T(C_6F_{13}H) = 2 \cdot 10^{-4}$$

The reason for the high C_T value for perfluorinated hexyl iodide may be seen in the low dissociation energy of the C-I bond compared to the C-Br and C-H bond. The bond dissociation energies (BDE) decrease as follows:¹⁰⁴

$$BDE(C-I) = 213 \text{ kJ}\cdot\text{mol}^{-1} < BDE(C-Br) = 284 \text{ kJ}\cdot\text{mol}^{-1} < BDE(C-H) = 414 \text{ kJ}\cdot\text{mol}^{-1}$$

The high bond dissociation energy of the C-H bond results in the comparably poor chain transfer activity of $C_6F_{13}H$.

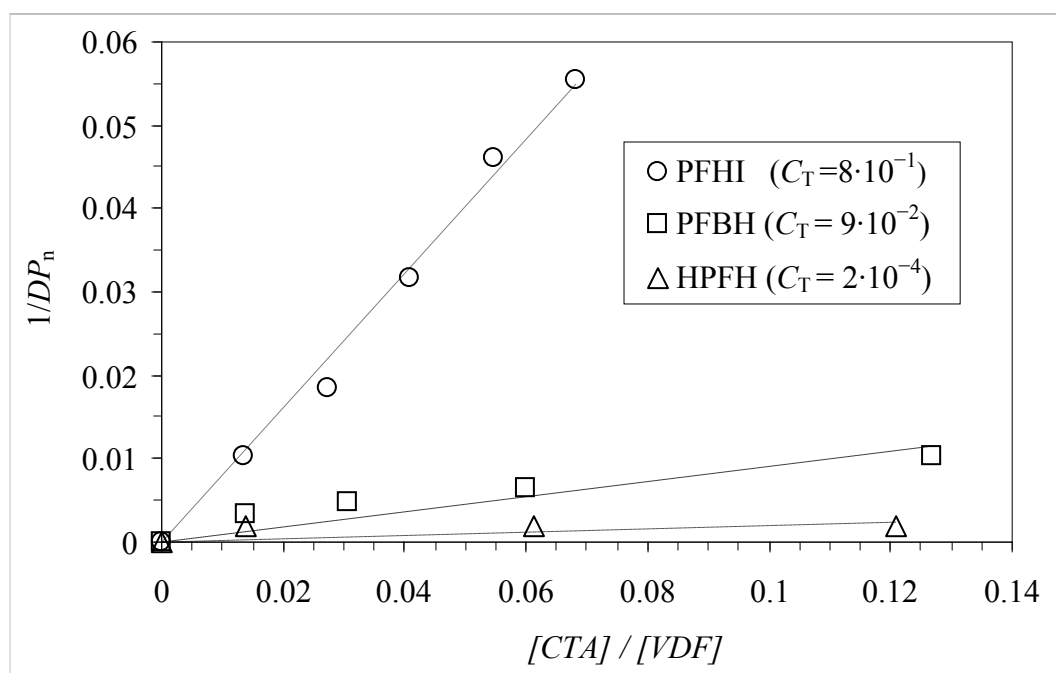


Figure 6.4.4: Mayo plot for VDF polymerizations at 120 °C and 1500 bar in the presence of different CTAs.

6.4.4 Effect of $CF_3-(CF_2)_5-X$ concentrations on rates of polymerization

The rates of polymerization were calculated from the NIR spectra recorded during the polymerization. The data analyses was restricted to 40 % of conversion to limit the influence of decreasing pressure due to volume contraction caused by the differences in polymer and

monomer density. The rate data for C₆F₁₃I was already reported in section 6.2.4, but will be repeated for comparison with the data related to C₆F₁₃Br and C₆F₁₃H as CTA. Rates of polymerization, r_p , and the ratio of the propagation and termination rate coefficients ($k_p/k_t^{0.5}$), derived for VDF polymerizations with CTA are listed in Table 6.4.4.

No.	BDE / kJ·mol ⁻¹	[CTA] / mol·L ⁻¹	M_n / g·mol ⁻¹	r_p / mol·L ⁻¹ ·s ⁻¹	$k_p/k_t^{0.5}$ / [L·mol ⁻¹ ·s ⁻¹] ^{0.5}	app. k_p / L·mol ⁻¹ ·s ⁻¹
PFHI	(C-I) 251	0.07 ^(a)	3000
PFHI-0	251	0.05	6700	2.72×10^{-3} ^(b)	1.03	10×10^3 ^(d)
PFHI-1	251	0.10	4000	4.02×10^{-3} ^(b)
PFHI-2	251	0.15	2500	4.90×10^{-3} ^(b)
PFHI-3	251	0.20	1800	6.33×10^{-3} ^(b)
PFHI-4	251	0.25	1600	7.32×10^{-3} ^(b)
PFBH-1	(C-Br) 284	0.051	16900	2.16×10^{-3} ^(c)	0.61	6.0×10^3 ^(d)
PFBH-2	284	0.112	11900	2.56×10^{-3} ^(c)	0.72	7.1×10^3 ^(d)
PFBH-3	284	0.220	8800	4.94×10^{-3} ^(c)	1.39	14×10^3 ^(d)
PFBH-4	284	0.464	5600	7.10×10^{-3} ^(c)	2.01	20×10^3 ^(d)
HPFH-1	(C-H) 414	0.051	32100	2.29×10^{-3} ^(c)	0.62	6.1×10^3 ^(d)
HPFH -2	414	0.224	34200	2.35×10^{-3} ^(c)	0.64	6.3×10^3 ^(d)
HPFH -3	414	0.442	32500	2.62×10^{-3} ^(c)	0.71	6.9×10^3 ^(d)

Table 6.4.4: Effect of CTA concentration on M_n , rate of polymerization, r_p , the ratio of propagation and termination rate coefficients ($k_p/k_t^{0.5}$) and apparent k_p . $k_p/k_t^{0.5}$ calculated with initiator efficiency $f_{DTBP}=1$, initiator decomposition coefficient $k_d=1.71 \cdot 10^{-5} \text{ s}^{-1}$. ^(a) no initiator, ^(b) r_p until 40 % conversion, ^(c) r_p at ~ 5% conversion, ^(d) estimated with $k_t=9.6 \cdot 10^7 \text{ L} \cdot \text{mol}^{-1} \cdot \text{s}^{-1}$.

For comparison, the rates of polymerization for VDF polymerizations with C₆F₁₃I, C₆F₁₃Br and C₆F₁₃H are depicted in Figure 6.4.5. In contrast to the data referring to C₆F₁₃I, the rate data for the two lowest concentrations of PFBH and HPFH are rather similar. Again, for C₆F₁₃Br the unexpected increase in r_p with higher amounts of CTA is found. The enhanced reaction rates are surprising since the molecular weight data indicate not only a much weaker

chain transfer activity, but also that living conditions are not established (high PDI). These findings are in line with the higher BDE of C–Br bonds. If the C–Br affords more energy to be cleaved, it was anticipated that C₆F₁₃Br does not contribute significantly to initiation. Of course, the corresponding data for $k_p/k_t^{0.5}$ in Figure 6.4.6 show a similar behaviour: data for the two lowest C₆F₁₃Br and C₆F₁₃I concentrations are rather similar, whereas the other experiments with these two CTAs yield significantly higher values. The rather weak variation of $k_p/k_t^{0.5}$ with conversion indicates that the lowering of r_p with conversion in Figure 6.4.5 was caused by the reduction in VDF concentration. In contrast to the other two CTAs, the rate data for polymerizations in the presence of 1H-perfluorohexane show no variation with CTA concentration. The reactions at the lowest and highest CTA concentration yield identical rates of polymerization and identical $k_p/k_t^{0.5}$. The corresponding conversion dependence of $k_p/k_t^{0.5}$ is plotted in Figure 6.4.6. Again, a rather weak variation with conversion is found, which suggests that the decreasing rate of polymerization seen in Figure 6.4.5 is due to the lowering in VDF concentration. The values for $k_p/k_t^{0.5}$ obtained with HPFH are consistently higher than the values obtained from polymerizations with BrCCl₃ as CTA (see chapter 6.3). This finding suggests that in case of BrCCl₃ side reactions with the DTBP-derived radicals, as reported for extremely high BrCCl₃,⁴⁹ may occur to some degree at lower concentrations. Thus $k_p/k_t^{0.5}$ derived from reactions with BrCCl₃ is expected to contain contributions from side reactions. Hence, these values are not considered reliable.

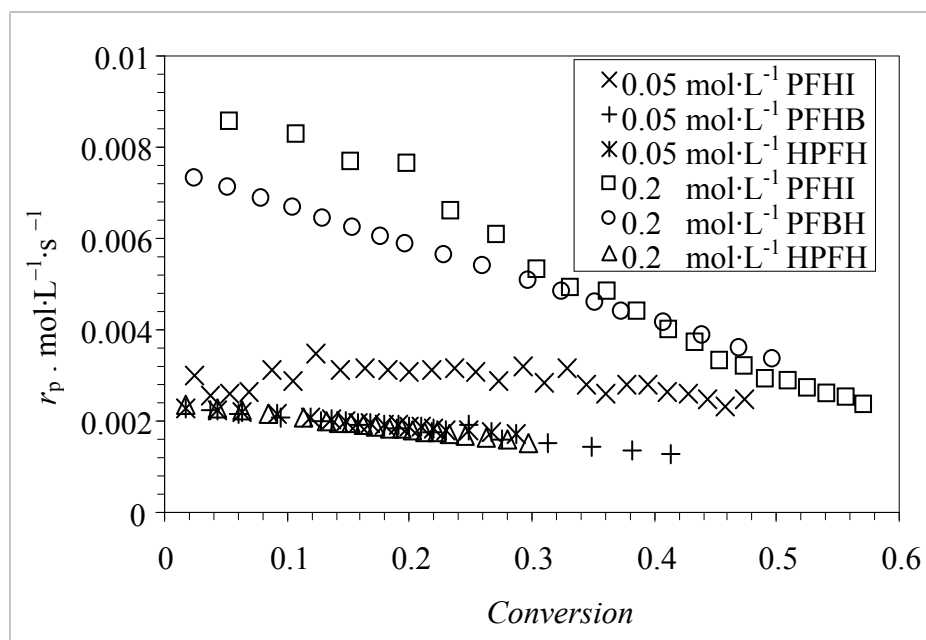


Figure 6.4.5: r_p - conversion plot from VDF polymerization at 120 °C, 1500 bar with 73 wt. % CO₂, 0.061 mol·L⁻¹ DTBP, 3.66 mol·L⁻¹ VDF with CTA concentrations as indicated.

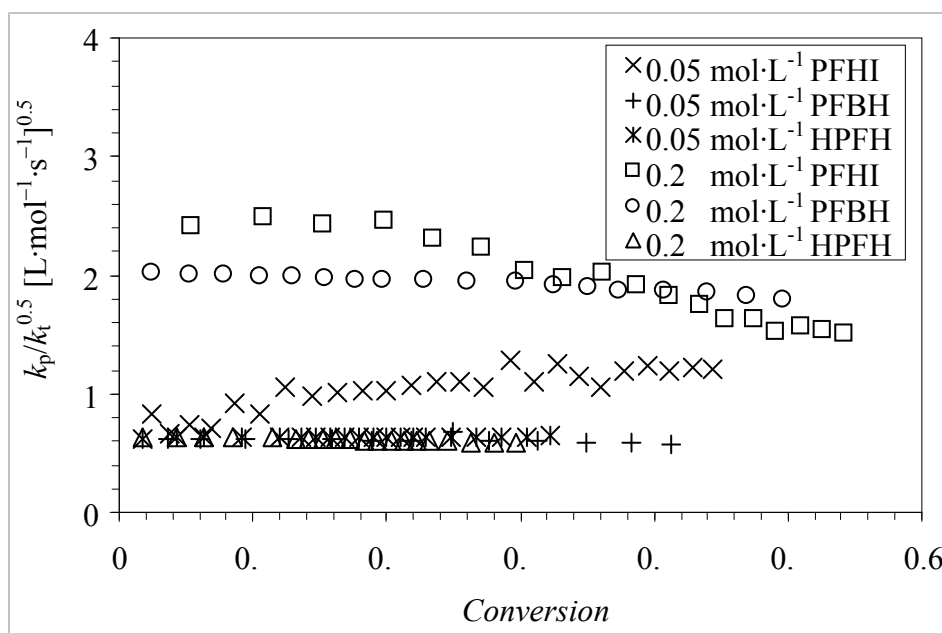


Figure 6.4.6: $k_p/k_t^{0.5}$ - conversion plot from VDF polymerization at 120 °C, 1500 bar with 73 wt. % CO₂, 0.061 mol·L⁻¹ DTBP, 3.66 mol·L⁻¹ VDF with CTA concentrations as indicated.

Since termination is a diffusion controlled reaction, it was assumed that k_t of the structural similar ethene should provide a reasonable estimate for k_t of VDF. Using a k_t value of $9.6 \cdot 10^7$ L·mol⁻¹·s⁻¹ calculated for 120 °C and 1500 bar according to ref. 95, apparent k_p values given in Table 6.4.4 were estimated. For polymerization in the presence of the lowest amount of C₆F₁₃H k_p in the order of $6 \cdot 10^3$ L·mol⁻¹·s⁻¹ is obtained. The same value is calculated for polymerizations with 0.05 mol·L⁻¹ C₆F₁₃Br. For polymerizations with C₆F₁₃Br an enhancement of CTA concentration is associated with an increase in $k_p/k_t^{0.5}$ and consequently with an increase in apparent k_p . At the highest C₆F₁₃Br concentration an apparent k_p of $20 \cdot 10^3$ L·mol⁻¹·s⁻¹ was obtained. For the lowest C₆F₁₃I concentration an apparent k_p of $10 \cdot 10^3$ L·mol⁻¹·s⁻¹ was obtained. Since it is highly unlikely that k_p is altered with molecular weight, the changes in apparent k_p reflect contributions from other reactions. The chain length dependence of k_t may be ruled out as a potential reason: with increasing CTA concentration the chain lengths are reduced and k_t will increase leading to a slower rate of polymerization. In contrast, an increase in r_p with CTA concentration was observed experimentally. A possible explanation may be seen in contributions of the CTA to the initiation reaction. The finding that r_p and $k_p/k_t^{0.5}$ are not affected by the concentrations of 1H-perfluorohexane suggests that this CTA induces no side reactions. Thus it can be concluded that reliable values for $k_p/k_t^{0.5}$ were determined. To test whether this 1H-perfluorohexane gives access to reliable

kinetic data and to decouple the rate coefficients for the termination and the propagation reaction, pulsed laser initiated polymerizations⁹⁵ should be carried out in the future.

6.4.5 Summary of results

This work has supplied kinetic data of the radical polymerization of VDF, initiated by di-*tert*-butyl peroxide, in the presence of three perfluorinated halogenated and non halogenated ($C_6F_{13}H$) chain transfer agents (CTAs): $C_6F_{13}X$. By using the method of Mayo and Lewis, the chain transfer constant, C_T , has been determined at 120°C for each CTA. The calculated values were $8 \cdot 10^{-1}$, $9 \cdot 10^{-2}$ and $2 \cdot 10^{-4}$ for $C_6F_{13}I$, $C_6F_{13}Br$ and $C_6F_{13}H$, respectively. The strong dependence of C_T on the X-atom in $C_6F_{13}X$ may be related to the bond dissociation energies of C-X. The stronger the C-X bond lowers the C_T value. The NMR analyses also show that there is insertion of monomer units between the two ends of the chain transfer agent in case of $C_6F_{13}I$ and $C_6F_{13}Br$. The fraction of DTBP-derived end groups is negligible. The CTA $C_6F_{13}H$ does not contribute to the initiation step, thus, it can be used to obtain reliable kinetic data $k_p/k_t^{0.5}$. At 120°C and 1500 bar the average value of $k_p/k_t^{0.5}$ is $0.65 (L \cdot mol^{-1} \cdot s^{-1})^{0.5}$.

The use of these CTAs has two major advantages. Firstly, by using these CTAs it is possible to obtain polymers in very different MW ranges. Secondly, the polymer end groups obtained are dissimilar: Polymer chains with $CF_3(CF_2)_5$ end groups at one end and I or Br at the other end are produced from these CTAs. This aspect is interesting as the type of terminal group in the polymer determines potential subsequent reactions and the properties of the polymer generated.

6.5 Polymer end groups effect on morphology and crystallization of PVDF

In chapter 6.1 it has been reported that VDF may be polymerized in scCO₂ in homogeneous phase using the conventional initiator di-*tert*-butyl peroxide (DTBP). After complete monomer conversion, expansion of the reaction mixture to ambient pressure conditions resulted in dry polymer material consisting of stack-like particles.⁶⁹ To reduce the amount of DTBP required, additional VDF polymerizations were carried out in the presence of perfluorinated hexyl iodide serving as a degenerative chain-transfer agent (see chapter 6.2).⁷⁰ Again, expansion of the reaction mixtures after polymerization resulted in particulate material. However, the visual appearance of these particles was different from the particles with DTBP-derived end groups. Thus, it seemed rewarding to study how polymer end groups of PVDF obtained from polymerization in scCO₂ affect the bulk and surface morphology as well as the melting and crystallization behaviour of the polymer. The polymers were analyzed by means of scanning electron microscopy, atomic force microscopy, Fourier transform infrared spectroscopy, wide angle X-ray diffraction and differential scanning calorimetry.

6.5.1 Polymers samples for analyses

PVDF samples with different end groups were applied to a detailed investigation into polymer properties. End groups analyses were carried out by ESI-MS and ¹H-NMR spectroscopy. The polymers under investigation are listed in Table 6.5.1. Number average molecular weights are based on polystyrene calibration of the SEC.

Sample	Appearance	MW control (mol·L ⁻¹)	End groups	M_n (g·mol ⁻¹)	<i>PDI</i>
DTBP-1 ^{a)}	fine powder	$c_{DTBP} = 0.307$	CH ₃ , (CH ₃) ₃ CO	2200	4.5
DTBP-2 ^{a)}	fine powder	$c_{DTBP} = 0.077$	CH ₃ ,(CH ₃) ₃ CO	6800	3.1
PFHI-1 ^{b)}	fine powder	$c_{PFHI} = 0.150$ ^{c)}	I, CF ₃ (CF ₂) ₅	2400	1.4
PFHI-2 ^{b)}	fine powder	$c_{PFHI} = 0.050$ ^{c)}	I, CF ₃ (CF ₂) ₅	6700	1.5
BTCM-1 ^{b)}	coagulated	$c_{BTCM} = 0.921$ ^{c)}	Br, CCl ₃	2100	1.6
BTCM-2 ^{b)}	fine powder	$c_{BTCM} = 0.230$ ^{c)}	Br, CCl ₃	6000	1.6

Table 6.5.1: Poly(vinylidene fluoride) samples employed in this work. Number average molecular weights, M_n ; polydispersity index, *PDI*; ^{a)}polymerization at 140 °C, 1500 bar ^{b)}polymerization at 120 °C, 1500 bar. ^{c)} concentration of di-*tert*-butyl peroxide (c_{DTBP}) = 0.061 mol·L⁻¹. c_{PFHI} and c_{BTCM} indicate the concentrations

of the CTA; $C_6F_{13}I$ and $BrCCl_3$, respectively. The monomer concentration was always 3.44 to 3.66 mol·L⁻¹.

The molecular weight data in Table 6.5.1 indicates that $C_6F_{13}I$ is a more efficient CTA than $BrCCl_3$. While 0.921 mol·L⁻¹ $BrCCl_3$ is required to yield polymer with M_n of 2100 g·mol⁻¹, only 0.15 mol·L⁻¹ $C_6F_{13}I$ was sufficient to yield a similar M_n value.

6.5.2 Positive ESI-MS analyses of PVDF

Electrospray ionization mass spectrometry (ESI-MS) has proven to be a valuable tool for end group analyses of synthetic polymers. Due to the soft ionization fragmentation may be omitted and end group functionalities may fully be retained in the ionized molecules. ESI-MS was applied to a large variety of polymers,¹⁰⁵⁻¹⁰⁸ including some fluoropolymers.¹⁰⁹ Here, ESI-MS was employed to characterize PVDF samples which were subsequently analyzed with respect to morphology and crystallinity. Unlike radical polymerizations of many other monomers chain growth in VDF polymerization predominantly proceeds via head to tail addition (see chapter 6.1).⁸¹ Thus, 94 to 97 % of all macroradicals carry terminal CF_2 groups. As a consequence termination occurs mainly via combination and contributions from disproportionation may be neglected. Therefore, species originating from bimolecular termination carry two end groups. As long as transfer of hydrogen is unlikely, hydrogen end groups will be scarce.

Firstly, PVDF from reactions with perfluorinated hexyl iodide is considered. Due to the high chain transfer constant of $C_6F_{13}I$ in VDF polymerizations,^{49,92} it was anticipated that chain growth was predominantly stopped by chain transfer events rather than by bimolecular termination with other radicals. In case of transfer being the major chain stopping event only a minor fraction of initiator-derived end groups are expected to be present in the macromolecules. To confirm that transfer is the major chain stopping event ESI-MS spectra were measured. Figure 6.5.1 gives such a spectrum for a PVDF sample with $M_n = 2400$ g·mol⁻¹ (PFHI-1). The spectrum shows a number of prominent peaks, which are periodically repeated. These peaks are separated by m/z of 64.03, the molar mass of the VDF monomer. The full spectrum exhibits a shape that is typical for the mass spectra of polymers produced by radical polymerization. The peak intensities do not quantitatively represent the actual chain-length distribution,¹¹⁰⁻¹¹² as the mode of ionization and further experimental parameters may affect mass sensitivity, in particular for low MW material. At higher molecular weights the observed shape is similar to the number distribution of the polymer, which decays towards

higher masses. These effects play a minor role upon considering the mass range of one monomer repeat unit, as shown in Figure 6.5.2. Ionization generally proceeds via sodium cations. The prominent peak occurring at $m/z = 1109.1$ is assigned to a species consisting of 10 VDF units, which was initiated by C_6F_{13} and terminated by transfer to "I". Formally, the mass of 1109.1 could also refer to a species with 7 VDF units that was initiated and terminated by C_6F_{13} , or to a species consisting of 13 VDF units that was initiated and terminated by "I". Based on the ESI-MS data a differentiation between these species is not possible. Thus, additional polymerizations were carried out with $C_8F_{17}I$. Corresponding ESI-MS spectra show prominent peaks at, e.g., $m/z = 1439.5$ which is unique for species of 13 VDF units carrying a C_8F_{17} and an iodine end group and a sodium cation from ionization. Thus, it may be concluded that using $C_6F_{13}I$ also species are formed, which carry one perfluorinated hexyl group and one iodine atom. This assignment is also in agreement with the finding that the use of $C_6F_{13}I$ leads to living radical polymerization conditions.⁸⁷ Considering the livingness of the systems containing $C_6F_{13}I$ M_n values may also be estimated according to $M_n = \alpha_{VDF} \times [C_6F_{13}I]_0 / [VDF]_0 \times M_{VDF}$, where α_{VDF} refers to VDF conversion, $[C_6F_{13}I]_0$ and $[VDF]_0$ to the initial concentrations of $C_6F_{13}I$ and VDF, respectively, and M_{VDF} is the molar mass of the monomer.⁸⁷ Knowing that complete monomer conversions were reached for PFHI-1 and PFHI-2 M_n values of 2000 and 5300 $g \cdot mol^{-1}$, respectively, were calculated. These values agree rather well with the SEC-derived values of 2400 and 6700 $g \cdot mol^{-1}$. The result indicates that SEC data for the low M_n samples are a good estimate of the absolute molecular weights, although polystyrene calibration was used.

PVDF species carrying DTBP-derived end groups, CH_3 or $(OC(CH_3)_3)$ are expected to occur at $m/z = 1125.3$ (CH_3 and I or C_6F_{13} as end groups) and at $m/z = 1119.3$ ($OC(CH_3)_3$ and I or C_6F_{13} as end groups) in Figure 6.5.2. The spectrum in Figure 6.5.2 indicates that these species are absent. Thus, it is concluded that chain initiation and chain termination are caused by the chain-transfer agent.

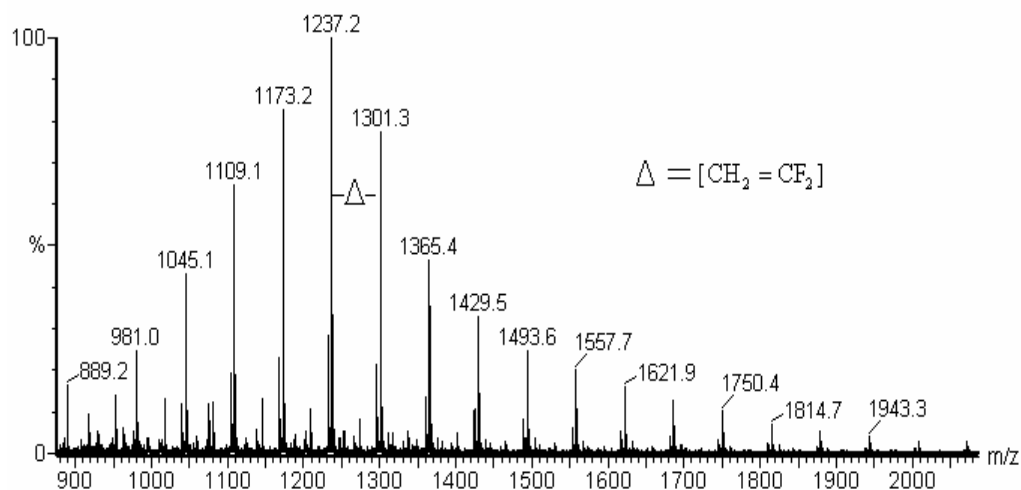


Figure 6.5.1: Electrospray mass spectrometry results for poly(vinylidene fluoride) polymerized at 120°C, 1500 bar initiated by 0.061 mol·L⁻¹ di-*tert*-butyl peroxide in the presence of 0.164 mol·L⁻¹ C₆F₁₃I (sample PFHI-1 in Table 6.5.1).

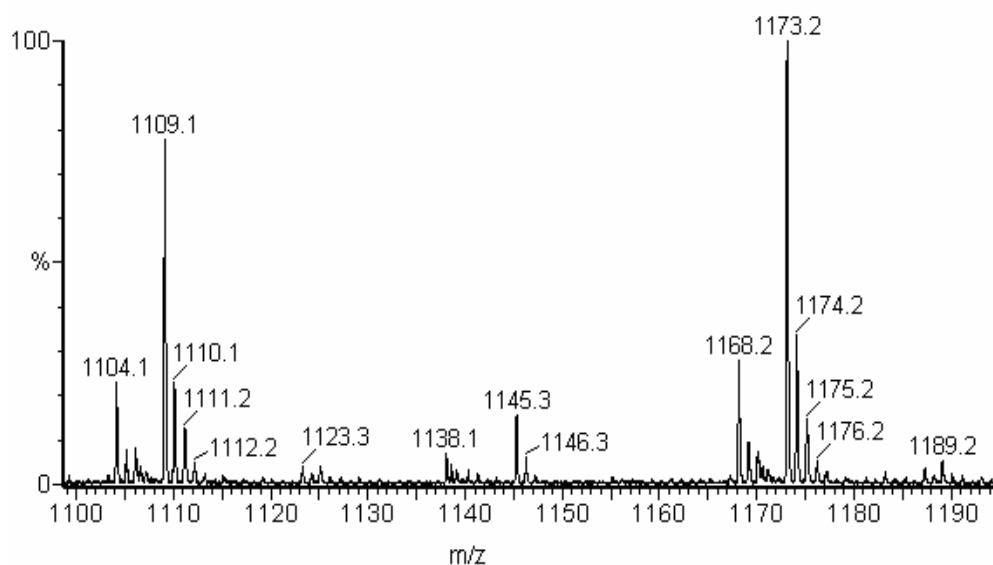


Figure 6.5.2: Expansion of the Electrospray ionization mass spectrometry results given in Figure 1 for poly(vinylidene fluoride) polymerized at 120°C, 1500 bar initiated by 0.061 mol·L⁻¹ di-*tert*-butyl peroxide in the presence of 0.164 mol·L⁻¹ C₆F₁₃I (sample PFHI-1 in Table 6.5.1).

ESI-MS analysis of PDVF samples with DTBP-derived end groups results in more complicated spectra. While still prominent peaks separated by $m/z = 64.03$ are observed, in between two neighbouring peaks a large number of smaller peaks are seen. These peaks may

be due to different DTBP-derived end groups. In addition, ESI-MS may also produce multiply charged ions and the ionization process may cause elimination of one or more HF molecules. The latter was not observed for PVDF from reactions in the presence of C₆F₁₃I. ESI-MS spectra for PVDF with BrCCl₃-derived end groups were not accessible. Thus, end groups had to be derived from ¹H-NMR spectra.

6.5.3 End groups analyses via ¹H-NMR spectroscopy

An ¹H-NMR spectrum of PVDF sample PFHI-1 is given in the upper part of Figure 6.5.3 in the spectral window from 0.9 to 4.5 ppm. Based on the detailed spectra discussion by the group of Ameduri and Boutevin the ¹H-NMR peaks may be assigned to the following groups:⁸⁷ 2.4 ppm is representative of tail to tail addition (-CF₂-CH₂-CH₂-CF₂-), whereas the peak at 2.9 ppm is assigned to normal head to tail addition (-CH₂-CF₂-CH₂-CF₂-). The peak at 3.3 ppm may be assigned to C₆F₁₃-CH₂-CF₂- groups. Iodine end groups give rise to peaks at 3.6 and 3.9 ppm, which are assigned to -CH₂-CF₂-I and -CF₂-CH₂-I, respectively. Acetone as solvent gives rise to a peak at 2.1 and a peak at 2.8 ppm is due to traces of water. Thermal decomposition of DTBP yields *tert*-butoxy radicals that will initiate polymerization and result in *tert*-butoxy end groups in the polymer. In principle, elimination of acetone from the *tert*-butoxy radicals may also occur. However, since the deacetonization yields a highly reactive methyl radical, this reaction is unlikely to occur. PVDF molecules carrying *tert*-butoxy end groups are expected to give rise to a NMR signal around 1.0 ppm for the methyl group. The ¹H-NMR spectrum in the upper part of Figure 6.5.3 indicates that even at a magnification by a factor of 10, as shown in the insert, there are no such contributions from methyl groups. Thus, the ¹H-NMR result indicates that DTBP-derived end groups are absent. Consequently, all PVDF chains are initiated and terminated solely by the action of C₆F₁₃I. This finding is in excellent agreement with analyses of the ESI-MS spectra. In addition, PVDF from polymerization with BrCCl₃ as chain transfer agent and DTBP as initiator was analyzed by ¹H-NMR spectroscopy. The peaks were assigned according to ref. 37. The ¹H-NMR spectrum in the lower part of Figure 6.5.3 contains the above-mentioned peaks at 2.3 and 2.9 ppm assigned to -CF₂-CH₂-CH₂-CF₂- and -CH₂-CF₂-CH₂-CF₂- sequences of the polymer backbone. Additional peaks at 3.9, 3.8 and 3.56 ppm may be assigned to -CF₂-CH₂-Br, CCl₃-CH₂-CF₂- and -CH₂-CF₂-Br units originating from chain transfer. The peak at 1.0 ppm characteristic for methyl protons is of negligible intensity compared to the other peaks (also illustrated by the tenfold magnification of the spectrum around 1.0 ppm given in the insert).

Thus, it is concluded that the fraction of initiator-derived end groups is negligible for PVDF from polymerizations with molecular weight control via both chain transfer agents.

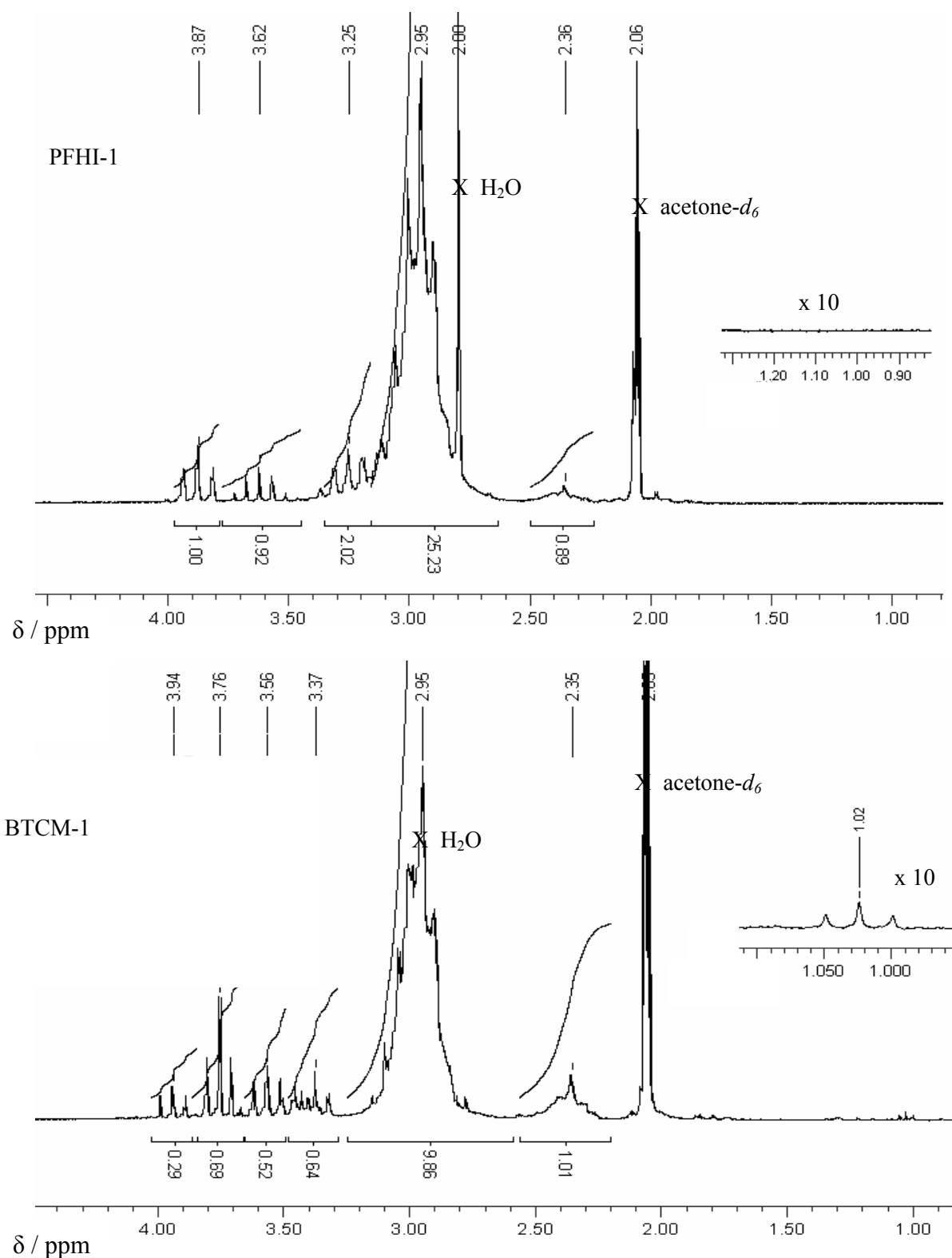


Figure 6.5.3: $^1\text{H-NMR}$ ($\text{acetone-}d_6$) of poly(vinylidene fluoride) polymerized at $120\text{ }^\circ\text{C}$ and 1500 bar initiated by $0.077\text{ mol}\cdot\text{L}^{-1}$ di-*tert*-butyl peroxide in the presence of $0.164\text{ mol}\cdot\text{L}^{-1}$ $\text{C}_6\text{F}_{13}\text{I}$ (upper spectrum, sample PFHI-1 in Table 6.5.1) or 0.921

$\text{mol}\cdot\text{L}^{-1}$ BrCCl_3 (lower spectrum, sample BTCM-1 in Table 6.5.1). The spectra around 1.0 ppm were magnified by a factor of 10 and are shown as inserts.

In addition to information on the polymer end groups, the ^1H -NMR spectra also allow for the detection of significant contributions from chain transfer to polymer resulting in $\text{H-CF}_2\text{-CH}_2$ sequences.⁷⁸ As discussed in literature these protons give rise to a peak at 6.3 ppm. For PVDF samples with $\text{C}_6\text{F}_{13}\text{I}$ - and BrCCl_3 -derived end groups the NMR spectra do not show any prominent peak at 6.3 ppm. For PVDF with DTBP-derived an end group a peak of very low intensity is observed. However, the intensity is too low for obtaining reliable results from spectra integration, since the integral is of similar value as the integral of the baseline calculated for the same range. Thus, it may be concluded that transfer to polymer occurs only to a very low extent, and thus, the high polydispersity of samples DTBP-1 and DTBP-2 is caused by the high DTBP concentrations required for MW control. This explanation is supported by the fact that the polydispersity is significantly larger for the low MW sample. Due to the absence of significant chain transfer to polymer linear chains were obtained.

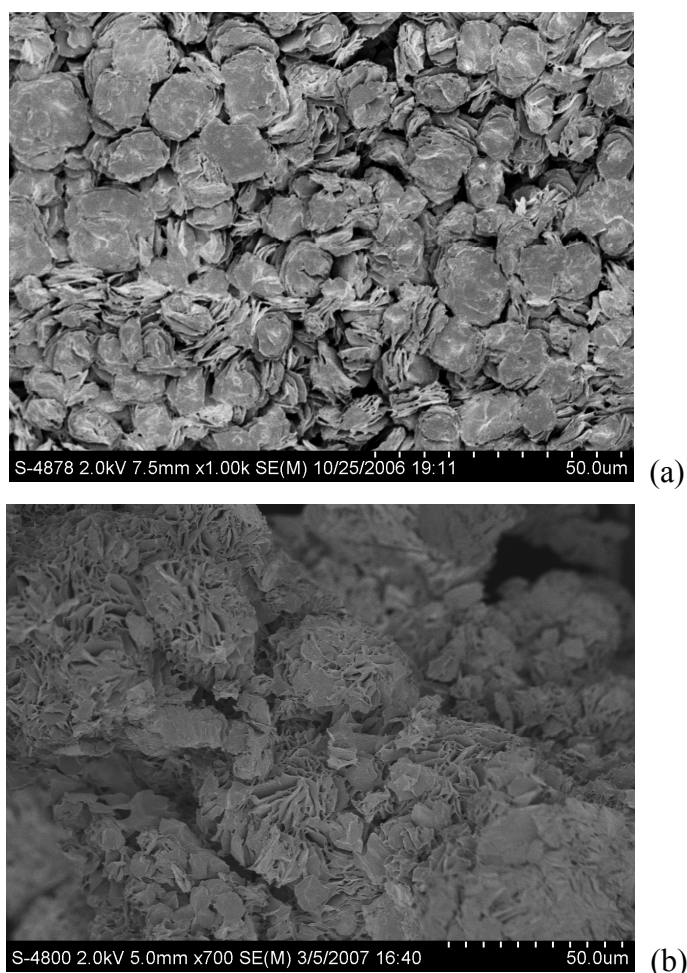
The results from ESI-MS and ^1H -NMR prove that the amount of DTBP-derived end groups is negligible, if polymer molecular weights are controlled by the chain transfer agents BrCCl_3 or $\text{C}_6\text{F}_{13}\text{I}$. Of course, polymers obtained from reactions in the absence of any chain transfer agents give rise to DTBP-derived end groups.⁶⁹ The predominant end groups of the polymers employed in the study on the morphology of PVDF polymers are listed in Table 6.5.1. Further, ^{19}F -NMR spectra were recorded, which also confirm the end group analyses.

Besides allowing for end group analyses, NMR spectra were used to estimate absolute M_n values and the fraction of the so-called defect structures resulting from tail to tail addition. The M_n values derived are within 30 % of the M_n values derived from SEC employing polystyrene calibration, e.g., the NMR-derived value of M_n for sample PFHI-1 is $2000 \text{ g}\cdot\text{mol}^{-1}$ compared to $2400 \text{ g}\cdot\text{mol}^{-1}$ from SEC. The fraction of defect structures amounts to 7 % for PFHI-1 and DTBP-1 and to 12 % for BTCM-1. These numbers are rather high, however, it has to be kept in mind that the polymerizations were carried out up to complete monomer conversion and consequently accumulating more defect structures than in low conversion polymerizations generally reported in literature.⁴⁹

6.5.4 Morphology of different PVDF samples

Visual observation of the PVDF samples listed in Table 6.5.1 indicated that different morphologies ranging from fine free-flowing powder to coagulated material were found. To

get further information on the morphology SEM images were measured for the samples listed in Table 6.5.1. The SEM images obtained for PVDF with M_n between 2100 and 2400 $\text{g}\cdot\text{mol}^{-1}$ are given in Figure 6.5.4. The upper SEM image (a) for sample DTBP-1 shows small stacks of layered material. The size of these stacks is around 10 μm and the particle size distribution is rather narrow. The SEM image (b) in the middle was obtained for PVDF with $\text{C}_6\text{F}_{13}\text{I}$ -derived end groups. Here, a sponge-type morphology is observed. Finally, BrCCl_3 -derived PVDF end groups result in coagulated material that does not show any distinct structures. The observation of these very different morphologies is in accordance with the visual impression of the polymers.



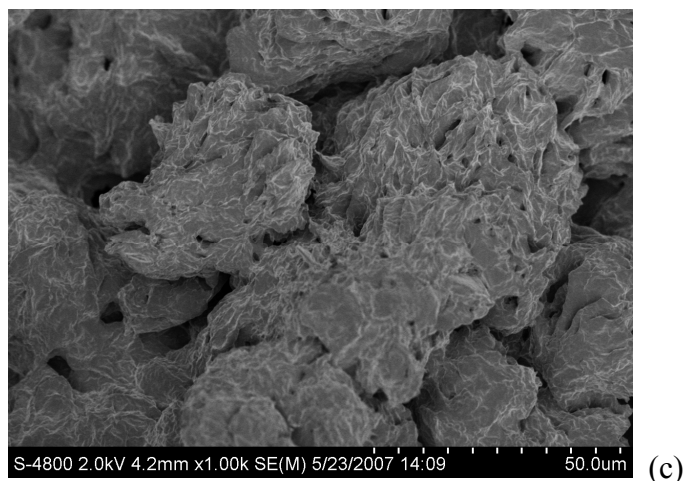


Figure 6.5.4: Scanning electron microscopy images of poly(vinylidene fluoride) (PVDF) samples collected after expansion of the reaction mixture at polymerization conditions to ambient conditions. PVDF samples with number average molecular weights range from 2100 to 2400 $\text{g}\cdot\text{mol}^{-1}$ and end groups originating from di-*tert*-butyl peroxide (a), $\text{C}_6\text{F}_{13}\text{I}$ (b), and BrCCl_3 (c).

It was anticipated that the influence of the polymer end groups is more pronounced for low molecular weight (MW) material than for higher molecular weights. To test whether differences also occur for higher MW material a second set of SEM images shown in Figure 6.5.5 was measured for polymers with M_n ranging from 6000 to 6800 $\text{g}\cdot\text{mol}^{-1}$. As expected the images of the three polymers seem to be less different. In all cases material with small-scale morphology is found. Again, for DTBP-derived end groups stack-type particles are observed, which are not significantly different from the particles for the low MW sample of Figure 6.5.4. Using $\text{C}_6\text{F}_{13}\text{I}$ as transfer agent also results in polymer with lamellar structures. In case of BrCCl_3 as transfer agent small rose petal like structures, having a diameter of around 25 μm , are seen. In contrast, the low MW polymer (BTCM-1) resulted in coagulated material.

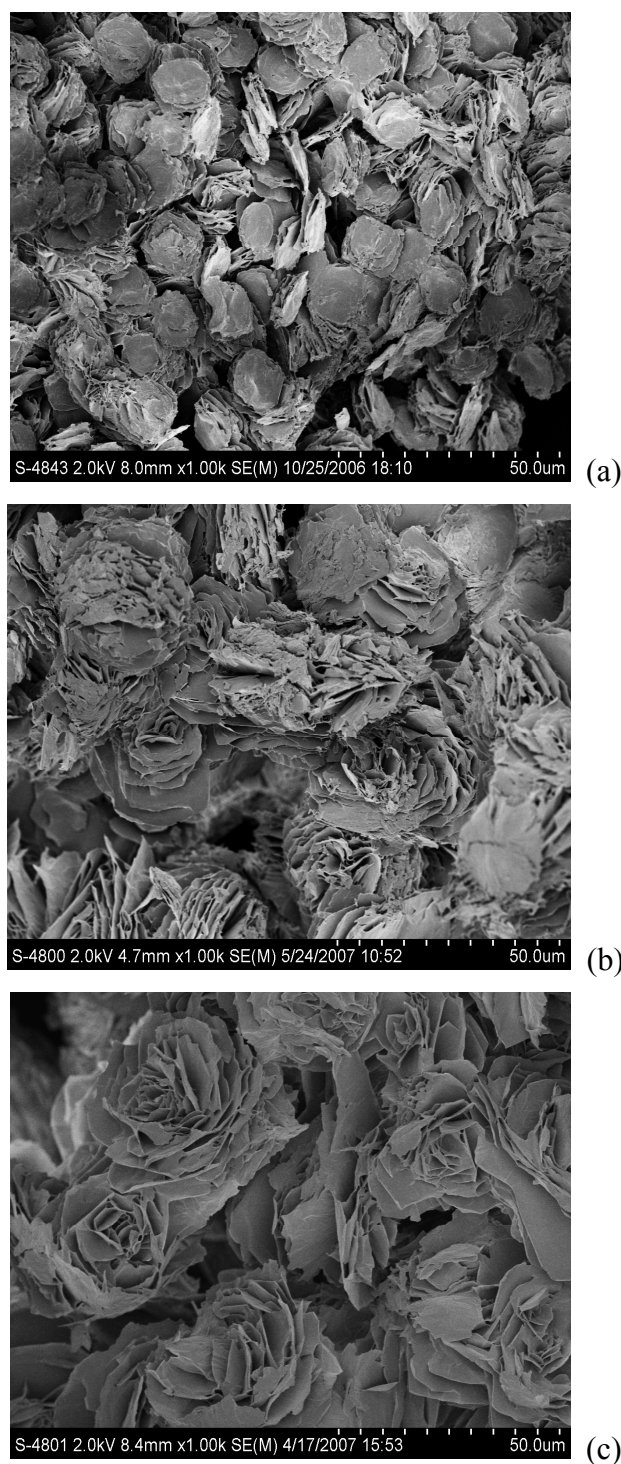


Figure 6.5.5: Scanning electron microscopy images of poly(vinylidene fluoride) (PVDF) samples collected after expansion of the reaction mixture at polymerization conditions to ambient conditions. PVDF samples with number average molecular weights ranging from 6000 to 6800 $\text{g}\cdot\text{mol}^{-1}$ and end groups originating from di-*tert*-butyl peroxide (a), $\text{C}_6\text{F}_{13}\text{I}$ (b), and BrCCl_3 (c).

6.5.5 DSC and crystallinity

The SEM images indicate that polymer end groups as well as polymer MW influence polymer morphology upon expansion to ambient conditions. To understand why the above-described differences in morphology occur, the degree of crystallinity of the polymer samples was investigated applying DSC. Figures 6.5.6a and 6.5.6b give the heating curves of the low and high MW samples, respectively.

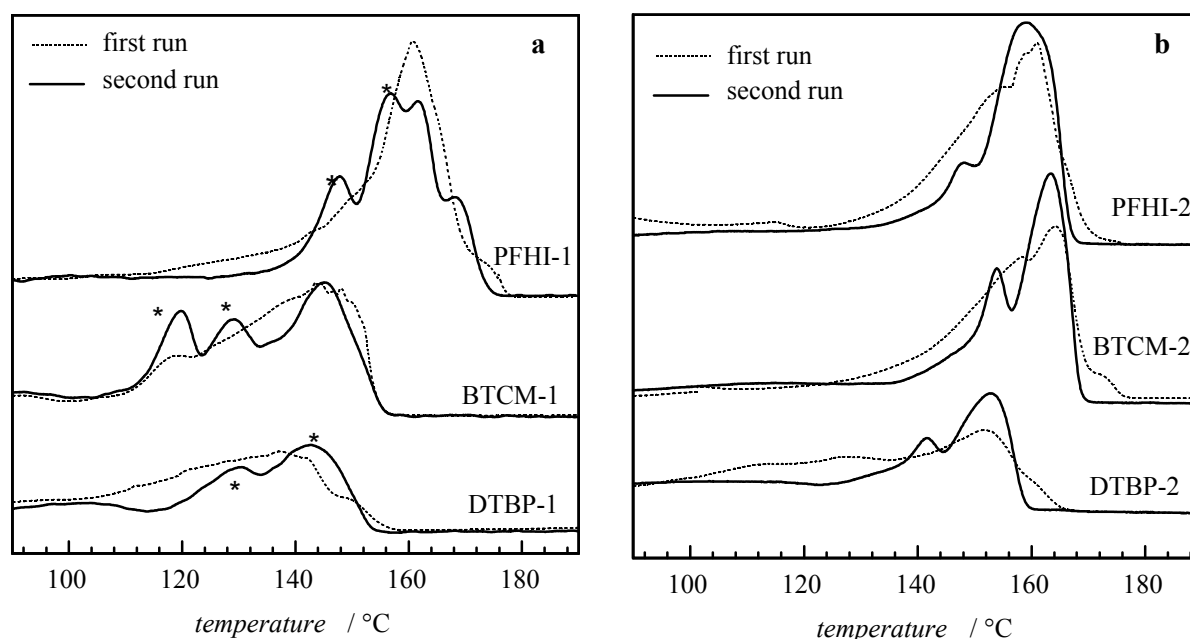


Figure 6.5.6: Differential scanning calorimetry results for poly(vinylidene fluoride) samples with different end groups and number average molecular weights, M_n . Dotted lines: first heating cycle, full line: second heating cycle. The acronyms in the diagrams refer to Table 6.5.1.

From literature it is well known that the morphology of PVDF may be varied by many experimental parameters, e.g., such as the speed of cooling,¹¹³ the CO₂ pressure or the pressure at which crystallization occurs.^{114,115} In addition, the polymers obtained upon expansion from CO₂ + polymer mixtures to ambient pressure may contain varying amounts of CO₂ dissolved in the polymer. Moreover, in contrast to most PVDF crystallization studies reported in literature, expansion of CO₂ + polymer mixtures is a non-equilibrium process, in which temperature and pressure change occurs very rapidly, typical values are 10⁷ bar·s⁻¹ and 10⁹ K·s⁻¹.¹³⁰ As a consequence expansion may give rise to heterogeneous material. Thus, it seemed important to measure two heating cycles. Due to crystallization of the material in the

DSC instrument at a constant cooling rate of $10\text{ }^{\circ}\text{C}\cdot\text{min}^{-1}$ the samples employed in the second heating run underwent identical treatment prior to melting. In Figures 6.5.6a and 6.5.6b the curves from the first heating cycle are represented by the dotted line and the second cycle by the full line. Generally, the first heating curve is less structured than the second. Firstly, the DSC results of the low MW samples depicted in Figure 6.5.6a are considered. The curves from the second heating cycle are almost as broad as the first curves. For sample BTCM-1, which showed the glue-type structure in the SEM image, the temperature range for melting extends from around 108 to 138°C . Material with DTBP-derived end groups melts at slightly higher temperature. For $\text{C}_6\text{F}_{13}\text{I}$ -derived end groups the temperature range for melting is the highest and starts at around 149°C . As for the low MW material the first heating cycles result in less structured curves, which show indications of bimodality. For all three samples the second heating cycle results in well resolved bimodal curves. The DSC results for the higher MW samples are depicted in Figure 6.5.6b. The temperature range for melting is very similar for BTCM-2 and PFHI-2. Sample DTBP-2 melts at slightly smaller temperatures. For comparison the two peak maxima are listed in Table 6.5.3. For the low MW samples the peaks marked with a star in Figure 6.5.6a are listed.

Sample	$T_m^{\text{I}} / ^{\circ}\text{C}$	$T_m^{\text{II}} / ^{\circ}\text{C}$	$T_c / ^{\circ}\text{C}$	$\Delta H_m (\text{J}\cdot\text{g}^{-1})$	$X (\%)$
PFHI-1	149.4*	156.7*	131.2	65.3	62
BTCM-1	108.1*	138.1*	104.2	44.2	42
DTBP-1	130.7	142.7	109.5	27.2	26
PFHI-2	148.1	158.9	123.6	67.2	64
BTCM-2	154.1	163.5	130.0	50.7	49
DTBP-2	141.6	152.6	117.8	30.0	29

Table 6.5.3: Results from differential scanning calorimetry. Melting temperatures, T_m^{I} , T_m^{II} refer to the first and second peak maximum observed in the second heating cycle. * T_m^{I} and T_m^{II} as indicated by the stars in Figure 6.5.6a. T_c : crystallization temperature, ΔH_m : melting enthalpy; X : crystallinity.

For comparison with literature the melting temperatures of the higher MW samples are considered. The first melting temperature, T_m^{I} , lies between 141.6 and $154.1\text{ }^{\circ}\text{C}$, the second melting temperature, T_m^{II} , between 152.6 and 163.5°C . Typical melting temperatures for high

MW α phase PVDF are in the range of 163 °C. Recently, bimodal DSC curves were reported for PVDF. The peak around 165 °C was assigned to β phase material and the peak around 173 °C to α phase material.¹¹⁶ In contrast, Greorgio reported that the melting temperature of α and β phase material determined by DSC is not significantly different.¹¹⁷ The occurrence of different DSC peaks for α phase PVDF was assigned to the mode of crystallization, rapid crystallization by temperature quenching or slow crystallization at isothermal conditions. Moreover, Shieh et al. reported that the size of the crystallites influences the DSC heating curve.⁴⁷ Multimodal crystal size distributions result in broad DSC curves. Already this small selection of potential influences on the DSC curves indicates that an assignment of the peaks observed to the various polymorphs of PVDF is not advisable.

However, the DSC results allow for the calculation of the degree of crystallinity, X . To allow for the calculation of X according to $X = \Delta H_m / \Delta H_c$ the melting enthalpy, ΔH_m , was determined by integration of the DSC curve of the second heating cycle. The results are listed in Table 6.5.3. $\Delta H_c = 104.5 \text{ J}\cdot\text{g}^{-1}$ for perfectly crystalline PVDF was used to calculate X , assuming that the heat of fusion for both crystalline forms is the same for 100 % crystalline material.¹¹⁶ For the low MW samples, the highest melting enthalpy of $63.5 \text{ J}\cdot\text{g}^{-1}$ associated with a crystallinity degree of 62 % is found for PFHI-1, whereas for DTBP-derived end groups (DTBP-1) a melting enthalpy of $27.2 \text{ J}\cdot\text{g}^{-1}$ and a crystallinity of 26 % was derived. It is interesting to note that the most massive and heavy chain end groups give rise to the highest melting temperature, which suggests that the entropy of melting decreases with an increase in the weight of the chain end group, because of suppression of the chain mobility by the heavy chain end group in the melt.

For all samples the degree of crystallinity for the higher MW sample is enhanced compared to the low MW sample. This enhancement is very similar for all samples: for PVDF with $\text{C}_6\text{F}_{13}\text{I}$ or DTBP derived end groups crystallinity increases by almost 2-3 %. PVDF samples obtained in the presence BrCCl_3 chain transfer agent show an increase in crystallinity by 7 % with increasing M_n . The variation of crystallinity with MW for the three different polymer end groups is illustrated in Figure 6.5.7.

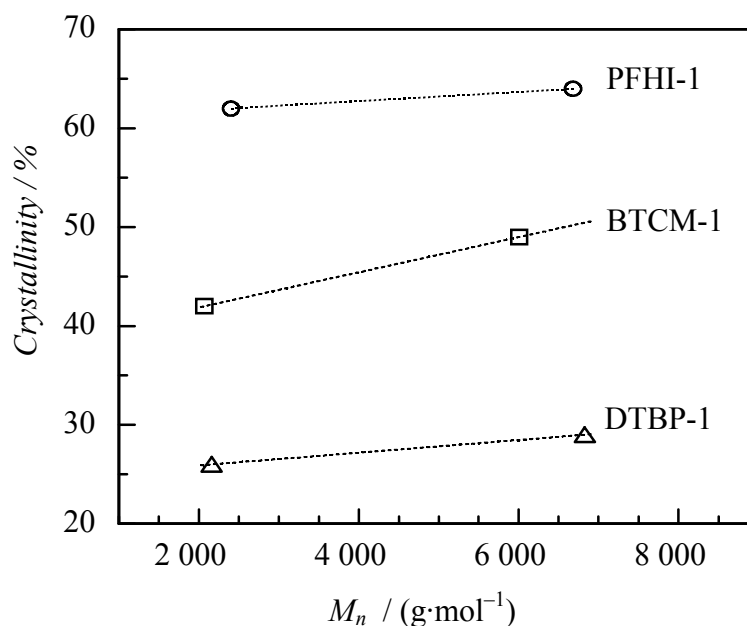


Figure 6.5.7: Crystallinity, as a function of the number average molecular weight, M_n , for poly(vinylidene fluoride) samples with end groups originating from di-*tert*-butyl peroxide (triangles), BrCCl_3 (squares) and $\text{C}_6\text{F}_{13}\text{I}$ (circles).

Table 6.5.3 indicates that the melting temperature is higher for the higher MW samples. In contrast to the observation for the crystallinity, this enhancement is not uniform. For comparison T_m^{II} is considered: For $\text{C}_6\text{F}_{13}\text{I}$ -derived end groups corresponding to samples with highest crystallinity at each MW, the increase in T_m^{II} is only 2.2°C. For BrCCl_3 -derived end groups T_m^{II} increases by 25.4°C and for DTBP-derived end groups by 9.9°C. The findings for T_m are paralleled by the crystallization temperatures, T_c , derived from the cooling curves. All cooling curves show a single sharp peak. Different cooling scans of a single sample do not result in significant differences. The T_c values are contained in Table 6.5.3. Keeping the end group constant and increasing M_n yields an increase in T_c . For BrCCl_3 -derived end groups T_c increases by 25.8°C, whereas for the other two end groups T_c is enhanced by 8.0°C upon increasing M_n . The high MW samples show at most a variation in T_c by 12.2°C, whereas the low MW samples lead to T_c values varying by as much as 27°C. With respect to melting and crystallization temperatures sample BTM-1, whose SEM image indicated a glue-type surface rather than distinct structures, shows exceptional behaviour. However, with respect to crystallinity both BTM samples are intermediate between the corresponding PFHI and DTBP samples.

Since the first and second heating curves show close proximity it may be concluded that the differences in crystallinity observed for the samples with different end groups are not due to the expansion process but are inherent to the constitution of the PVDF material. While the

degree of crystallinity may be derived from DSC analysis, the unambiguous assignment of the types of polymorphs present is not possible. To determine the different PVDF crystal phases FTIR and WAXD analyses were applied.

6.5.6 Polymorphs of PVDF and FT-IR analyses

PVDF was reported to have at least four important crystalline phases, α , β , γ and δ . These different forms are distinguished by the conformation of C–C bonds along the polymer main chain. The α phase has alternating trans and gauche bonds (TGTG), the β phase has all trans bonds (TTTT), the γ phase has a gauche bond every fourth repeat unit (T_3GT_3G), and the δ phase is very similar to the α -crystalline phase except that every other chain is rotated.¹¹⁸ As reported in literature, the different crystalline phases may be distinguished by differences in their IR spectra.^{117,119-122} The characteristic bands of the α phase are 530 cm^{-1} (CF_2 bending), 615 and 765 cm^{-1} (CF_2 bending and skeletal bending), 796 cm^{-1} (CH_2 rocking), 976 cm^{-1} (CH_2 twisting) and a peak at 1178 cm^{-1} . The β phase is associated with absorptions at 510 cm^{-1} (CF_2 bending) and 840 cm^{-1} (CH_2 rocking). Absorptions at 512 , 776 , 812 , 833 and 840 cm^{-1} are characteristic for the γ phase.

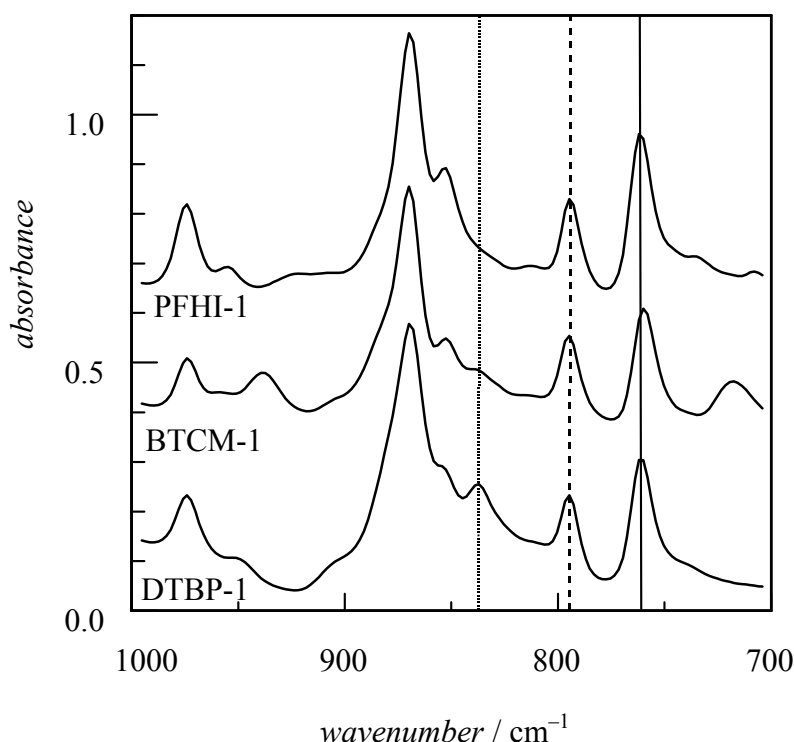


Figure 6.5.8: Fourier Transform Infrared spectra of poly(vinylidene fluoride) samples with number average molecular weights between 2100 and $2400\text{ g}\cdot\text{mol}^{-1}$ and end groups originating from the initiator di-*tert*-butyl peroxide (DTBP-1), from $\text{C}_6\text{F}_{13}\text{I}$ (PFHI-1), and from BrCCl_3 (BTCM-1).

Figure 6.5.8 gives IR spectra of samples PFHI-1, BTCM-1 and DTBP-1. The absorptions at 763 and 795 cm^{-1} (indicated by full and dashed line) characteristic for α phase PVDF are clearly seen in all samples. The IR spectrum of sample BTCM-1 shows two peaks at 717 and 938 cm^{-1} not seen in the other spectra. The peaks may be assigned to CCl_3 and Br as polymer end groups, respectively. The characteristic band at 840 cm^{-1} (indicated by the dotted line), that may be assigned to the β and γ phase, is present in all spectra, whereas the bands at 776, 812 and 833 cm^{-1} characteristic for the γ phase are absent in all three samples. Thus, it may be anticipated that the peak at 840 cm^{-1} refers to the β phase.

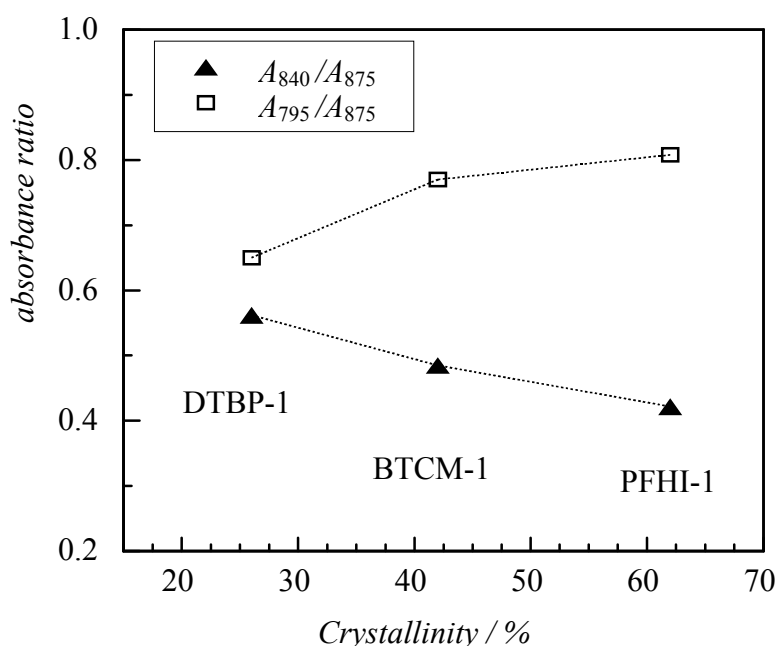


Figure 6.5.9: Absorbance ratios A_{795}/A_{875} and A_{840}/A_{875} as calculated from FT-IR spectra given in Figure 6.4.8. A_{795} , A_{840} and A_{875} are the absorbances at 795 cm^{-1} , 840 cm^{-1} and 875 cm^{-1} , respectively.

As previously reported the band at 875 cm^{-1} (CH_2 bending) is observed for α and β phase polymorphs and may be used as an internal standard for comparison of different spectra.⁴⁷ The ratios of A_{795}/A_{875} and A_{840}/A_{875} provide information on the fraction of α and β polymorphs contained in the sample. A_{795} , A_{840} and A_{875} are the absorbances at 795 cm^{-1} , 840 cm^{-1} and 875 cm^{-1} , respectively. Figure 6.4.9 gives the ratios of A_{795}/A_{875} and A_{840}/A_{875} derived from the IR spectra as a function of the degree of crystallinity. The diagram indicates that the lowest degree of crystallinity is associated with the least differences in the ratio of A_{795}/A_{875} and A_{840}/A_{875} : The differences in the fraction of α and β phase material present in the sample are the lowest. The ratio A_{795}/A_{875} and thus the amount of α crystal phase present in the

sample are enhanced as the overall crystallinity increases. These changes are associated with a decrease in the β phase ratio as overall crystallinity is increasing.

FT-IR spectra recorded for the high MW samples are very similar to the corresponding low MW spectra in Figure 6.5.8. Generally, the absorption at 840 cm^{-1} is slightly weaker than for the low MW samples indicating that the fraction of α phase material is enhanced with increasing molecular weight.

Analyses of the absorptions at 840 cm^{-1} and 795 cm^{-1} in Figure 6.5.9 indicated that the lowest fraction of β -phase material was found for the rather large iodine end group. Literature information on the influence of polymer end groups on the polymorphs of PVDF is scarce. One article reports that iodine end groups give rise to α phase material, contributions from β phase material were not considered.¹²³ Qualitatively, this result is in agreement with the finding of this work that the lowest fraction of β crystal phase occurs for PVDF with an iodine end group. To confirm the assignments of our IR absorption peaks to α and β phase PVDF, additional wide angle X-ray diffraction analyses were carried out.

6.5.7 Wide angle X-ray diffraction: (WAXD)

According to Lovinger¹²⁴ the diffraction peaks of (100), (020), and (110) of the α form appear at 17.4, 18.6, 19.5, while the diffraction peak of the β form appears at 20.5 and the diffraction peak of the γ form appears at 14.8. The spectra shown in Figure 6.5.10 clearly indicate no significant contributions from the γ phase, which confirms the above-given peak assignment of the FTIR absorptions. Further, the diffraction peaks shown in Figure 6.5.10 indicate a predominant occurrence of the α phase, since contributions from the β phase are weak as shown by the rather small diffraction peak at 20.4 - 21.1 (#4). The ratio of the intensities of peaks #1, #2 and #3 assigned to the α phase are very similar for PVDF with DTBP or PFHI-derived end groups, whereas peaks #2 and #3 are more intense for sample BTCM-1. The biggest difference, however, is seen for #4 assigned to the β phase. According to Lovinger, the diffraction peaks of (100) and (200) corresponding to the β -phase polymorph overlap at 20.7. The sharpness of this diffraction peak (#4) is found to decrease with increasing β -phase, indicating that the degree of crystallinity of PVDF decreases. While a strong diffraction peak at 20.68 is seen for PVDF with DTBP and BTCM-derived end groups, this peak is rather weak for PFHI-1. To analyze the WAXD spectra the intensity of the diffraction peak at 26.2 - 26.7 (#5)^o for the α phase and at 20.4 - 21.1 (#4) for the β phase are listed in Table 6.5.4. To characterize the α phase peak #5 was considered rather than peaks #1, #2 or #3, since #5 is more isolated showing a flat baseline which increases the accuracy of the intensity

determination. While very similar intensities for the α phase are found for DTBP and BTCM-derived end groups, PFHI-1 shows a slightly higher intensity. Conversely, PFHI shows the weakest intensity of peak #4 in comparison to the other two samples. This finding is in excellent agreement with the results from FTIR, which also indicated lower amounts of β phase in both PFHI samples.

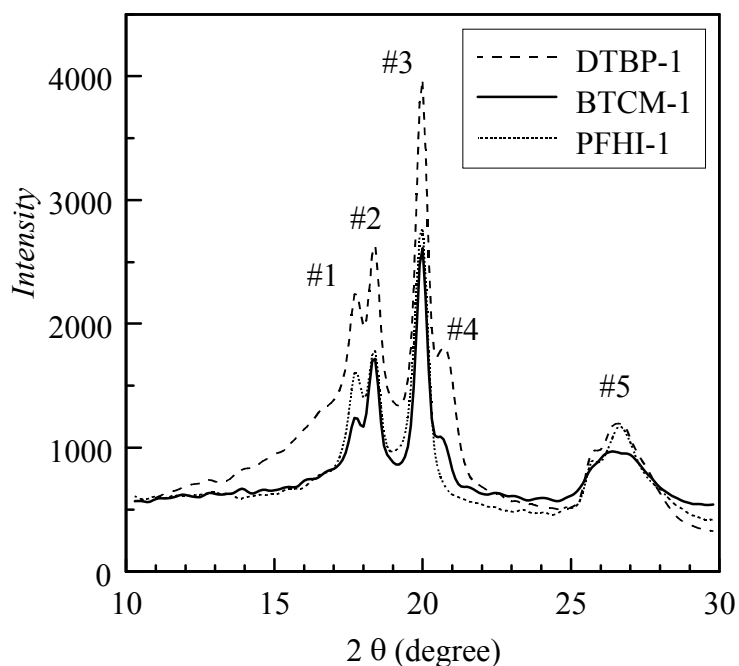


Figure 6.5.10: Wide angle X-ray diffraction spectra of poly(vinylidene fluoride) samples with number average molecular weights between 2000 and 2400 $\text{g}\cdot\text{mol}^{-1}$ and end groups originating from the initiator di-*tert*-butyl peroxide (DTBP-1), from $\text{C}_6\text{F}_{13}\text{I}$ (PFHI-1), and from BrCCl_3 (BTCM-1). The acronyms refer to Table 6.5.4, where further details are given.

sample	intensity of peak #4 (β phase)	intensity of peak #5 (α phase)	X / %
PFHI-1	723	1068	62
BTCM-1	971	900	42
DTBP-1	1625	920	26

Table 6.5.4: Comparison of crystallinity, X , and intensities of wide angle X-ray diffraction (WAXD) peaks in the 2θ range from 22.2 to 26.7 (#5) and from 20.4 to 21.1 (#4) assigned to α and β phase material, respectively. Details of the samples are given in Table 6.5.1.

6.5.8 AFM images of PVDF

Since morphologies after expansion of the reaction mixture as well as crystallinity and the content of α and β phase were strongly affected by the type of end group, it seemed rewarding to examine the surface morphology and the 3D topology applying AFM. Sample preparation for AFM required the dissolution of the polymer in DMSO and subsequent evaporation of the solvent. As detailed above, DSC analyses showed that differences in crystallinity of the samples remain even after several melt and crystallization cycles. Thus, sample preparation for AFM measurements is not expected to eliminate differences due to the polymer end groups.

The AFM images of the low MW samples are given in Figure 6.5.11. In all cases no homogeneous coverage of the substrate was achieved. The images indicate some organization of the polymer leading to different patterns on the surface. As can be seen in Figure 6.5.11a, the surface of the PFHI-1 sample is rather smooth with distinct indentations leading to round flower-like structures with overall diameters of roughly 20 μm . The average height of the structure is in the order of 4 nm. In case of DTBP-derived end groups the AFM image in Figure 6.5.11b shows two mostly flat circles, which have a diameter of around 4 μm and an average height of 4 nm, as observed for the material with $\text{C}_6\text{F}_{13}\text{I}$ -derived end groups. In contrast to the image in Figure 6.5.11a, in the centre of these cyclic structures some spikes are seen. Even more spikes are visible in the AFM image for the BTCM-1 sample depicted in Figure 6.5.11c, which make it difficult to identify the surface structure. However, again spherical structures are seen and the height of the material is below 10 nm. It may be concluded that the surface is not as flat and smooth as for the other two samples. This finding is in agreement with the SEM image of sample BTCM-1, which shows glue-type material rather than any clear structure.

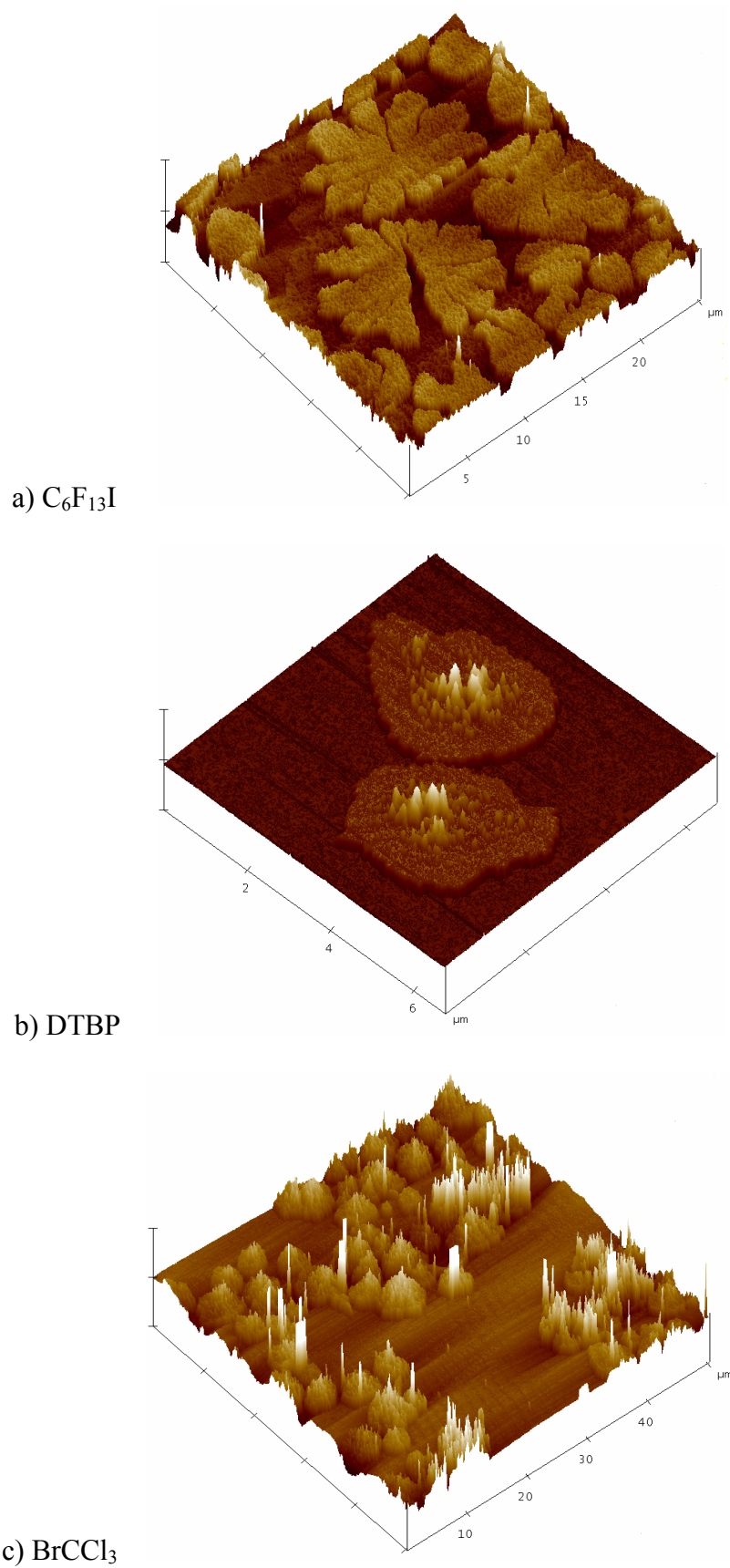


Figure 6.5.11: Atomic force microscopy images of the surface of poly(vinylidene fluoride) samples with number average molecular weights around $2200 \text{ g}\cdot\text{mol}^{-1}$.

Despite the differences observed in Figures 6.5.11a-c, in all cases round structures with diameters being below 25 μm and a thickness below 10 nm were obtained. The formation of flat-on lamella as shown in Figures 6.5.11a and 6.5.11b was reported for crystallization from films with a thickness below 300 nm. For films thinner than 15 nm it was observed that they tend to break-up and form dendritic structures.¹²⁵ The AFM images shown in Figure 6.5.11 indicate that not only the film thickness, but also the polymer end groups significantly affect the surface morphology of PVDF deposited on a substrate. The formation of structures as shown in Figure 6.5.11a for PVDF with $\text{C}_6\text{F}_{13}\text{I}$ -derived end groups were assigned to dewetting phenomena.¹²⁶ The break-up of the PVDF films is in accordance with the generally weak cohesion energies of fluoropolymers.

The spikes seen on the surfaces may be artefacts, since AFM measurements were carried out using routine procedures. However, since spikes are almost absent for sample PFHI-1, the polymer with the lowest fraction of β phase material, and since it was shown that AFM may be used to study the ferroelectricity of PVDF¹²⁷ or to polarize ferroelectric domains,¹²⁸ it cannot be excluded that the spikes are due to interactions between the piezoelectric material and the cantilever.

6.5.9 Summary of results

The results reported indicate that polymer end groups have a significant influence on polymer morphology, the ratio of α and β phase material, the overall degree of crystallinity, melting and crystallization temperature as well as the film formation on silica. For example, based upon choice of end groups and molecular weight PVDF with overall degrees of crystallinity ranging from 26 to 64% are accessible. The differences in melting and crystallization temperatures remained even after three heating cycles. Although rather low molecular weight material was used, the lower MW samples still consisted of polymer molecules containing around 30 monomer units (estimated from M_n) and the higher MW samples of polymer molecules with 91 to 104 monomer units. In addition, it should be noted that the end group induced differences are larger than the changes induced by molecular weight. Further, AFM results show that thin films in the range of nanometers were obtained on silica. The type of end groups determines the structure of these films.

6.6 Rapid expansion of supercritical solution (RESS) for PVDF

As shown in section 6 PVDF with end groups derived from di-*tert*-butyl peroxide resulted in stack-type particles. Using perfluorinated hexyl iodide or BrCCl₃ as chain transfer agents led to polymers with sponge-type or rose-type morphology after expansion, respectively. Besides characterization by SEM, AFM also showed that different end groups result in change of the surface appearance. FT-IR and DSC analyses revealed that the degree of crystallinity is changed by up to a factor of two and that the type of crystal phase strongly depends on polymer end groups.¹²⁹

Based on the strong impact of scCO₂ and end groups on PVDF morphology additional RESS (rapid expansion from supercritical solution) experiments were carried out, in which a small amount of PVDF was dissolved in scCO₂ at 200 bar and 50°C. The particle formation was studied for PVDF with different end groups and different polymer molecular weights.

6.6.1 Effect of RESS process on molecular weight of PVDF

To study the influence of polymer end groups and molecular weight on the RESS process the polymers listed in Table 6.6.1 were used. The entries in Table 6.6.1 refer to the polymer before applying RESS. The SEM images for most of the polymers prior to RESS show that coagulated material was obtained.

Sample	End groups	M_n (g·mol ⁻¹)	PDI	M_n^* (g·mol ⁻¹)	PDI^*
PFHI-A	I, CF ₃ (CF ₂) ₅	4000	1.42	6000	1.32
DTBP-A	CH ₃ , (CH ₃) ₃ CO	4300	3.77	7500	2.56
BTCM-A	Br, CCl ₃	4400	1.71	5600	1.48
DTBP-B	CH ₃ , (CH ₃) ₃ CO	16000	2.39	17100	1.85
PFHI-B	I, CF ₃ (CF ₂) ₅	2200	1.37	2300	1.35

Table 6.6.1: Poly(vinylidene fluoride) samples employed in the RESS process. M_n and PDI , refer to material before RESS. M_n^* and PDI^* refer to the material collected from the extractor unit after RESS.

During the RESS process the temperature in the extractor, T_E , was 50°C and the temperature prior to expansion, T_0 , was 60°C. The pressure during RESS was 200 bar. After the RESS process was stopped, the polymer remaining in the extractor unit was analyzed by SEC to test whether a fractionation of the polymer occurred. Table 6.6.1 gives the molecular weight of the polymers with different end groups taken from the extractor unit. It is evident that with exception of sample PFHI-B, the number average molecular weight, M_n^* , is higher than for the original material. The reason for higher MWs may be seen in a higher solubility of low MW polymer in scCO₂, resulting in a fractionation of the polymer. The amount of material obtained after the RESS process was too small for SEC analysis, thus the material from the extractor had to be analyzed. This explanation is supported by the observed decrease in polydispersity. The SEM images for all polymers show that the polymers are obtained in the form of small particles.

6.6.2 Particle formation

In all cases processing of the polymers by RESS resulted in small particles. For example the SEM images of the unprocessed (PFHI-B, $M_n = 2200 \text{ g}\cdot\text{mol}^{-1}$) and micronized PVDF are shown in Figure 6.6.1. These pictures are typical examples of the obtained product and indicate that the small primary particles are strongly agglomerated.

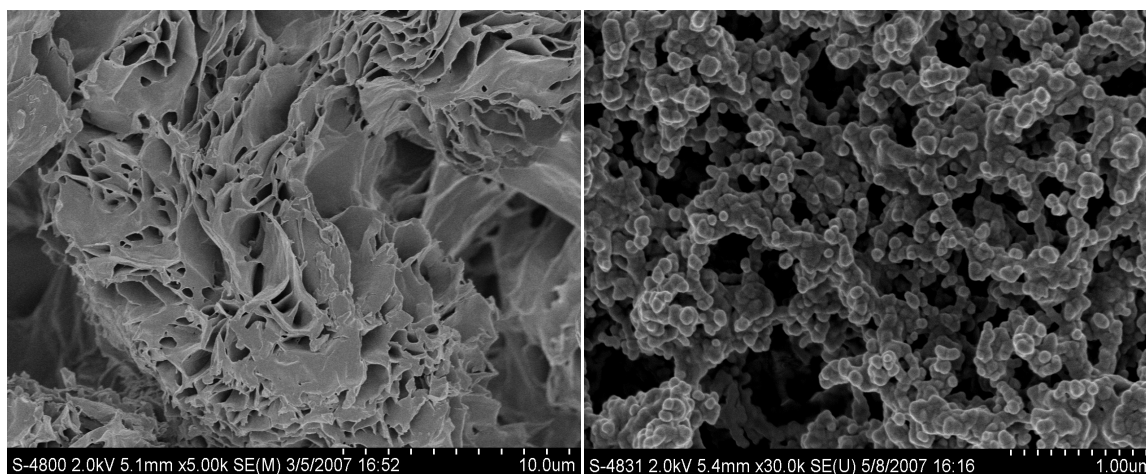


Figure 6.6.1: Typical SEM images of unprocessed PFHI-B (left) and of particles obtained from RESS experiment (right).

As a second example, PVDF with PFHI-derived end groups and $M_n = 4000 \text{ g}\cdot\text{mol}^{-1}$ (PFHI-A) is considered. The SEM images of the unprocessed (left) and micronized PVDF (right) are shown in Figure 6.6.2. These pictures indicate that the small primary particles are less agglomerated as compared to the particles from lower molecular weight material shown in

Figure 6.6.2. In addition, the primary particles obtained from sample PFHI-A are somewhat smaller. Details on the particle sizes of all samples are discussed in the following sections.

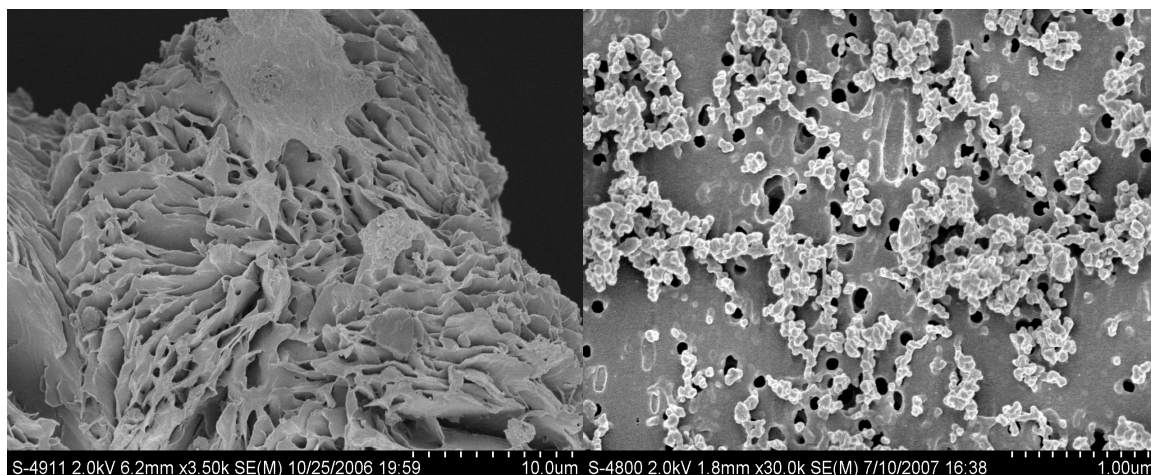


Figure 6.6.2: Typical SEM images of unprocessed PFHI-A (left) and of PFHI-A particles obtained from a RESS experiment at (right).

6.6.3 Influence of polymer molecular weight on particle size distribution (PSD)

The SEM images of the polymer material after the RESS process were analyzed with respect to the particle size distribution (PSD) using the programme image analysis (Image J Version 1.38). The PSDs obtained by image analysis are depicted in Figure 6.6.3 for polymers with different molecular weights. In case of the lower molecular weight sample of PVDF with PFHI-derived end groups (PFHI-B), the RESS precipitated PVDF powders are formed by particles ranging from 58 (d_{10}) to 119 nm (d_{90}), with 50 % of the particles being smaller than 82 nm (d_{50}). Increasing the molecular weight from $M_n = 2200$ to $M_n = 4000 \text{ g}\cdot\text{mol}^{-1}$ leads to a PSD ranging from 46 (d_{10}) to 100 nm (d_{90}) with 50 % of the particles being smaller than 69 nm (d_{50}). Figure 6.6.3 shows the relation of Q_0 and particle diameter. It is the ratio of individual particles n_i divided by number of total particles n_{total} . For example the number of particle counts of PFHI-A between 0 and 30 nm is 26 and the number of total particle counts of PFHI is 1730. Q_0 (frequency distribution) is calculated using Equation 6.4.

$$Q_0 = \frac{n_i}{n_{\text{total}}} = \frac{26}{1730} = 0.015 \quad (6.4)$$

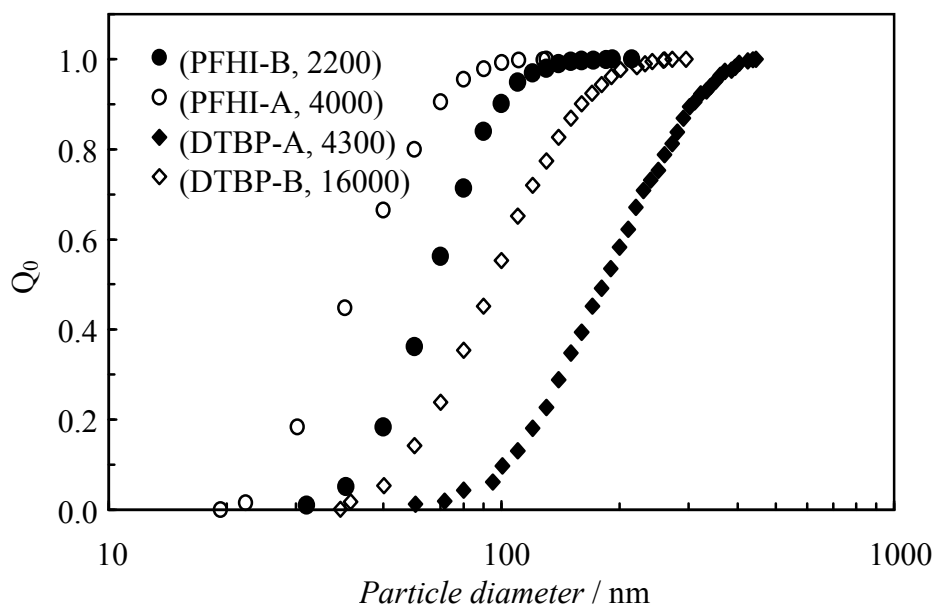


Figure 6.6.3: Abundance ratio of low molecular weight polymer and high molecular weight polymer with DTBP- and PFHI derived end groups.

The d_{50} is defined as the diameter where 50 % of the particles have a larger diameter, and the other 50 % have a smaller diameter. d_{10} (d_{90}) is the diameter where 10 % (90) of the particles have a smaller diameter and hence the remaining 90 % (10) a larger diameter. As a rule, about 600 particle diameters were considered in each PSD calculation.

In addition, Figure 6.6.3 contains data for polymers with DTBP-derived end groups. The RESS precipitated powders of sample DTBP-A are formed by particles ranging from 144 (d_{10}) to 358 nm (d_{90}), with 50 % of the particles smaller than 222 nm (d_{50}). Increasing the molecular weight of the original material from $M_n = 4300$ to $M_n = 16000 \text{ g}\cdot\text{mol}^{-1}$ leads to a PSD ranging from 74.0 (d_{10}) to 194.3 nm (d_{90}) with 50 % of the particles smaller than 119.2 nm (d_{50}).

The observed decrease of particle size with increasing polymer molecular weight can be explained as follows: the increase of molecular weight leads to a lower solubility of the polymer in scCO_2 and the lower solubility results in noticeably lower number concentrations and therewith in smaller particles.¹³⁰ Thus, the observed relationship between molar mass and particle size is consistent with classical nucleation theory, since particle collision rate is directly proportional to the square of particle concentration. These calculations show that a lower solubility and hence a higher dilution of the particles in the expansion chamber inhibit post-expansion particle growth and results in smaller particles.¹³¹

Within this work, for the first time primary nanoscale particles of fluoropolymers were obtained. So far the formation of small primary polymer particles by the RESS process was

only reported for biodegradable polymers, e.g., PLLA nanoparticles produced by Sane and Thies.^{58, 61, 62}

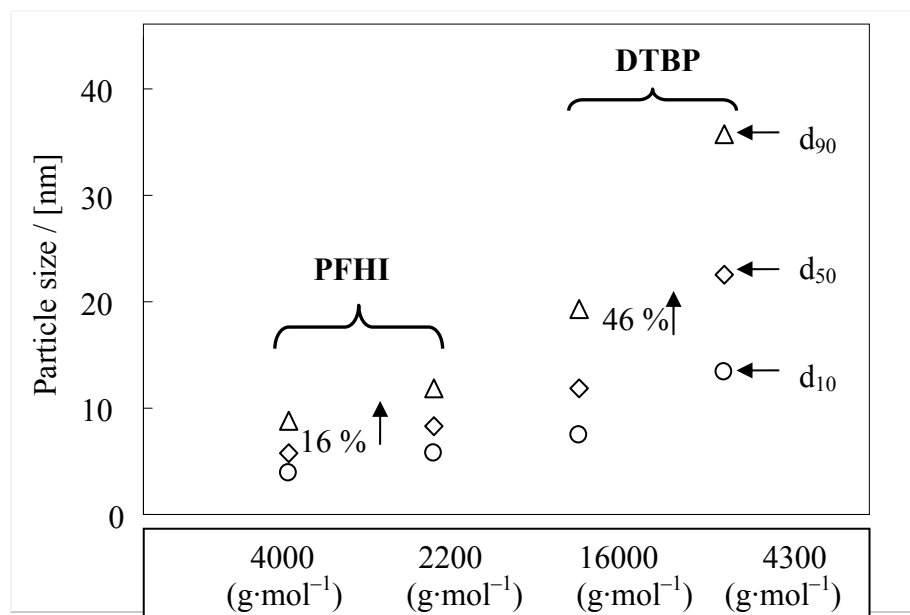


Figure 6.6.4: Particle diameter of low molecular weight polymer and high molecular weight polymer with DTBP- and PFHI derived end groups.

The above reported particle sizes are summarized in Figure 6.6.4. It shows that in the case of PFHI and DTBP the particle size increases about 16 % and 46 %, respectively, as the molecular weight increases. The increase in particle size (inc), with molecular weight is calculated using Equation 6.5.

$$\text{inc} = \left(1 - \frac{d_{50}(M_n, \text{high})}{d_{50}(M_n, \text{low})}\right) \cdot 100 \quad (6.5)$$

The SEM images indicate that polymer MW as well as polymer end groups influence the PSD of particles obtained upon expansion to ambient conditions. To understand why the above-described differences in PSD occur, the degree of crystallinity of the polymer samples taken from the extractor after the RESS processⁱⁱ was investigated applying DSC. As described before, the degree of crystallinity was calculated according to $X = \Delta H_m / \Delta H_c$. Where $\Delta H_c = 104.7 \text{ J} \cdot \text{g}^{-1}$ is the melting enthalpy for a 100 % crystalline sample of PVDF.¹¹⁶

The DSC results, such as melting enthalpy (ΔH_m) and crystallinity (X) are listed in Table 6.6.2. The observed increase of particle size with decreasing polymer molecular weight can be

ⁱⁱ In the remainder of this chapter the wording “after the RESS process“in combination with M_n , PDI or DSC results refers to the material taken from the extractor unit after the RESS process.

explained by considering the crystallinity of polymer. The increase of molecular weight is associated with a high crystallinity and leads to a lower solubility of the polymer in scCO₂. The lower solubility results in noticeably lower number concentrations of polymer and therewith in smaller particles. The DSC results of PVDF samples before and after the RESS process are presented in Table 6.6.2 for low and high molecular weight.

Sample	d_{50} / nm	M_n^* g·mol ⁻¹	ΔH_m J/g	Crystallinity “X” (%)	ΔH_m^* J/g	Crystallinity “X” (%)*
PFHI-A	69	6000	60.6	58	61.9	59
PFHI-B	82	2300	38.3	37	22.3	21
DTBP-B	119	17100	32.5	31	35.5	34
DTBP-A	222	7500	29.60	28	34.2	33

Table 6.6.2: Results from differential scanning calorimetry before and after the RESS process. ΔH_m , melting enthalpy; X , crystallinity; ΔH_m^* , melting enthalpy; X^* , crystallinity. (*) after the RESS process.

6.6.4 Influence of polymer end groups on particle size distribution

The PSD obtained by image analysis showed that in case of the same molecular weight but different end groups, the RESS precipitated PVDF powders are formed by particles of different size. Table 6.6.3 shows that PSD ranging from 46 (d₁₀) to 144.6 nm (d₁₀) depending on the nature of end groups. The DSC results of PVDF samples before and after the RESS process are presented in Table 6.6.3 for different end groups.

Sample	d_{50} [nm]	M_n^* g·mol ⁻¹	ΔH_m J/g	Crystallinity “X” (%)	ΔH_m^* J/g	Crystallinity “X” (%)*
DTBP-A	222.5	7500	29.6	28	34.2	33
BTCM-A	160.2	5600	49.2	47	58.0	55
PFHI-A	68.8	6000	60.6	58	61.9	59

Table 6.6.3: Poly(vinylidene fluoride) samples employed in this work. M_n^* ; particle size distribution (PSD). ΔH_m , melting enthalpy; X , crystallinity; ΔH_m^* , melting enthalpy; X^* , crystallinity. (*) after the RESS process

The DTBP samples generally have a high *PDI* which indicates the presence of low MW chains. Therefore, after the RESS process there is a significant reduction in *PDI* and the strongest variation in M_n is found for sample DTBP-A. The observed change of particle size with end group of polymers with similar molecular weight may be explained by the polymer solubility in scCO₂. Solubility plays a key role for the size of primary particles, the results listed in Table 6.6.3 suggest that PVDF with C₆F₁₃I-derived end groups show the lowest solubility and DTBP-derived end groups leads to material with the highest solubility. At first sight, this finding is unexpected, because the perfluorinated hexyl (C₆F₁₃) group should contribute to a higher solubility in CO₂. However, DSC results indicated that sample PFHI-A has a much higher crystallinity than sample DTBP-A after the RESS process. The polymer with the higher crystallinity is expected to have the lower solubility and is expected to yield the smaller particles. Thus, it may be concluded that again polymer solubility controls the size of the primary particles. Thus, the observed relationship between crystallinity of polymer and particle size is consistent with classical nucleation theory. To obtain deeper insights and to allow for modelling, data for the solubility of the polymers in scCO₂ are required. These data will be obtained in future studies.

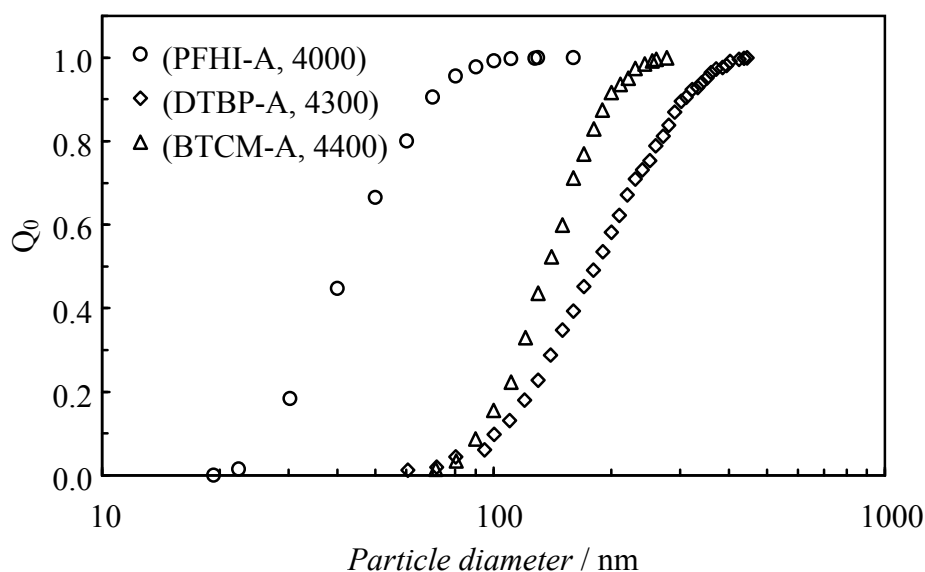


Figure 6.6.5: Abundance ratio and particle size of polymer with different end groups (DTBP-A, PFHI-A and BTCM-A).

The PSD obtained by image analysis is given in Figure 6.6.6 shows that in case of the PFHI-A, the RESS precipitated PVDF powders are formed by particles ranging from 46 (d_{10}) to 99.8 nm (d_{90}), with 50 % of the particles being smaller than 68.8 nm (d_{50}). By changing the end groups (DTBP-A) and keeping the same molecular weight ($M_n = 4300 \text{ g}\cdot\text{mol}^{-1}$) a PSD ranging from 144.6 (d_{10}) to 358.4 nm (d_{90}) with 50 % of the particles being smaller than 222.5 nm (d_{50}) was obtained. Particle sizes obtained for sample BTCM-A with BrCCl_3 -derived end groups are intermediate and range from 109.7 (d_{10}) to 217.3 nm (d_{90}) with 50 % of the particles being smaller than 160.2 nm (d_{50}) was obtained. The observed increase of particle size with polymer end group can be explained as follows: PFHI-derived end groups lead to a lower solubility of the polymer in scCO_2 and the lower solubility results in noticeably lower number concentrations and therewith in smaller particles.¹³⁰ DTBP-derived end groups lead to higher solubility of the polymer in scCO_2 and higher particle size.

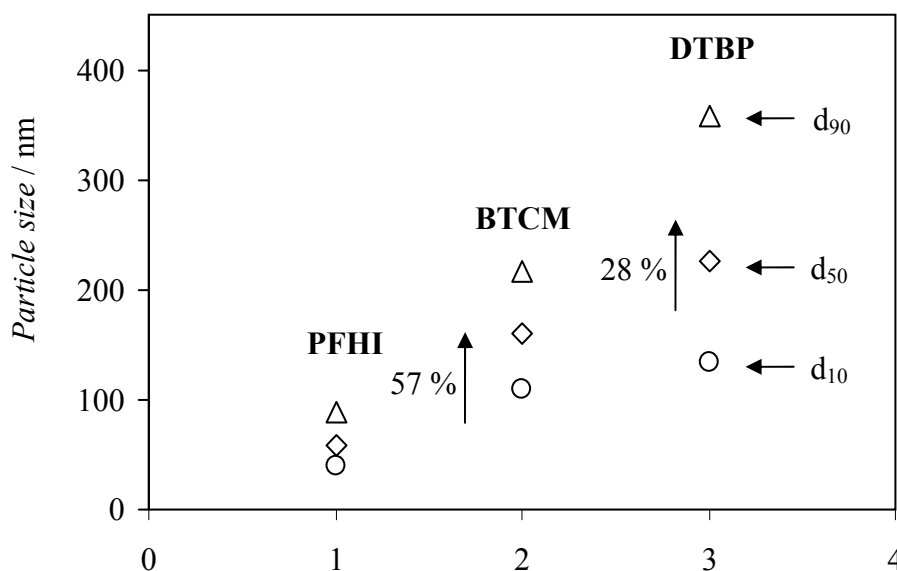


Figure 6.6.6: Particle diameter of particle size of polymers with different end groups (DTBP-A, PFHI-A and BTCM-A).

Figure 6.6.6 shows that in the case of PFHI and BTCM particle size (d_{50}) increases about 57 %, and for BTCM and DTBP the increase is 28 % as the molecular weight is similar. This increase is related to the different end groups of the polymers.

6.6.5 Summary of results

For the first time, it has been demonstrated that RESS can be used to produce primary PVDF nanoparticles with diameters less than 100 nm without the use of liquid solvents, surfactants,

or other additives. The rapid expansion of scCO₂ + polymer mixtures enables the formation of nanoparticles with diameters as small as 69 nm. The results indicate the strong impact of polymer molecular weight and polymer crystallinity on the particle size distributions. Higher M_n or higher crystallinity, both associated with a lower solubility in scCO₂, lead to a decrease in particle sizes. Since, the experimental data demonstrate that primary nanoparticles may be obtained. It seems important to study in future experiments how agglomeration may be avoided.

7. Summary and conclusions

The aim of this work was to synthesize PVDF in homogeneous phase under supercritical carbon dioxide. In addition, kinetics investigations into polymerization and into the characterization of the polymers were carried out. Two strategies for polymer synthesis were used: polymerization with MW control via initiation and MW control via chain transfer agents.

Although PVDF is a semicrystalline polymer its solubility in scCO₂ is sufficiently high to allow for homogeneous phase polymerization of VDF up to complete monomer conversion for CO₂ contents ranging from 61 to 83 wt.%. Polymer molecular weights were derived from ¹H-NMR and SEC. As expected, M_n is decreasing upon increasing DTBP concentration or lowering VDF concentration. For M_n of 19000 g·mol⁻¹ the reaction mixture turned heterogeneous during the polymerization. The reaction mixture remained homogeneous for polymers having M_n values up to 8000 g·mol⁻¹. Generally, large polydispersities ranging from 3.1 to 5.7 were obtained. The high-temperature, high-pressure and high DTBP concentration conditions applied did not alter the microstructure of PVDF: from ¹H-NMR spectra it was concluded that structural defects amount to 6.4 mol.%, which is close to the literature value of 6 mol.%. SEM analyses showed that polymer obtained in a homogeneous phase reaction lead to regular stack-type particles upon expansion, whereas expansion following a heterogeneous polymerization yields polymer particles with high polydispersity. The present work indicated that VDF polymerizations may be carried out in an environmentally benign reaction medium (CO₂) in the absence of any fluorinated stabilizers. This homogeneous phase polymerization of VDF may serve as a basic step for the development of continuous polymerization processes.

In polymerization with perfluorinated hexyl iodide as chain transfer agent excellent control of molecular weight may be achieved. In agreement with literature the linear increase in M_n with time and conversion indicated that a living radical polymerization is occurring. It is remarkable to note that polymer from reactions up to complete monomer conversion shows a polydispersity of 1.2. The monomer conversion – time data may be used to estimate the rate of polymerization. The rate data indicated that C₆F₁₃I does not only control molecular weight but also significantly contributes to the initiation rate. The presence of C₆F₁₃I along with controlling the molecular weight also improved the phase behaviour of the reaction. In this case the reaction remained homogeneous up to complete monomer conversion at the temperature of 120°C instead of 140°C as required in the absence of C₆F₁₃I.

PVDF obtained from iodine transfer polymerization in supercritical CO₂ with iodide end groups allowed for efficient functionalization of the polymer. After substitution of the iodide end group by an azide group 1,3 dipolar cycloadditions with alkynes yield polymers with 1,2,3 triazole end groups. Using symmetrical alkynes the reactions may be carried out in the absence of any catalyst. This end-functionalized PVDF has higher thermal stability as compared to the normal PVDF. These polymers may be used as cross linkers.

This work has supplied kinetic data of the radical polymerization of VDF, initiated by di-*tert*-butyl peroxide in the presence of three chain transfer agents (C₆F₁₃X) perfluorinated (halogenated) and non halogenated (C₆F₁₃H). By using the method of Mayo and Lewis, the chain transfer constant (C_T) has been determined at 120°C for each CTA. The calculated values are $8 \cdot 10^{-1}$, $9 \cdot 10^{-2}$ and $2 \cdot 10^{-4}$ for C₆F₁₃I, C₆F₁₃Br and C₆F₁₃H, respectively. The transfer efficiency is dependent on the X group of the C₆F₁₃X. The NMR and ESI-MS analyses also showed that there is insertion of monomer unit between two ends of chain transfer agent in case of C₆F₁₃I and C₆F₁₃Br. The results obtained for M_n and C_T are also in agreement with the rate of polymerization with different CTAs.

The polymer material obtained from polymerizations with MW control via initiation and via the use of CTAs was analyzed by various characterizations techniques. The results indicated that polymer end groups have a significant influence on polymer morphology, the ratio of α and β phase material, the overall degree of crystallinity, melting and crystallization temperature as well as the film formation on silica. For example, based upon choice of end groups and molecular weight PVDF with overall degrees of crystallinity ranging from 26 to 64 % are accessible. The differences in melting and crystallization temperatures remained even after three heating cycles indicating that the end groups rather than synthesis in the presence of CO₂ or expansion from supercritical solution are determining the polymer properties. Although rather low molecular weight material was used, the lower MW samples still consisted of polymer molecules containing around 30 monomer units (estimated from M_n) and the higher MW samples of polymer molecules with 91 to 104 monomer units. In addition, it was noted that the end group induced differences are larger than the changes induced by molecular weight.

It has been demonstrated that the RESS process can be used to produce primary PVDF nanoparticles with diameters less than 100 nm without the use of liquid solvents, surfactants, or other additives. The rapid expansion of scCO₂ + polymer mixtures enabled the formation of nanoparticles with diameters as small as 69 nm. The results indicate the strong impact of polymer molecular weight and polymer crystallinity on the particle size distributions. Higher

M_n or higher crystallinity, both associated with a lower solubility in scCO₂, led to a decrease in particle sizes. The results suggest that the size of polymer particles produced by RESS depends on the processing conditions (pressure and temperature), phase behaviour (solubility in scCO₂), and on the polymer properties (molar mass and end group). The rapid expansion of scCO₂ + polymer with different end groups enabled the formation of nanoparticles with diameters of 68.8 (d_{50}), 160.2 (d_{50}) and 222.5 nm (d_{50}) depending on the nature of the polymer end groups. These nanoparticles provide a base to prepare nanocomposites for applications such as dielectric materials.

Outlook

Within this work it was demonstrated that VDF polymerizations may be carried in the absence of any stabilizer in solution with scCO₂. In future experiments it should be investigated to what extent the CO₂ content and the pressure may be reduced to allow for a more efficient process. Additionally, it should be tested how polymer morphology may be modified. It is particularly interesting to increase the β -phase fraction, because it would lead to an increase of the piezoelectric character of the polymer material. To obtain more insights into the factors affecting the PVDF properties, future experiments should be carried out with, e.g., polymers of higher MW and with additional end groups.

The end-functionalization of PVDF-I with symmetric alkynes showed very interesting results. In the future, the work should be extended to functionalization of the end groups with asymmetric alkynes using a catalyst. Asymmetric alkynes with additional functional groups may allow for functionalization to different groups giving access to polymers with a wide range of properties.

The RESS process gave access to material consisting of primary particles with sizes in the range from 45 to 120 nm. Depending on molecular weights and end groups these particles showed different degrees of agglomeration. It seems important to study polymers with additional end groups in future RESS experiments. Furthermore, it is important to modify the RESS experiments to avoid agglomeration of polymer particles. The nanoparticles obtained from the RESS process may be used to prepare the nanocomposites for applications such as dielectric materials.

As a first estimate the kinetic coefficients derived from VDF polymerizations in the presence of C₆F₁₃H should be used to model polymerizations using the program PREDICI[®]. To allow for the optimization of the polymerizations via modeling, however, the knowledge of reliable rate coefficients over a wide range of temperatures and pressures is required. To obtain these

kinetic data pulsed laser initiated polymerizations in combination with polymer analysis by size-exclusion chromatography, which give access to the individual propagation rate coefficients, should be carried out. Aiming for kinetic coefficients at lower pressures and temperatures, it should be tested whether homogeneous phase VDF homopolymerizations may be carried out in solution with, e.g., pentafluorobutane.

8. List of abbreviations

A	absorbance
AFM	atomic force microscopy
BDE	bond dissociation energy
BTCM	bromotrichloromethane
c	concentration
c_{CTA}	concentration of chain transfer agent
c_I	initial initiator concentration
CLD	chain length distribution
c_M	initial monomer concentration
C_p	chain-transfer constant for transfer to polymer
c_{R0}	effective initial radical concentration
C_T	chain-transfer constant
CTA	chain-transfer agent
d_{10}	diameter of 10 % particles
d_{50}	diameter of 50 % particles
d_{90}	diameter of 90 % particles
DMAc	dimethylacetamide
DMSO	dimethylsulfoxide
DP_n	number average degree of polymerization in the presence of CTA
DP_{no}	number average degree of polymerization in the absence of CTA
DSC	differential scanning calorimetry
DTBP	di- <i>tert</i> -butyl peroxide
E_A	activation energy
E_λ	energy of one mole of photons at the wave length λ
ESI-MS	electrospray ionization mass spectroscopy
f	initiator efficiency
FT-NIR	Fourier Transform-Near Infrared Spectroscopy
HPFH	1H-perfluorohexane
$Int(t=0)$	peak integral at time zero
$Int(t)$	peak integral at time t
K	overall rate coefficient
k_d	decomposition rate coefficient

k_p	propagation rate coefficient
k_t	termination rate coefficient
$k_{t,c}$	termination rate coefficient for termination by combination
$k_{t,d}$	termination rate coefficient for termination by disproportionation
$k_{tr,I}$	chain transfer rate coefficient for transfer to initiator
$k_{tr,M}$	chain transfer rate coefficient for transfer to monomer
$k_{tr,P}$	chain transfer rate coefficient for transfer to polymer
$k_{tr,X}$	chain transfer rate coefficient for transfer to chain-transfer agent
LiBr	lithium bromide
M	monomer
M_n	number average molecular weight
MW	molecular weight
MMA	methyl methacrylate
M_w	weight average molecular weight
MWD	molecular weight distribution
NMR	nuclear magnetic resonance
p	pressure
P_o	pre-expansion pressure
P_c°	critical pressure
<i>PDI</i>	polydispersity
PFHI	perfluorinated hexyl iodide
PFBH	perfluorinated hexyl bromide
PMMA	poly(methyl methacrylate)
PSD	particle size distribution
PVDF	poly (vinylidene fluoride)
Q_o	frequency distribution
RESS	rapid expansion of supercritical solution
r_p	rate of polymerization
R_p	rate of propagation
R_t	rate of termination
R_{tr}	rate of transfer
SADT	self accelerating decomposition temperature
scCO ₂	supercritical carbon dioxide
SEC	size-exclusion chromatography

SEM	scanning electron microscopy
t	time
T_c°	critical temperature
T_c	crystallization temperature
T_E	Extractor temperature
T_m	melting temperature
T_0	pre-expansion temperature
V	volume
ΔV^\ddagger	activation volume
VDF	vinylidene fluoride
WAXD	wide angle X-ray diffraction
x	monomer conversion
X	crystallinity of polymer

9. Acknowledgments

I want to express my profound gratitude to the staffs of scientists and technicians and other persons directly or indirectly involved in the completion of this work. The findings within this dissertation would never have been so fruitful without the help of these people.

First of all, I would like to thank sincerely *Prof. Dr. Sabine Beuermann* (University of Potsdam) for giving me the opportunity to carry out my PhD thesis under her supervision, on a research topic of polymer science. Furthermore, I am grateful for the real autonomy she gave me so that I could “explore” the topic by myself and fulfil my own ideas. I appreciated her availability for discussions, during which I definitely benefited from her knowledge and experience in chemistry. Likewise, I thank her for her encouragement, trust and for interesting conversations on open subjects. Finally, I gratefully acknowledge her for allowing me to present our results at international conferences.

I am grateful to *Prof. Dr. Michael Buback* (Georg-August University Goettingen) who permitted me to work in his research group for one year. At the practical level in Goettingen, many thanks to Dr. Hans-Peter Vögele for his ability to keep everything running. Many thanks to Dr. Moritz Gadermann, Dr. Duc Hung Nguyen, Pascal Hesse, Olaf Janssen, Daniel Boschmann, Fabian, Durga and Undrakh, for their guidance and help during my stay in Goettingen. Many thanks to the Buback Abteilung as a whole for the very pleasant and cooperative working environment. Special thanks to Sandra Lotze for help to perform high pressure experiments.

I am thankful to *Prof. Dr. Michael Türk* and E. Breininger (TU Karlsruhe) for RESS process and particles size measurements along with interesting discussions on polymer particles obtained from RESS process.

I am thankful to *Prof. Dr. Markus Antonietti* (Max Planck Institute of Colloids and Interfaces, Golm) and his coworkers for permitting me to use the DSC, TGA, AFM and WAXD analysis. Dr. Brigitte Tiersch and Dr. Ines Starke (University of Potsdam) are gratefully acknowledged for the SEM and ESI-MS analysis.

I am thankful to the *Dyneon GmbH* for financial support of this research. Additional support within the European Graduate School on “Microstructural Control in Free-Radical Polymerization” by the Deutsche Forschungs-gemeinschaft is acknowledged.

Special thanks to the lab and office mates for the nice work atmosphere and their guidance and help during my stay: Eleonore Möller, Sascha Prentzel, Diana Hill and Aleksandra Jeličić for her vigilant proof reading.

Finally, I am indebted to my parents for their understanding, help and encouragement whatever I have carried out in my life. I send my heartfelt thanks to my brothers and all friends in Pakistan and Germany for their important support all over these years.

10. Publications

1. “Homogeneous phase polymerization of vinylidene fluoride in supercritical carbon dioxide.”
Sabine. Beuermann, M.Imran ul-haq,: J. Polym. Sci, Part A, Polym. Chem. 2007, 45, 5626.
2. “Homogeneous phase polymerization of vinylidene fluoride in supercritical carbon dioxide; surfactant free synthesis and kinetics”
Sabine. Beuermann, M.Imran ul-haq,: Macromol Symp. 2007, 259, 210.
3. “Influence of polymer end groups on the morphology of poly (vinylidene fluoride) synthesized in supercritical carbon dioxide.”
M.Imran ul-haq, Sabine. Beuermann,: Macromolecules (accepted).
4. “Effect of chain transfer agents on kinetics of poly (vinylidene fluoride) synthesized under supercritical carbon dioxide”
M.Imran ul-haq, Sabine. Beuermann,: (submitted to Macromol Symp).
5. “Effect of polymer end groups on particles produced by RESS process from poly (vinylidene fluoride) synthesized under supercritical CO₂”
M. Imran ul-haq, E. Breininger, S. Beuermann, M. Türk,: (submitted to Journal of Supercritical Fluids).
6. “Living Radical Polymerizations of vinylidene fluoride in supercritical carbon dioxide”
S. Beuermann, M. Imran ul-haq,: Polymer Preprints, 2008, 49(2), 167.
7. “Morphological control of poly (vinylidene fluoride) obtained from surfactant free homogeneous phase polymerization in supercritical CO₂”
S. Beuermann, M. Imran ul-haq,: (Proceedings, 11th European Meeting on Supercritical Fluids 2008, Barcelona, Spain).
8. “Submicron poly (vinylidene fluoride) particles from rapid expansion of Supercritical solution”
M. Imran-ul-haq, E. Breininger, S. Beuermann, M. Türk,: (Proceedings, 11th European Meeting on Supercritical Fluids 2008, Barcelona, Spain).
9. “Influence of Polymer End groups on Particle Properties Produced by Rapid Expansion of Poly(Vinylidene Fluoride) – scCO₂ Solutions”
M. Imran-ul-haq, E. Breininger, S. Beuermann, M. Türk,: (Proceedings, 4th Symposium, Produktgestaltung in der Partikeltechnologie 2008, Pfinztal, Germany).

Patent

1. “M. Jürgens, K. Hintzer, S. Beuermann, M. Imran ul-haq, “Combination of click chemistry and vinylidene fluoride polymerization in supercritical carbon dioxide”
(to be filed)

Poster presentations

1. M. Imran ul-haq, Sabine Beuermann, “*Homogeneous phase free radical polymerization of vinylidene fluoride in supercritical carbon dioxide*” 4th IUPAC Sponsored International Symposium on Radical Polymerization: Kinetics and Mechanism. September 03-08, 2006, Il Ciocco/, Italy.
2. M. Imran ul-haq, Sabine Beuermann, “*High pressure free radical polymerization of vinylidene fluoride in supercritical carbon dioxide*” The bi-annual international meeting on Polymers, Polydays. October 4 - 6, 2006, Berlin, Germany.
3. M. Imran ul-haq, Sabine Beuermann, “*Influence of polymer end groups on the morphology of poly (vinylidene fluoride)*” Day of Chemistry. June 27, 2007, Berlin, Germany.
4. M. Imran ul-haq, E. Breininger, S. Beuermann, M. Türk. “*Influence of polymer end groups on particle properties produced by rapid expansion of poly (vinylidene fluoride) – scCO₂ solutions*”. 9th International workshop on polymer reaction engineering. October 7-10, 2007, Hamburg, Germany.
5. M. Imran ul-haq, E. Möller, Sabine Beuermann, “*Surfactant-Free Homogeneous Phase Polymerization of Vinylidene fluoride in Supercritical CO₂*” 5th Conference on Formulation Technology, Formula V. November 19-22, 2007, Potsdam, Germany.
6. M. Imran ul-haq, E. Breininger, S. Beuermann, M. Türk. “*Formation of nanoscale polymer particles via rapid expansion of supercritical polymer / scCO₂ solution*”. High pressure meets advanced fluids. March 11- 13, 2008, Aachen, Germany.
7. M. Imran ul-haq, E. Breininger, S. Beuermann, M. Türk. “*Effect of polymer end groups on crystallization, morphology and particles produced by RESS process for poly (vinylidene fluoride) synthesized under supercritical carbon dioxide*” 11th European Meeting on Supercritical Fluids. May 4-7, 2008, Barcelona, Spain.

11. Literature

- [1] Jessop, P. G.; Leitner, W. *Chemical Synthesis using Supercritical Fluids*, Wiley-VCH, Weinheim **1999**.
- [2] McHugh, M. A.; Krukonis, V. J. J. *Supercritical Fluid Extraction: Principles and Practice*, 2nd Ed. Butterworth-Heinemann: Stone-ham, **1993**.
- [3] Cooper, A. I. *J. Mater. Chem.* **2000**, 10, 207.
- [4] <http://www.tyndall.ie/nap/NormaScully-NAP34.pdf>
- [5] DeSimone, J. M.; Guan, Z.; Elsbernd, C. S. *Science* **1992**, 257, 945.
- [6] Beuermann, S.; Buback, M.; Schmaltz, C.; Kuchta, F.-D. *Macromol. Chem. Phys.* **1998**, 199, 1209.
- [7] Beuermann, S.; Buback, M.; Schmaltz, C. *Macromolecules* **1998**, 31, 8069
- [8] Beuermann, S.; Buback, M.; Schmaltz, C. *Ind. Eng. Chem. Res.* **1999**, 38, 3338.
- [9] David, G.; Boyer, C.; Tonnar, J.; Ameduri, B.; Lacroix-Desmazes, P.; Boutevin, B. *Chem. Rev.* **2006**, 106, 3936.
- [10] Buback, M. *Angew. Chem. Int. Ed.* **1991**, 30, 1654.
- [11] Beuermann, S.; Buback, M.; Isemer, C.; Wahl, A. *Macromol. Rapid. Commun.* **1999**, 20, 26.
- [12] Beuermann, S.; Buback, M.; Jürgens, M. *Ind. Eng. Chem. Res.* **2003**, 42, 6338.
- [13] Hoeffling, T. A.; Newman, D. A.; Enick, R. M.; Beckman, E. J. *J. Supercrit. Fluids.* **1993**, 6, 165.
- [14] Sarbu, T.; Styranec, T.; Beckman, E. J. *Nature (London)* **2000**, 405, 165.
- [15] Kazarian, S. G.; Vincent, M. F.; Bright, F. V.; Liotta, C. L.; Eckert, C. A. *J. Am. Chem. Soc.* **1996**, 118, 1729.
- [16] Shah, V. M.; Hardy, B. J.; Stern, S. A. *J. Polym. Sci., Polym. Phys. Ed.* **1993**, 31, 313.
- [17] Mertdogan, C. A.; Byun, H. S.; McHugh, M. A.; Tuminello, W. H. *Macromolecules* **1996**, 29, 6548.
- [18] Kirby, C. F.; McHugh, M. A. *Chem. Rev.* **1999**, 99, 565.
- [19] Beuermann, S.; Buback, M.; Jürgens, M. *Ind. Eng. Chem. Res.* **2003**, 42, 6338.
- [20] Lovinger, A. J. in: *Development in Crystalline Polymers-I*; D. C. Bassett, Ed., Applied Science Publishers: London, **1982**; pp 195.
- [21] Hougham, G.; Johns, K.; Cassidy, P. E.; Davidson, T. "Fluoropolymers: Synthesis and Properties", Plenum, New York, **1999**.

- [22] Scheirs, J. “*Modern Fluoropolymers*”, Wiley: New York, **1997**.
- [23] Ameduri, B.; Souzy, R. *Prog. Polym. Sci.* **2005**, 30, 644.
- [24] Wood, C. D.; Yarbrough, J. C.; Roberts, G.; DeSimone, J. M. in: *Supercritical Carbon Dioxide in Polymer Reaction Engineering*; Kemmere, M. F.; Meyer, T. eds., Wiley-VCH, **2005**, 189.
- [25] Giesy, J. P. ; Kannan, K. *Environ. Sci. Technol.* **2001**, 35, 1339.
- [26] Woods, H. M.; Silva, M. M. C. G.; Nouvel, C.; Shakesheff, K. M.; Howdle, S. M. *J. Mater. Chem.* **2004**, 14, 1663.
- [27] Kendall, J. L.; Canelas, D. A.; Young, J. L.; DeSimone, J. M. *Chem. Rev.* **1999**, 99, 543.
- [28] DeSimone, J. M.; Maury, E. E.; Menciloglu, Y. Z.; McClain, J. B.; Romack, T. J.; Combes, J. R. *Science* **1994**, 265, 356.
- [29] Hsiao, Y. L.; Maury, E. E.; DeSimone, J. M.; Mawson, S.; Johnston, K. P. *Macromolecules* **1995**, 28, 8159.
- [30] O'Neill, M. L.; Yates, M. Z.; Johnston, K. P.; Smith, C. D.; Wilkinson, S. P. *Macromolecules* **1998**, 31, 2838.
- [31] Beginn, U.; Najjar, R.; Ellmann, J.; Vinokur, R.; Martin, R.; Moeller, M. *J. Poly. Sci., Part A: Polym. Chem.* **2006**, 44, 1299.
- [32] Tai, H.; Wang, W.; Martin, R.; Liu, J.; Lester, E.; Licence, P.; Woods, H. M.; Howdle, S. M. *Macromolecules* **2005**, 38, 355.
- [33] Saraf, M. K.; Gerard, S.; Wojcinski, L. M.; Charpentier, P.A.; DeSimone, J. M.; Roberts, G. W. *Macromolecules* **2002**, 35, 7976.
- [34] Kendall, J. L.; Canelas, D. A.; Young, J. L.; DeSimone, J. M. *Chem. Rev.* **1999**, 99, 543.
- [35] Bonavoglia, B.; Storti, M.; Morbidelli, M.; Rajendran, A.; Mazzotti, M. *J. Polym. Sci., Part B: Polym. Phys.* **2006**, 44, 1531.
- [36] Dinoia, T. P.; Conway, S. E.; Lim, J. S.; McHugh, M. A. *J. Polym. Sci., Part B: Polym. Phys.* **2000**, 38, 2832.
- [37] Pianca, M.; Barchiesi, E.; Esposito, G.; Radice, S. *J. Fluorine Chem.* **1999**, 95, 71.
- [38] Lu, F. J.; Hsu, S. L. *Macromolecules* **1986**, 19, 326.
- [39] Takahashi, Y.; Mataubara, Y.; Tadokoro, H. *Macromolecules* **1982**, 15, 334.
- [40] Matsushige, K.; Nagata, K.; Imada, S.; Takemura, T. *Polymer* **1980**, 21, 1391.
- [41] Kasmynin, B. P.; Gal'Perin, E. L. *Vysokomol. Soedin., Ser. A* **1972**, A14, 1603.

- [42] Matsushige, K.; Takemura, T. *J. Polym. Sci., Polym. Phys. Ed.* **1978**, 16, 921.
- [43] Kochervinskii, V. V. *Crystallography Reports* **2003**, 48, 649.
- [44] Dang, T.-M.; Wang, L.; Yin, Y.; Zhang, Q.; Lei, Q.-Q. *Adv. Mater.* **2007**, 19, 852.
- [45] Chen, Y.; Deng, Q.; Xiao, J.; Nie, H.; Wu, L.; Zhou, W.; Huang, B. *Polymer* **2007**, 48, 7604.
- [46] Mokrini, A.; Huneault, M. A.; Gerard, P. *J. Membr. Sci.* **2006**, 283, 74.
- [47] Shieh, Y.-T.; Hsiao, T.-T.; Chang, S.-K.; *Polymer* **2005**, 47, 5929
- [48] <http://www.gl.ciw.edu/~cohen/meetings/ferro2004/Ferro2004Presentations/Nakhmanson.pdf>.
- [49] Duc, M.; Ameduri, B.; David, G.; Boutevin, B. *J. Fluorine. Chem.* **2007**, 128, 144.
- [50] Jung, J.; Perrut, M. *J. Supercrit. Fluids.* **2001**, 20, 179.
- [51] Yeo, S.-D.; Kiran, E. *J. Supercrit. Fluids.* **2005**, 34, 287.
- [52] Reverchon, E.; Adami, R. *J. Supercrit. Fluids.* **2006**, 37, 1.
- [53] Bahrami, M.; Ranjbarian, S. *J. Supercrit. Fluids.* **2007**, 40, 263.
- [54] Türk, M.; Hils, P.; Helfgen, B.; Schaber, K.; Martin, H.-J.; Wahl, M.A. *J. Supercrit. Fluids.* **2002**, 22, 75.
- [55] Charoenchaitrakool, M.; Dehghani, F.; Foster, N. R. *Int. Journal of Pharmaceutics.* **2002**, 239, 103.
- [56] Perrut, M.; Jung, J.; Leboeuf, F. *Int. Journal of Pharmaceutics.* **2005**, 288, 3.
- [57] Türk, M.; Upper, G.; Hils, P. *J. Supercrit. Fluids.* **2006**, 39, 253.
- [58] Sane, A.; Thies, M.C. *J. Supercrit. Fluids.* **2007**, 40, 134.
- [59] Chernyak, Y.; Henon, F.; Harris, R. B.; Gould, R.D.; Franklin, R. K.; Edwards, J. R.; DeSimone, J. M.; Carbonell, R. G. *Ind. Eng. Chem. Res.* **2001**, 40, 6118.
- [60] Blasig, A.; Shi, Ch.; Enick, R.M.; Thies, M C. *Ind. Eng. Chem. Res.* **2002**, 41, 4976.
- [61] Sane, A.; Taylor, S.; Sun, Y.-P.; Thies, M. C. *Chem. Commun.* **2003**, 2720.
- [62] Sane, A.; Thies, M.C. *J. Phys. Chem. B.* **2005**, 109, 19688.
- [63] Moad, G.; Solomon, D. H. *The chemistry of Free Radical Polymerization*; Pergamon: Oxford, **1995**.
- [64] Mayo, F. R. *J. Am. Chem. Soc* **1943**, 65, 2324.

- [65] Buback, M.; Hinton, C. in: *High Pressure Techniques in Chemistry and Physics*; Holzappel, W. B.; Isaacs N. S. eds. Oxford University Press **1997**, 151.
- [66] Buback, M.; Latz, H. *Macromol. Chem. Phys.* **2003**, 204, 638.
- [67] Türk, M.; Hils, P.; Helfgen, B.; Schaber, K.; Martin, H. -J.; Wahl, M. A.; *J. Supercrit. Fluids.* **2002**, 22, 75.
- [68] Jürgens, M. PhD. *Thesis* **2002**, Göttingen.
- [69] Beuermann, S.; Imran-ul-haq, M. *J. Polym. Sci., Polym. Chem. Ed.* **2007**, 45, 5626.
- [70] Beuermann, S.; Imran. ul-haq, M. *Macromol. Symp.* **2007**, 259, 210.
- [71] Becker, P.; Buback, M.; Sandmann, J. *Macromol. Chem. Phys.* **2002**, 203, 2113.
- [72] Becker, P. PhD. *Thesis* **2001**, Göttingen.
- [73] Bosch, C. M.; Velo, E.; Recasens, F. *Chem. Eng. Sci.* **2001**, 56, 1451.
- [74] Brandrup, J.; Immergut, E. H.; eds. *Polymer Handbook*, 3rd edition, Wiley, New York **1989**.
- [75] Schmaltz, C. PhD. *Thesis* **1997**, Göttingen.
- [76] Buback, M.; Kuchta, F.-D. *Macromol. Chem. Phys.* **1995**, 198, 1455.
- [77] Wahl, A. PhD. *Thesis* **2000**, Göttingen.
- [78] Guiot, J.; Ameduri, B.; Boutevin, B. *Macromolecules* **2002**, 35, 8694.
- [79] Pianca, M.; Barchiesi, E.; Esposito, G.; Radice, S. *J. Fluorine. Chem.* **1999**, 95, 71.
- [80] Russo, S.; Behari, K.; Chengji, S.; Pianca, M.; Barchiesi, E.; Moggi, G. *Polymer* **1993**, 34, 4777.
- [81] Duc, M.; Ameduri, B.; Boutevin, B.; Kharroubi, M.; Sage, J. M. *Macromol. Chem. Phys.* **1998**, 199, 1271.
- [82] Maccone, P.; Apostolo, M.; Ajroldi, G. *Macromolecules* **2000**, 33, 1656.
- [83] Saraf, M. K.; Wojcinski, L. M.; Kennedy, K. A.; Gerard, S.; Charpentier, P. A.; DeSimone, J.; Roberts, G. W. *Macromol. Symp.* **2002**, 182, 119.
- [84] Gorlitz, M.; Minke, R.; Trautvetter, W.; Weisgerber, G. *Angew. Makromol. Chem.* **1973**, 29, 30, 137.
- [85] Jung, J.; Perrut, M. *J. Supercrit. Fluids.* **2001**, 20, 179.
- [86] Diefenbacher, A.; Türk, M. *J. Supercrit. Fluids.* **2002**, 22, 175.
- [87] Boyer, C.; Valade, D.; Sauguet, L.; Ameduri, B.; Boutevin, B. *Macromolecules* **2005**, 38, 10353.

- [88] Baradi, B.; Shoichet, M. *Macromolecules* **2002**, 35, 3569.
- [89] Janssen, O. Diploma. *Thesis* **2004**, Göttingen.
- [90] Tsarevsky, N. T.; Matyjaszewski, K. *Chem. Rev.* **2007**, ASAP article, published on the web 05/27/2007
- [91] Buback, M.; Hinton, C. *Z. Phys. Chem. (Munich)*, **1996**, 193, 61.
- [92] Boyer, C.; Valade, D.; Lacroix-Desmazes, P.; Ameduri, B.; Boutevin, B. *J. Polym. Sci., Part A: Polym. Chem.* **2006**, 44, 19, 5763.
- [93] Mueller, P. A.; Storti, G.; Morbidelli, M.; Costa, I.; Galia, A.; Scialdone, O.; Filardo, G. *Macromolecules* **2006**, 39, 6483.
- [94] Buback, M.; Schweer, J. *Z. Phys. Chem. (Munich)* **1989**, 161, 153.
- [95] Beuermann, S.; Buback, M. *Prog. Polym. Sci.* **2002**, 27, 191.
- [96] Langer, R.; Tirrell, D. A. *Nature* **2004**, 428, 487.
- [97] Klok, H.-A. *J. Polym. Sci., Part A: Polym. Chem.* **2005**, 43, 1.
- [98] Pyun, J.; Matyjaszewski, K. *Chem. Mater.* **2001**, 13, 3436.
- [99] Rostovtsev, V. V.; Green, L. G.; Fokin, V. V.; Sharpless, K. B. *Angew. Chem. Int. Ed.* **2002**, 41, 2596.
- [100] Link, A. J.; Vink, M. K. S.; Tirrell, D. A. *J. Am. Chem. Soc.* **2004**, 126, 10598.
- [101] Kolb, C.; Finn, M. G.; Sharpless, K. B. *Angew. Chem. Int. Ed.* **2001**, 40, 2004.
- [102] Huisgen, R. *1,3-Dipolar cycloaddition - introduction, survey, mechanis.* in: *1,3-Dipolar Cycloaddition Chemistry*, A. Padwa, Ed., Wiley, New York, **1984**.
- [103] Coessens, V.; Nakagawa, Y.; Matyjaszewski, K. *Polymer Bulletin*, **1998** 40, 135.
- [104] <http://www.cem.msu.edu/~reusch/OrgPage/bndenrgy.html>.
- [105] Hanton, S. D. *Chem. Rev.* **2001**, 101, 527.
- [106] Buback, M.; Frauendorf, H.; Günzler, F.; Vana, P. *J. Polym. Sci., Part A. Polym. Chem.* **2007**, 45, 2453.
- [107] Szablan, Z.; Lovestead, T. M.; Davis, T. P.; Stenzel, M. H.; Barner-Kowollik, C. *Macromolecules* **2007**, 40, 26.
- [108] Quan, C. L.; Soroush, M.; Grady, M. C.; Hansen, J. E.; Simonsick, W. J. *Macromolecules* **2005**, 38, 7619.
- [109] Marie, A.; Fournier, F.; Tabet, J. C.; Amedurid, A.; Walker, J. *Anal. Chem.* **2002**, 74, 3213.

- [110] Axelsson, J.; Scrivener, E.; Haddleton, D. M.; Derrick, P. J. *Macromolecules* **1996**, *29*, 8875.
- [111] Hunt, S. M.; Sheil, M. M.; Belov, M.; Derrick, P. J. *Anal. Chem.* **1998**, *70*, 1812.
- [112] Zammit, M. D.; Davis, T. P.; Haddleton, D. M.; Suddaby, H. G. *Macromolecules* **1997**, *30*, 1915.
- [113] Yang, D.; Chen, Y. *J. Mater. Sci. Lett.* **1987**, *6*, 599.
- [114] Koga, Y.; Saito, H. *Polymer*, **2006**, *47*, 7564.
- [115] Hattori, T.; Kanaoka, M.; Oigashi, H. *J. Appl. Phys.* **1996**, *79*, 2016.
- [116] Neidhöfer, M.; Beaume, F.; Ibos, L.; Bernes, A.; Lacabanne, C. *Polymer* **2004**, *45*, 1679.
- [117] Gregorio, R.; Cestari, M. *J. Polym. Sci. Part B., Polym. Phys.* **1994**, *32*, 859.
- [118] Hsu, S.L.; Lu, F.J.; Waldman, D.A.; Muthukumar, M. *Macromolecules* **1985**, *18*, 2583.
- [119] Tashiro, K.; Kobayashi, M.; Tadokoro, H. *Macromolecules* **1981**, *14*, 1757.
- [120] Benedetti, E.; Catanorchi, S.; D'Alessio, A.; Moggi, G.; Vergamini, P.; Pracella, M.; Ciardelli, F. *Polym. Int.* **1996**, *41*, 35.
- [121] Benz, M.; Euler, W. B. *J. Appl. Polym. Sci* **2003**, *89*, 1093.
- [122] Peng, Y.; Wu, P. *Polymer* **2004**, *45*, 5295.
- [123] Herman, Uno. T.; Kubono, A.; Umemoto, S.; Kikutani, T.; Okui, N. *Polymer* **1997**, *38*, 1677.
- [124] Lovinger, A. J. *Polymer* **1980**, *21*, 1317.
- [125] Chan, C.-M.; Li, L. *Adv. Polym. Sci.* **2005**, *188*, 1.
- [126] Reiter, G. *J. Polym. Sci: Part B: Polym. Phys.* **2003**, *41*, 18697.
- [127] Noda, K.; Ishida, K.; Kubono, A.; Horiuchi, T.; Yamada, H.; Matsushige, K. *Jpn. J. Appl. Phys.* **2001**, *40*, 4361.
- [128] Kimura, K.; Kobayashi, K.; Yamada, H.; Horiuchi, T.; Ishida, K.; Matsushige, K. *Appl. Phys. Lett.* **2003**, *82*, 4050.
- [129] Imran-ul-haq, M.; Beuermann, S. *Macromolecules* (accepted)
- [130] Türk, M. *J. Supercrit. Fluids.* **2000**, *18*, 3, 169.
- [131] Türk, M.; Lietzow, R. *J. Supercrit. Fluids.* in press

Curriculum Vitae

Personal information

13.07.1978 Born in Gujrat, Pakistan

Education & qualification

1984 – 1994 SSC, F. G. High School G.7/4 Islamabad, Pakistan.

1994 – 1996 HSSC, ICB college G.6/3 Islamabad, Pakistan.

1997 – 1999 Graduation at the University of Punjab, Lahore, Pakistan.

2000 – 2002 Master of Science in Chemistry, Quaid-i-Azam University, Islamabad, Pakistan.

2002 – 2004 Master of Philosophy in Chemistry, Quaid-i-Azam University, Islamabad, Pakistan.

Sept.2004 – Mar.2005 Short term research project, University of Tübingen, in the research group of Prof. Dr. Wolfgang Voelter, Germany.

Jun.2005 – Aug.2006 Research toward doctorate at the Institute for Physical Chemistry, University of Göttingen, in the research group of Prof. Dr. M. Buback / Prof. Dr. Sabine Beuermann, Germany.

Since Aug.2006 Research toward doctorate at the Institute of Chemistry, University of Potsdam, in the research group of Prof. Dr. Sabine Beuermann, Germany.

.

Since Sept. 2006 Member of the European Graduate School "Microstructural Control in Free-Radical Polymerization".

Experience

Sept.2004 – Mar.2005 Scientific worker at the University of Tübingen, Germany.

Jun.2005 – Aug.2006 Scientific worker at the University of Göttingen, Germany.

Since Aug.2006 Scientific worker at the University of Potsdam, Germany.